POLITECNICO DI MILANO

Facoltà di Ingegneria Industriale

Corso di Laurea in
Ingegneria Spaziale

OBISAT: A CUBESAT PROJECT FOR TELEPATHOLOGIC PURPOSES

Relatrice: Prof. MICHÈLE LAVAGNA
Co-relatore: Ing. Riccardo LOMBARDI

Tesi di Laurea di:

Filippo Tommaso Lopes Matr. 725675

Anno Accademico 2011 - 2012

Acknowledgments

First of all I would like to thank all those doctors who, with passion and love dedicate their life to save other people's one. Thus I am saying thank to my father who has supported me and always does, together with my mother and my sister.
Special thanks to Patologi oltre Frontiera, and especially to Dr. Agostino Faravelli who, besides the great work he does, has always been kind and available to be bothered by me.
I would like to thank Professor Amalia Ercoli Finzi who suggested and supported this work from the first beginning together with Prof. Lavagna and Eng. Riccardo Lombardi whom I could never thank enough.
Sincere thanks go to Prof. Capsoni for his constant and patient help and to Eng. Galli from General Electric for his precious technical support.
Finally I want to thank all my friends and roommates who had to deal with me during my stressful and critical moments.

Contents

LIST OF FIGURES

LIST OF TABLES

Abstract

One of the primary needs of Telepathology is to transfer histological slides from place A where they are collected and digitalized to the designed center B, namely the site of analysis and diagnosis. When places are destitute and hard to be reached a valid and reliable satellite transfer link is required.
This work tries to design a space system which could achieve this goal in restricted times, being competitive on the market with a low cost philosophy.
The system here designed is namely a Cubesat. Because of the high demand in terms of service and performance, it uses some atypical devices, not properly thought for Cubesat systems, on an already proven and standardized base.
What will be demonstrated is that the use of such a system, even if with open-ended debatable costs, leads to the satisfaction of the prearranged requirements.

Key words: Telepathology; Pathologists beyond Borders; Oncological Prevention; Space System Design; Cubesat; Equinoctical Orbital Elements; S-Band Satellite Link.

Sommario

Uno dei bisogni primari della Telepatologia è il trasferimento dei vetrini istologici dal luogo A, sede della raccolta e digitalizzazione, al luogo B, centro di studio e diagnosi. Se A è una zona del terzo mondo, difficile da essere raggiunta una comunicazione satellitare diviene indispensabile.
Nello specifico, questo lavoro si propone di studiare un sistema ingegneristico spaziale che possa offrire tale servizio in economia di costi, competitività di mercato ed efficienza tecnologica in termini di qualità delle immagini trasferite.
Viene dunque analizzato e dimensionato un sistema spaziale dedicato, propriamente un Cubesat, che a seguito delle elevate prestazioni richiestegli, innesta su una base standardizzata degli elementi di innovazione che non appartengono propriamente al mondo dei Cubesat.
Si dimostra pertanto che l'utilizzo di questo satellite piccolo e compatto si traduce in un mezzo di trasmissione, che se pur con costi discutibili, soddisfa i requisiti prefissati.

Parole chiave: Telepatologia; Patologi Oltre Frontiera; Prevenzione Oncologica; Progetto di Sistema Spaziale; Cubesat; Parametri Orbitali Equinoziali; Trasmissione Satellitare in Banda S.

1 OBISAT: Mission Overview

Africa: the world's second-largest and second-most-populous continent. These are the first words you encounter by typing Africa on Google. The geographical and population size is unfortunately accompanied by equal dimensions in terms of problems.

Figure 1.1. Africa Area and population

Several issues afflict this continent: lack of water, famine, poverty, diseases and lack of progress and scientific culture.
Many nonprofit organizations (NPO) work and operate in this contest, trying to help population in a specific field. One of them is called Patologi Oltre Frontiera (POF). This work was supposed to be developed in 3 directions: To build a satellite system which was able to connect POF from African venues with the desired Italian hospitals to transfer histological diagnosis, to solve collateral problems relating Africa such as water lack in dry region and to develop an e-learning system. Going forward with the work for different reasons due to costs and nowadays radar technologies, it has been decided to deal with the first issue only, in order to develop an ad-hoc system. In this introductive chapter the main objectives of this work are presented, along with a brief overview of who POF are and what they do. The contribution given by this work and the main issues that have been faced through, they will be described together with an overview of the next chapters' structure.

1.1 Patologi Oltre Frontiera

Patologi Oltre Frontiera (Pathologists Beyond Borders) is a non-governmental association founded in Venice in 1999 with the aim of realizing projects to develop pathological anatomy and oncologic diagnostics in the South of the world. Born for an initiative of a group of Anatomic pathologists, members of the Committee of the International activities of SIAPEC (Società Italiana di Anatomia Patologica e Citologica Diagnostica - the Italian Society of Anatomic Pathology and Diagnostic Cytopathology), it began in the same year its activity, taking part in a project aimed to start-up a Patologic anatomy Service in Tanzania, proposed by the "Associazione Cultura e solidarietà Vittorio Tisòn".
During 2001 Patologi Oltre Frontiera was officially acknowledged as ONLUS, while in 2006, following the acknowledgement of the Ministry of foreign affairs, it was included in the list of qualified non governmental organizations. For a decade, Patologi Oltre Frontiera has been realizing projects in Africa, Latin America, Europe and Middle East. One of the topics POF deals with is Telepathology.
Telepathology is a branch of the telemedicine which envisages the possibility of transferring, from a point to another, images (macroscopic or microscopic images) allowing the sharing of information or even the formulation of a remote diagnosis. Today this technology allows us more ways of action:

Static telepathology: the pathologist A (less expert) choices some microscopic fields in a slide and takes some images at the microscope with a camera. Through internet, he sends images to the pathologist B (more expert) for an advice. The pathologist B answers, via e-mail, giving his opinion. It is the cheapest system: it needs cheap equipment and it works with a satellite dish; but, it requests, from both parties, the presence of pathologists with a good experience. This process was applied for the vaginal cytology in projects in Zambia and Madagascar and in the project Tanzania for the quality control of the histological diagnostics.

Dynamic telepathology: the pathologist A (less expert) puts the slide on the robotized microscope which, via internet, can be manipulated at distance by the pathologist B. Due to this remote system, the latter can, increase or decrease magnifications and moves on the substance as he prefers. Once a diagnosis is made, he invites, via phone or chat, the pathologist B to change the slide to make another diagnosis. This process was used at the beginning of the project Zambia and Palestine but then it was abandoned mainly for high costs and for organizational problems. The costs are at an intermediate level between the first and the third solution, described below.

***Static and dynamic telepathology*:** in a lab at site A, unattended by any pathologist, a technician inserts in a special scanner some slides which are quickly scanned at high magnification and transformed in a virtual slide. The virtual slide digitized images of about 4-5 gigabytes are then downloaded to a server. The pathologist at site B, regardless the presence of pathologists or technicians at site A, can access with a pw the server and see the slide, moving himself, modifying the magnifications, and taking photos. This solution is the most expensive one and it was adopted in the projects Zambia and Madagascar, since a pathologist was not available on site

What do they need?

To conduct their work they must have a reliable and efficient network which could connect them among the different locations, with an affordable cost held by an NGO.

According to this, my task is to build a satellite system which could perform such a job.

1.2 Aperio scanner

Successful digital pathology depends upon effective and timely creation of high-quality digitized glass slides (digital slides). The Scanner utilized by the Patologi Oltre Frontiera is a new developed system, made by Aperio. ScanScope digital scanners are precision instruments that scan glass slides and create seamless, true-color digital slide images of entire glass slides in a matter of minutes. The main characteristics of the used Scan scope are:

- 20X and 40X scanning magnification capabilities
- Rapidly create seamless well-focused whole-slide scans
- Scan a slide in minutes, then view and edit digital slides with the user-friendly ImageScope viewing software
- Manage digital slides, search data tables, and autopopulate fields with barcode data with Spectrum information management system
- Appropriate for multi-user, multi-site, or laboratory workflow-integrated deployments.

Once digitalized, slides need to be transferred to the desired hospital. Actually they are not transferred, but stored in a server accessible from outside. Generally a digital slide server (DSR) is simply a PC with a lot of disk space. The most important attributes of a digital slide server (DSR) are network bandwidth and disk capacity. Network bandwidth is typically the rate-limiting factor in accessing digital slides over a network. Aperio recommends GB Ethernet if possible, otherwise 100MB works also fine. The shared traffic on an education

network is often a factor; sometimes it isn't the total bandwidth available which is limiting, but rather the other traffic which is competing for the bandwidth. In terms of disk capacity, the size of a digital slide file can be calculated as follows:

$$3\ x\ \frac{width\ x\ height\ x\ resolution}{compression}$$

Where:
width = average width of sample area in mm
height = average height of sample are in mm
resolution = Mpixels / mm2. For 20x scans this is 4, for 40x scans this is 16.
3 = number of bytes per pixel
compression = lossy compression ratio. Typically 15 is a good average value.

Although digital slides created are different in dimensions and can vary depending on the size of the sample, in average a picture is about 4 GB.
When scanning or creating images, a type code must be specified. The type code determines the file format and the compression type.

Table 1.1. Compression rates and types

Type code	file format	file extension	compression type	compression ratio	quality?	comment
0	TIFF	.tif	Nome	1:1	lossless	
1	TIFF	.tif	LZW	2-3:1	lossless	
2 (default)	TIFF	.svs	JPEG	15-20:1	good	fastest to process
3	TIFF	.svs	JPEG2000/MIL	20-25:1	excellent	best image quality, 32-bit Windows only.
4	TIFF	.svs	JPEG/YCC	15-20:1	slightly > 2	hardly ever used: a variation on type 2
5	TIFF	.svs	JPEG2000/ Kakadu	20-25:1	excellent, same as 3	best image quality,
7	TIFF	.svs	YUYV	3:2	lossless	just for testing
8	JFIF	.jpg	JPEG	15-20:1	good	for interchange, not suitable for BIG files.
9	PPM	.ppm	Nome	< 1:1	lossless	interchange format, only supported on input
10	CWS	<directory>	JPEG	15-20:1	good	klunky to manage,
11	PFF	.pff	JPEG	15-20:1	good	for interchange, not supported yet
12	JP2	.jp2	JPEG2000/ Kakadu	20-25:1	excellent	for interchange
13	NDPI	.ndpi	JPEG	15-20:1	good	Olimpus / Hamamatsu Nanozoomer
14	VMS	.vms	JPEG	15-20:1	good	older
15	VMU	.vmu	nome	1:1	lossless	older
16	MRXS	.mrxs	JPEG	15-20:1	good	Zeiss / 3DHistech Mirax

SVS, TIFF,JP2 and JFIF are file formats. JPEG, JPEG2000 and LZW are compression types. Some file formats only support one compression type, like JP2 which always use JPEG2000 and JFIF which only use JPEG compression. In the following table, it is possible to see the different type codes supported by Aperio's software:
The most common types are type 2, which is JPEG compression in a TIFF/SVS file and type 3, which is JPEG2000 compression in a TIFF/SVS file [1].

1.3 Mission Requirements

Patologi Oltre Frontiera's need is to make histological slides, collected among African population, be sent to a Milan designed hospital where they can receive a proper diagnosis. The lack of in situ pathologists compelled them to develop several programs dealing with teaching, exchanging and sharing all the resources they can offer between Africa and Europe. In the past, the service was provided by a rental of a Vatican satellite, which nowadays is completely inappropriate due to the obsolete technology and the lack of broadband. When costs and practical issues made this specific satellite connection no more affordable, they started to deliver images through traditional mail express, by storing them in common USB sticks which were occasionally sent in order to be analyzed by Italian Pathologies for receiving a diagnosis.
The sites that have been involved in this program are currently three, reported in the map below:

Lusaka, capital of Zambia

Brazzaville, capital of Congo

Antananarivo, capital of Madagascar.

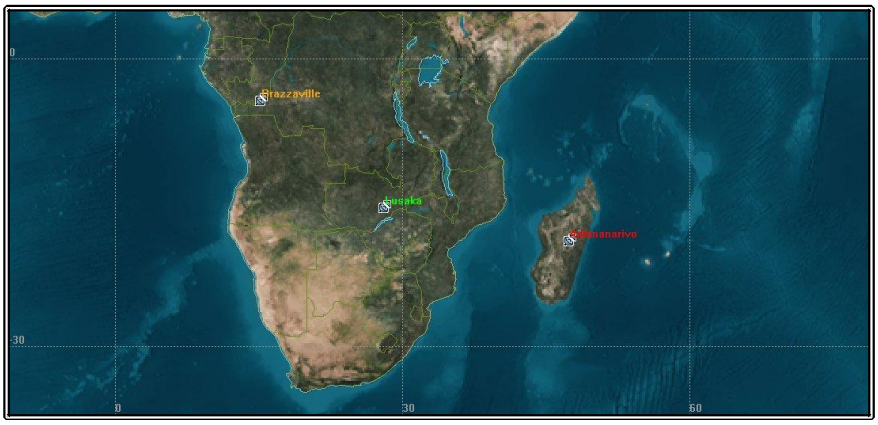

Figure 1.2. Venues of Pathologists activity (2011)

Histological slides are collected and sent from each of the previous sites, but the number of slides varies and it is never the same. It depends on the availability of local specialists to make pap tests and from many other local factors, like local people inclination and culture, villages' accessibility, doctors' availability.

- The goal is to transmit about 20 pictures per week with a minimum cost.
- The digitized images, compressed in formats defined by the scanner technology, need to preserve their high quality.

1.4 Solutions on the market and costs analysis

In order to understand whether a study of an appropriate satellite system dedicated to the specified mission was appropriate or not, a comparison analysis of existing on the market solutions has been carried out.
A first proposal and estimate was asked to Milano Teleport. They offer an innovative product based on the Evolution® X3 Satellite Router by iDirect. The Evolution X3 Satellite Router maximizes the efficiency of satellite capacity to enable new opportunities for star topology networking, thanks to DVB-S2 and Adaptive Coding and Modulation (ACM) on the outbound and deterministic TDMA on the return. The Evolution X3 Satellite Router is an integrated satellite modem and IP router supporting a wide range of carrier IP data rates. Services Price List for the iDirect X3 Evolution platform over the T11N satellite for the African coverage have the following monthly fees:

Table 1.2 Fees for Milano teleport service for different CIRS

CIR Committed Information Rate	**CIR Return [Kbps]**	**Cir Forward [Kbps]**	**Price/Month/Kbps [USD]**
Low CIR	1 – 64	1 - 64	5.40
High CIR	> 64	> 64	5.20

Such a satellite does not cover Madagascar facility yet so the solution is partially comparable.
The average size of a picture is about 4 GB. Applying a compression rate of 1:15 and multiplying times 8 (byte/bit rate), one obtains the size of a picture in Gbits, namely about 2.13 Gbits.
Pathologists enter the server in Africa in order to upload pictures; estimating the time for the picture to be fully visualized in 1 hour, a speed connection of at least 590 Kbps is required.,

With such a rate, the connection's cost for a two years period is estimated to be approximately 70.000 USD in addition to a one-time service start-up cost of 1750 USD for total cost of 71.750 USD.
Another quotation was asked to Skylab. The cost for a transmission of 19 pictures per week, which is 42.6 Gbits/week, was estimated to be about 45000 €.

Considered the commercial service limits in terms of access and costs, it would be interesting to study a satellite system which could offer the same service at lower or equal costs. Among the possible solutions, one could surely be represented by Cubesat systems.

2 Cubesat Solution Overview

2.1 Cubesat Approach

The budgets analyzed above are important financial constraints that made us consider that if a customized system is the best solution to comply to all technical requirements, it also needs to be designed in order to gain the maximum cost saving. Consequently, it is necessary and mandatory to use a small satellite that has less implementation costs as possible.

These satellites, often called picosats, nanosats, or microsats are generally less than 200 kg in weight and, in many cases, are as little as 1 - 5 kg. Such satellites, which range in size from refrigerators to small soda cans, offer many potential benefits over traditional space satellites and provide an amazing alternative to traditional space satellites. Such projects are driven by a "smaller, faster, better, cheaper, smarter" mentality which allows for a fully functioning space satellite to be built in a fraction of the time and cost of a traditional space satellite. Small satellite projects are also able to accept higher risk payloads, allowing for more interesting satellite experiments. Furthermore, as a result of resource limitations, small satellite developers are often forced to experiment with new and innovative designs, techniques, and procedures. One of the driving philosophies of small satellite design is the use of standard, easy to use, COTS (Commercial off-the-shelf) components designed for non-space applications. This allows for fast and inexpensive construction, reducing satellite complexity. The use of standardized platforms and reusable components further shortens the development process. For this reason some brands have been considered in this analysis through all the design, according to reliability and costs.

To both further speed up the development process and aid in obtainment of a launch opportunity, many university small satellite projects choose to follow the Cubesat specification. This standard outlines a set of physical launch interfaces as well as mechanical requirements for a small satellite. According to this specification, a standard Cubesat satellite is a 10 x 10 x 10 cm cube with a weight of one kilogram tops. According to how many cube are assembled, the name varies; the first 3 of an extendable series are reported in Table 2.1.
The limited surface area of a Cubesat restricts the amount of solar power that may be generated, restricting power available for computation, communications, and payloads. Restrictions on space, time, and power necessitate that Cubesat satellites incorporate limited payloads, slow communications links, little redundancy, and minimal information processing capabilities.

Table 2.1. Main standard combination of multiple units

Name	Dimensions [cm]
1 U	10 x 10 x 10
1.5 U	10 x 10 x 15
2 U	10 x 10 x 20
3 U	10 x 10 x 30

The widespread standard and the high demand made a lot of companies be dedicated to the production of these systems. Many providers, have been considered; the main ones are: Cubesatshop, Clyde space, AeroAstro and GomSpace from which the different components have been selected.

2.2 OBISAT

The project that is going to be discussed is namely a Cubesat which has been called Obisat. Obi is the character of a tale, invented by POF, who takes pictures of the symptoms caused by a disease present in his village, and through a "magic" link to the hospital, he manages to save his people life.

This system is foreseen to have higher costs than this on-the-market solution, since even the launch cost itself is approximately 60.000 USD.
Nevertheless it could be possible to use a "piggyback" approach, namely it consists in exploiting an already existing mission letting the launcher bring you to the desired altitude. For example, ESA (European Space Agency) launched in 2007 a space program which allowed to a limited number of Cubesat to be launched on the maiden flight of the Vega launch vehicle. The announcement of opportunity issued by ESA's Education Office in February 2008 offered the possibility of launching up to nine university Cubesats free-of-charge on Europe's newest launcher. Since it has happened once, it could be possible to study special agreements with ESA which could help in saving a part of the launch cost.

Moreover, higher costs could have higher return on investments if one considers extending the scope of such a system to as many sites as possible in Africa, and to as many potential customers who may need the service for private use. Moreover further missions in different locations could be developed due to the whole Africa Obi access expansion. To comply with this larger scope, an alternative solution consisting of a little more complex system has also been designed for utilization by different customers and for different purposes and applications.

It is clear that the rental income can provide consistent revenues, thus increasing profits and getting higher return on investments in a shorter period of time.
As an example of what explained above, Table 2.2 shows the minimal price by month/rate needed to have returns at least on launch costs within the period of service of 24 months, considering the same connection speed rate conditions of 590 Kbps, 4 hours connection a day, 25 days a month for the period of service. It shows also how the elapsed time of returns of launch costs is decreasing as number of customer increases.

Table 2.2. ROI (return on investment) calculation

Price Month/Kbps	Period (months)	hours/day	Kbps	Price/ period	# Customer	Total Price [K]	Launch Cost [K]	ROI Period
$4,7	24	5	590	$66.5	1	$66	$60	0,90
$4,7	24	5	536	$66.5	2	$133	$60.	0,45
$4,7	24	5	536	$66.5	4	$266	$60	0,23

A two year life time is fixed as a target, but other similar Cubesats have been operative for more time than the expected life. CUTE-I a Japanese Cubesat had been operating for more than 5 years [2]. A longer life time would give a big contribution in terms of costs distribution and saving.
The satellite is a typical Cubesat with the exception of the communication block that is an atypical one

2.3 Configuration

Cubesats subsystems normally lay on a printed circuit board, or PCB; which it is used to mechanically support, electrically connect and thermal link electronic components using conductive pathways; it is made of tracks or signal traces etched from copper sheets laminated onto a non-conductive substrate of FR4 composite. The subsystems present on a typical space system are:

- EPS Electric Power System
- TT&C Telemetry, Tracking and Communication Subsystem
- OBDH On board data handling Subsystem
- TCS Thermal Control Subsystem
- ADCS Attitude Determination and Control Subsystem

Every module, mounted on its PCB takes a single slot of 1.5 / 2 cm thickness (as usual from Cubesat standards), with the exception of the communication block

which has particular needs. Figure 2.1 shows both external and internal configurations for the Obisat system.

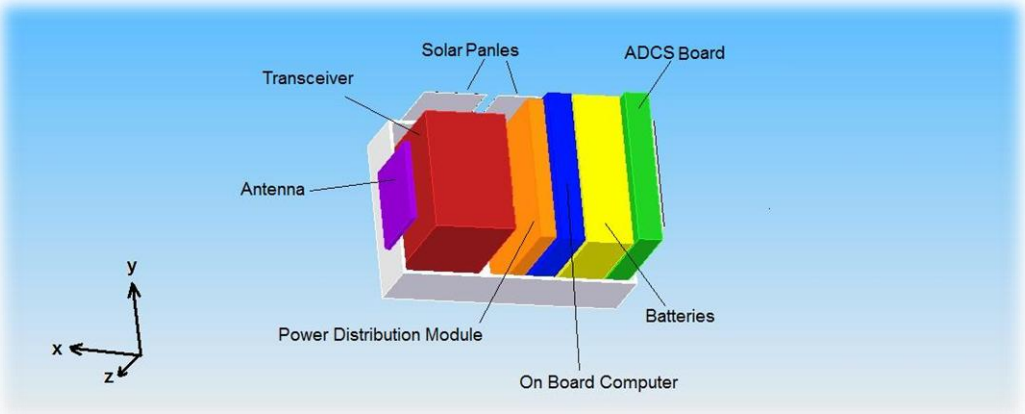

Figure 2.1 Obisat Configuration

The final Obisat design has been achieved and defined after several configurations have been dumped, as all of them resulted not to be the optimal ones for different reasons. The first one analyzed has been a Cubesat 1 U. This system was good until the choice of the Communication block, which with its large dimensions took more slots than the standard one. Due to this constraint, the selected solution has been the 1.5 U Cubesat module.

2.4 Operative Modes

The mission presents three main operative modes:

Downloading phase: every time the satellite gets access to Milan facility to download the stored pictures. It is the most critical one since power consumption and thermal dissipation reach very high level for such a small system.

Uploading phase: it's usually two or three times longer than the first one, it happens every time the satellite passes on the desired African facility.

Stand–by: Obisat is not communicating; it charges its batteries waiting for the next communication phase.

The whole design is mainly driven by the first mode's requirements. This one is more demanding in terms of satellite performance and subsystems' contribution demand.

2.5 Environment

The main features of the environment in a 800 km Leo orbit that have an impact on the Obisat system are listed below:

- Different radiations: Earth Albedo, Earth infrared radiation, Sun ultraviolet radiation and Solar flares
- Ionosphere
- Orbital debris
- Vacuum

Earth

From the Earth the Cubesat is under the Albedo irradiation; Earth Albedo is the fraction of sunlight which is reflected off the planet. The average albedo of the Earth is about 0.3. For short periods it can vary considerably between about 0.05 and 0.6. For albedo radiation, it is assumed the same spectral shape as for sunlit. Besides the reflected energy there is the proper Earth emitted energy, the infrared Earth radiation. For this one a black body spectrum with a characteristic temperature of 288 K is assumed. The average infrared radiation emitted by Earth is 230 W/m^2. On a short time scale it can vary between 150 W/m2 to 350 W/m2. The diurnal variations can amount to about 20 % over desert areas while it is small over oceans. The main source for radiation is of course the Sun. When solar activity is high, ultraviolet and extreme ultraviolet radiation from the Sun heats and expands the Earth's upper atmosphere, increasing atmospheric drag and the orbital decay rate of spacecraft. Solar flares are a major contributor to the overall radiation environment.

Ionosphere

The environment in which the satellite will operate is the Ionosphere, a region of the Exosphere. It sees the presence of Plasma, a partly or wholly ionized gas whose particles exhibit a collective response to magnetic and electric fields. Solar radiation contains sufficient energy at short wavelengths to cause considerable photoionization in the upper atmosphere of the Earth. This process is responsible for maintaining the ionosphere, a partially ionized layer mainly located between 50 and 200 km and extending to an upper boundary of about

2000 km from the surface of the Earth. In the ionosphere, the intense plasma density means there is an ample supply of ions and electrons which tend to neutralize high potential surfaces on spacecraft.
Effects attributed to spacecraft charging can be of serious engineering concern:

- Increased surface contamination
- Physical surface damage
- Operation anomalies

In the following chart, atmosphere density as function of the quote, for low, medium and high sun activity is reported.
For the selected 800 Km Leo orbit with these characteristics, the spacecraft will go through ionosphere including aural zones. This could cause Power leakage, high spacecraft "ground" potential, ram/wake effects, surface charging.
In addiction the particles associated with ionizing radiation, which are categorized in three main groups depending on the source, trapped radiation belt particles, cosmic rays and solar flare particles may cause atomic displacement or may leave streams of charged atoms in the incident particle's wake.

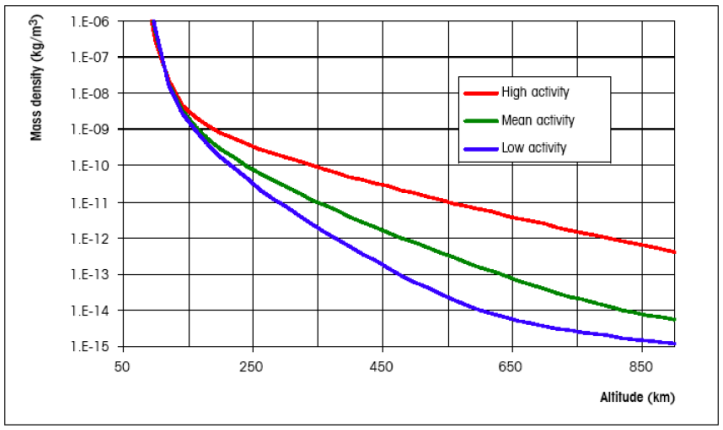

Figure 2.2 Density values as a function of altitude for different solar activitieslevels

Therefore spacecraft damage includes:

- decreased power production by solar arrays
- Failure of sensitive electronics
- increased background noise in sensors

Debris

Due to the high number of orbital debris that populate the LEO orbit, there is a non-negligible chance that a newly launched satellite could be damaged -or even totally destroyed- by one of these roaming fragments.. Therefor an evaluation of the probability of impact needs to be performed
First of all, it is possible to estimate the density of orbital debris for the selected orbital altitude from the graph in Figure 2.3: at an altitude of 800 Km a density of 2.4×10^{-8} objects/Km^3 is foreseen. The next step is to evaluate the probability to incur in a debris impact. For this aim Figure 2.4 is needed.
Choosing for example a 0.01 cm diameter space object one obtains that the approximate number of them to impact a surface of 0.02 m^2 (considering the area given from the product of the diagonal of the top face times the Cubesat's height) is estimated in 0.2 objects in the whole lifetime; that is considered to be a good result in terms of probability of possible impacts.

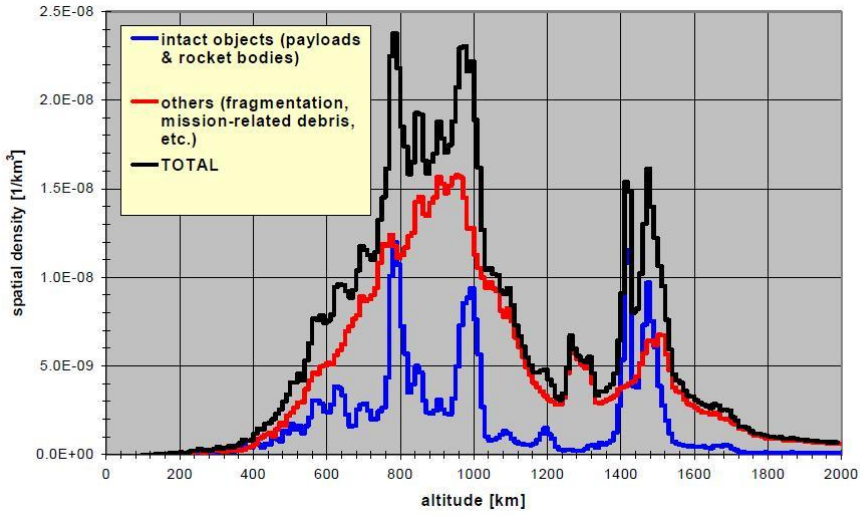

Figure 2.3. The near Earth altitude population [3]

Vacuum

Outer space has very low density and pressure, and is the closest physical approximation of a perfect vacuum.
This factor makes some materials and structures go through a process called outgassing. Outgassing is the release of a gas that was dissolved, trapped, frozen or absorbed in some material. All materials, solid or liquid, have a small vapor pressure, and their outgassing becomes important when the vacuum pressure

falls below this vapor pressure. In man-made systems, outgassing has the same effect as a leak and can limit the achievable vacuum.

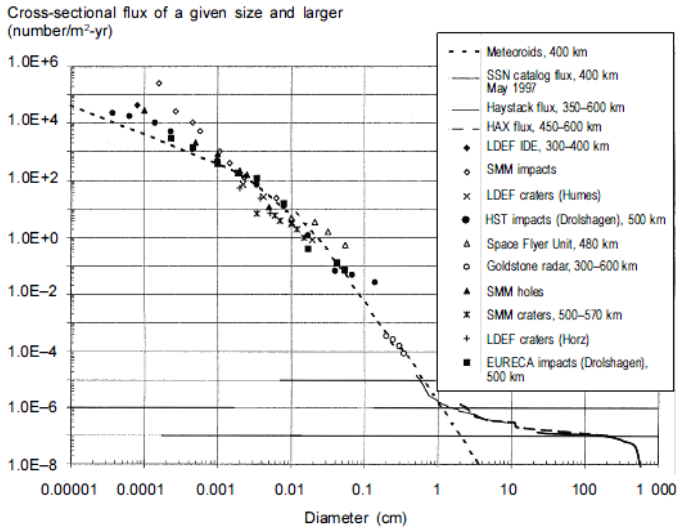

Figure 2.4. Approximate measured debris flux in low Earth orbit,by object size [4]

Outgassing products may condense on nearby colder surfaces, which can be troublesome if they obscure optical instruments or react with other materials.
This is of great concern to space missions, where an obscured telescope or solar cell can ruin an expensive mission. It is a challenge to create and maintain clean high-vacuum environments; therefore NASA and ESA maintain a list of low-outgassing materials to be used for spacecraft. Moisture, sealants, lubricants, and adhesives are the most common sources, but even metals and glasses can release gases from cracks or impurities. The rate of outgassing increases at higher temperatures because the vapor pressure and rate of chemical reaction increases. For most solid materials, the method of manufacture and preparation can reduce the level of outgassing significantly.

3 Mission Analysis

3.1 Mission analysis requirements

The requirements for the mission analysis are strongly dependent on all the others subsystems. The requirements for this mission, resulting from a preliminary analysis of the satellites subsystems, are:

- Orbit altitude < 800 Km because Cubesat products can't overcome this threshold.
- Limited eclipses times, if needed, to maximize power generation
- High access time both for data upload and download.
- No orbit maintenance can be provided
- Lifetime of at least 2 years.

3.2 Orbit trade off

The first step in finding the appropriate orbit for an Earth referenced mission is to determine if a specialized orbit applies. In Table 3.1 a list of the most common specialized orbits used for communication is reported.

The following list of orbits is made of those that do not match Obisat requirements for different reasons:

- Geosynchronous: Apogee out of requirements and too expensive to be reached;
- Molniya: Apogee out of requirements and high costs required
- Repeated Ground Track: Its parameters will be quickly modified because of the action of perturbative forces. Their advantages would be lost.

For the two types of orbits from Table 3.1 which match the mission requirements, a sensitivity analysis has been conducted.
The easiest way to begin the orbit trade process is by assuming a circular orbit and then conducting altitude and inclination trades.

The results come from an analysis conducted in a 2 days period, choosing as uplink time the value averaged on the both days at an altitude of 800 Km. As the

location choice does not interfere with the results, reference data are those uploaded from Antananarivo.

Table 3.1. Specialized Orbits used for Earth-Referenced Missions.

Orbit	Characteristic	Advantages	Disadvantages	Good for Obisat
Geosynchronous	Maintains nearly fixed position over equator	Continuous view of continental Real time communications	High energy needed; very expensive to be reached; No worldwide coverage	No
Molniya	Apogee/Perigee do not rotate	High latitude communications	High energy requirement	No
Frozen/Sun synchronous	It bends together the two following orbit's types.	Stable conditions plus control of the sun direction	Very high apogee	No
Repeated Ground track	Sub satellite track repeats	Repeating viewing angle (marginal)	Restrict choice of altitude Some perturbation stronger	No
Frozen	Minimizes changes in orbit parameters	Guarantee stable conditions	None	Yes
Sun-synchronous	Orbit rotates so as to maintain approximately constant orientation with respect to Sun	Good controllability of solar incoming power	None	Yes

From Table 3.2 one can see that at a consistent difference in the downlink parameters, it does not correspond an equal distance in the uplinks ones. It is due to the fact that in the frozen orbits, communication windows even if more, they keep happening at the same time frames. This makes the increase in terms of times be poor.

Table 3.2. Comparison of performances of Sun-synchronous and frozen orbits per week

Orbit	i [deg]	Downlink time [s]	Uplink time [s]
Frozen	63.4	5320	1976
Sun-synchronous	98.6	4047	1903

Two factors that imply an increase in power demand to the EPS system are here listed:

- The increase of downlink time implies two connections of about 300 s each, during two consecutive orbits. It results in a rise of power demand to the power subsystem.
- The lack of RAAN variation stability would result in a rotation of the line of ascending node, causing a consistent time to be spent in eclipse.

The combination of these factors makes the power demand to solar arrays be 4.6W, while their production is estimated in 4W. This system could therefore not be sustained by the power subsystem.

The case of the frozen orbits applies to all those orbits whose inclination is different from the sun synchronous one.
The results show that, unless an increase of the power system performances were thought, an inclination which makes the orbit be sun synchronous is mandatory.

A trade off can be conducted for different altitudes; basing the calculations on a sun synchronous orbit model, and taking as reference parameter the downlink time, results give (Table 3.3)

Table 3.3. Orbit altitude VS connection time, per week.

Altitude [Km]	Downlink connection [s]
400	2992
600	3650
800	4047

As foreseeable, the higher the orbit, the longer is the access time.
Having worked the problem assuming a circular orbit, the potential advantages of using eccentric orbits should also be assessed. These orbits have a greater peak altitude for a given amount of energy, lower velocity at apogee than is possible, which makes more time available there. Unfortunately, eccentric orbits have a difficulty; because the oblateness of the Earth causes perturbations which cause the perigee rotate rapidly. The first order rotation of perigee is proportional to $2 - 2.5 \sin^2 i$ which equals zero at an inclination, i = 63.4 deg. This is again the case of the frozen orbits for which no possible use is foreseen.

The choice of a sun-synchronous orbit is also useful to keep Obisat under certain constant ranges of sun visibility and ground access. The inclination value comes from the following equation:

$$\dot{\bar{\Omega}} = -\frac{3}{2}\frac{\sqrt{\mu}}{\sqrt{a^7}} J_2 \frac{R_T^2}{(1-e^2)^2} \cos i = \dot{\bar{\Omega}}_{Earth} \qquad (3.1)$$

This comes from the exploitation the J2 perturbation factor which, with the proper inclination, makes the orbit plane to rotate with the same revolution speed of the Earth.

Figure 3.1 reports the necessary values that inclination has to have, for a sun-synchronous orbit VS orbit's altitude:

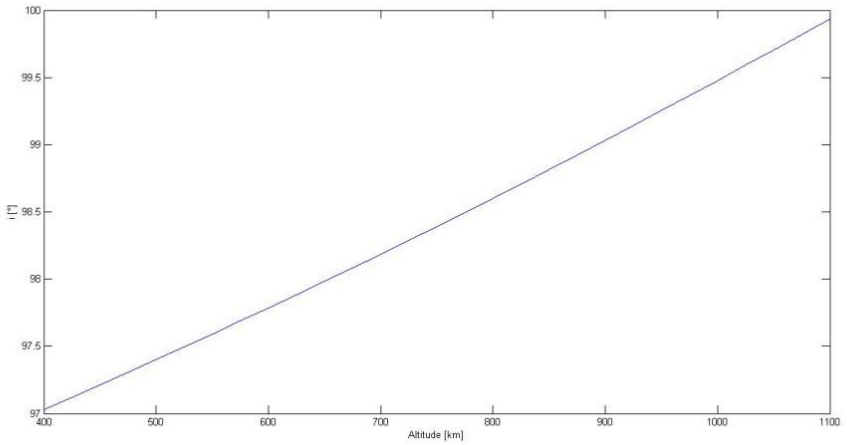

Figure 3.1. Sun synchronous orbits: inclination value VS function of altitude .

In fact, exploiting the J2 perturbation factor it is possible to make the orbit plane to rotate with the same speed of the Earth in its revolution motion around the Sun.
Special consideration needs to be paid to both thermal and power subsystems; eclipses are useful in terms of panels' temperatures; by lowering them, they help to increase the power income. So the RAAN choice has, as a main driver, the power generation requirement bent to the need to hold temperatures down. After a thermal simulation joint to the power gathering one, it was found out that no eclipse is necessary for thermal ranges; full visibility is moreover required to collect the necessary amount of energy. Thus, considering the initial date be the 25th of July 2025 from the right ascension of the Sun in this day and from the need to have a down dusk orbit, the RAAN is fixed in 214 deg. The ascending node line is therefore perpendicular to the sun vector avoiding thus the occurrence of eclipses' phases (except for the short one of about 1086 s maximum, occurring in the solstice summer period).

Table 3.4. Orbital Keplerian Parameters

Element	Value
a	7178 Km
e	0
i	98.6°
Ω	214°
ω	indefinite

Being *a* the semi major axis, *e* the eccentricity, *ω* the argument of perigee (indefinite as the orbit is circular), *i* the inclination, and *Ω* the right ascension of the ascending node.

3.3 Perturbation Analysis

Since no active control will be applied to the Obisat orbit, a detailed analysis of the acting forces has to be developed, as perturbations need to be put under control. One way to achieve such a goal is to choose a sun-synchronous orbit. This implies that the satellite will rotate of about 1° per day. Not only it will help the power system, which will be set under the same condition through all its lifetime, but also it will avoid undesired rotations of the RAAN and Latitude of perigee parameters. Two different kinds of analysis have been carried out: one in a short temporal window and the second in a longer one through all the satellite's life time.

First of all it is necessary to analyze the disturbing forces, their entities and where they come from; thus, the main perturbation causes are briefly discussed, with a quick look on the used equations for the model, They will be presented as perturbing accelerations in the 3 directions *r*, *t* and *h*: respectively the component along the radius vector outwards, the one perpendicular to the radius vector in the direction of motion and the component normal to the orbital plane in the direction of the angular momentum.

Simulation's results are shown for both 1 orbit and for the whole lifetime.

Atmospheric drag:

The acceleration due to this influence is not particular high. Nevertheless with this component in the direction of motion it changes the semi-major axis of the orbit. This will lead to a progressive orbit decrease until Obisat will burn with the impact with the atmosphere. Time to collapse has been calculated with the STK model and it is esteemed in about 250 years. A disposal procedure needs to be investigated. The atmospheric drag is given by:

$$a_{atm} = \frac{1}{2m}\rho A v^2 C_D \tag{3.2}$$

where C_D is estimated to be 3, A is the maximum area of the body which is perpendicular to the motion which can be 0.15m x 0.15m tops, v is the body velocity relative to the atmosphere [5]

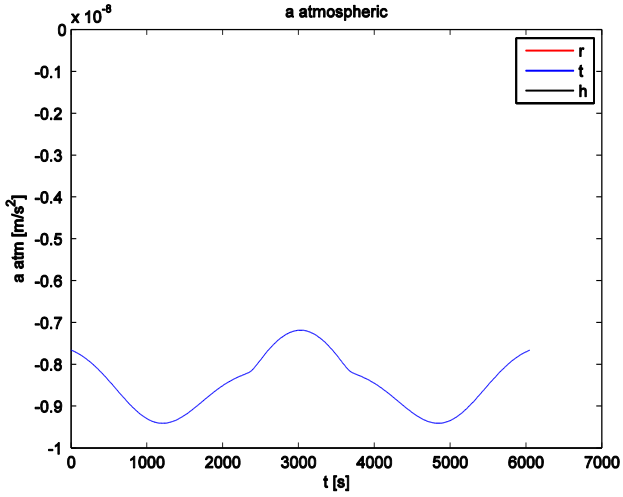

Figure 3.2. Atmospheric drag perturbation

Sun and Earth radiation:

This effect is caused by the reflection of electrical particles present in direct Sun radiation and in that part reflected by the Earth (albedo). It, like the atmospheric one, has an important impact when acting on large surfaces. Since our satellite is small with limited exposed area, it has not relevant effects. Its expression is given by equation (3.3) [6]:

$$\underline{F} = -AP\left[(1-c_s)\hat{S} + 2\left(c_s\cos\theta + \frac{1}{3}c_d\right)\hat{N}\right]\cos\theta \qquad (3.3)$$

With $P = \frac{P_{sun}}{c}$ where P_{sun} = 1367 W/m^2 it is the sun power per unitary surface at 1 AU and c is the light speed. *cs* and *cd* are respectively 0.12 and 0.08 [7]. Θ is the angle between the sun vector $\hat{S}$ and each surface normal $\hat{N}$.

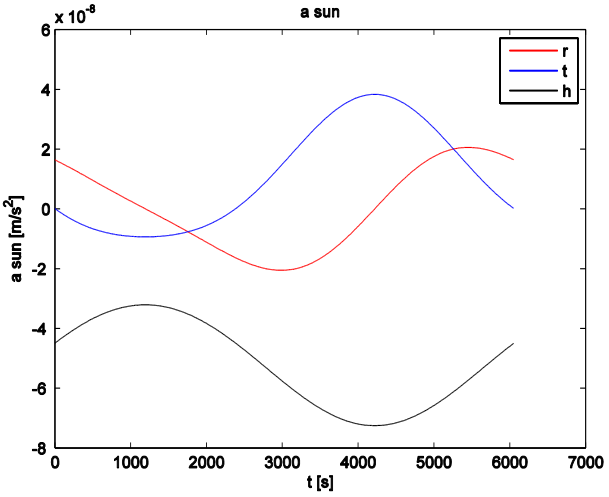

Figure 3.3. Sun perturbation

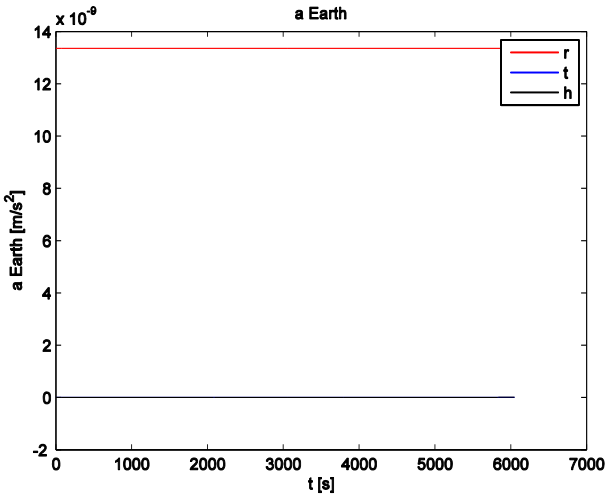

Figure 3.4. Earth Albedo perturbation

Third body effect:

When computing orbital dynamics, only 2 contributions are considered: the main attractor and the attracted body. Other presences which naturally influence the satellite motion are treated as perturbations and are here discussed. In particular the perturbing accelerations inducted by the Sun and Moon will be treated. The equation used to model this acceleration is [5]:

$$a_{3B} = \mu_m \left(\frac{r_{mS} - r}{r_m^3} - \frac{r_{mS}}{r_{mS}^3} \right) + \mu_\odot \left(\frac{r_{\odot S} - r}{r_\odot^3} - \frac{r_{\odot S}}{r_{\odot S}^3} \right) \quad (3.4)$$

Where the $\odot$ symbol stands for Sun, m for Moon and S for Satellite, r is the distance from the center of the Earth to the considered body and μ is the gravitational parameter. Thus one obtains:

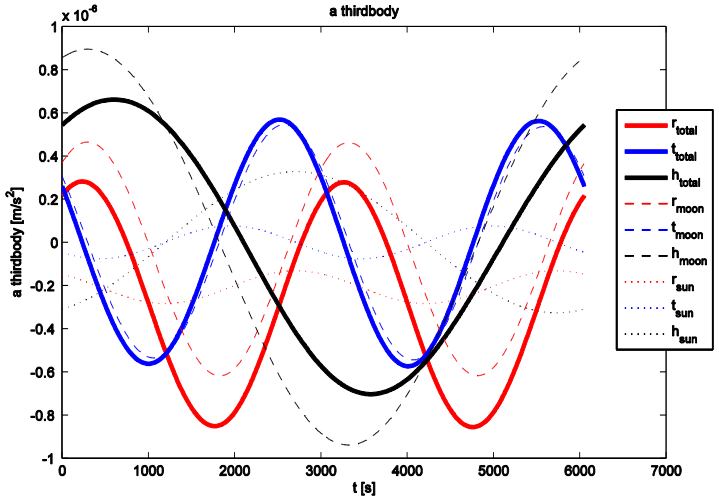

Equation 3.5. Third body perturbation: Moon and Sun influence

Earth oblateness effect:

One of the most impacting perturbations in near Earth satellites' orbits, it's the non-spherical distribution of mass inside the Earth and its not uniform density, hypotheses requested by a Keplerian model. The equipotential surfaces of the gravitational field are not spheres but more ellipsoids with many irregularities. Through the definition of the geoid potential, and its associated Legendre polynomials and constants it is possible to calculate the effect of such a mass distribution on an orbiting satellite. The most influent action is given by the biggest (the first) of the coefficients, also called zonal harmonics, whose value is J2 = 2.08 x 10^{-3}. The inducted acceleration is given by [5]:

$$a_{J2} = -\mu_\oplus J_2 R^2 \frac{3}{r^4} \left[\left(\frac{1}{2} - \frac{3}{2} \sin^2 i \, sin^2 u \right) \hat{\imath}_R + sin^2 i \, sin u \cos u \, \hat{\imath}_T + \cos i \sin i \sin u \, \hat{\imath}_N \right] \quad (3.6)$$

With the proper inclination, it causes the rotation of the line of the ascending node, as desired. The acceleration caused is:

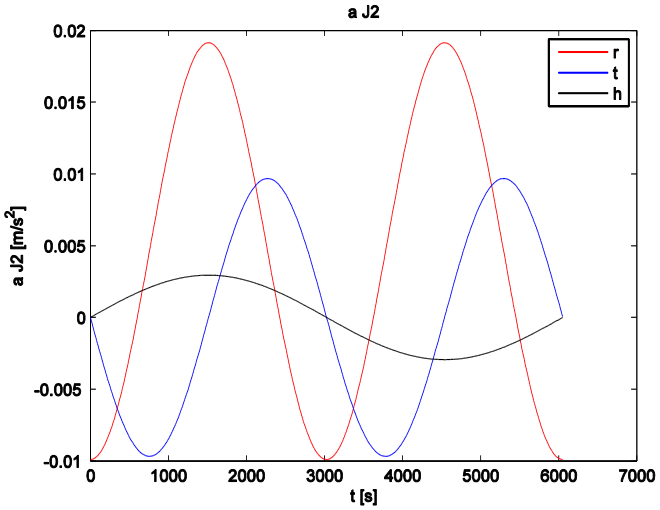

Figure 3.5. Perturbation from J2

The sum of all the single perturbations is shown in Figure 3.6.
From a computational point of view, it has been used the integration of the orbital parameters' derivative. Since the initial orbit is a circular one, the use of keplerian elements would cause singularities in all those elements' derivatives, as ω or ν in which the eccentricity value stands at denominator. For this reason a set of Modified Equinoctical Elements has been introduced.
Main schemes of orbital elements which avoid these difficulties have been developed, ranging from standard transformations applied to general canonical elements (Kaula, 1966), to specific sets of elements (e.g. Broucke and Cefola 1972; Giacaglia 1977). It is generally advisable to employ elements which are not too far removed from the classical ones; then transforming and interpreting them in terms of physically significant parameters is relatively easy.

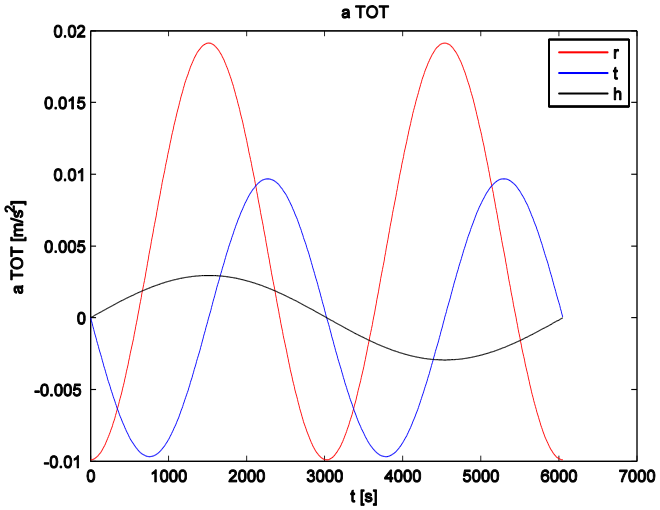

Figure 3.6. Total Perturbation

To this end, Cefola and his co-workers have made a good case for the use of Equinoctical Orbit Elements. For some purposes it is desirable to employ a "fast variable" (phase angle) as the sixth "element". In particular, the Stroboscopic Method (Roth 1979) assumes such a formulation, so that a regular perturbation technique can be used with the fast variable as independent variable. In such a case, it is natural to modify the Equinoctical Elements by choosing the true longitude L as the element fixing position in the orbit. Further by replacing the semi-major axis "a" by semi-latus rectum "p", a set of orbit elements of the prescribed form is obtained, which is applicable to all the orbits, and have non-singular equations of motion (excluding the case i=π). Modified Equinoctical Elements are thus (this follows European Space Agency Notation):

$$p = a(1 - e^2)$$

$$f = \mathrm{e}\cos(\omega + \Omega)$$

$$g = \mathrm{e}\sin(\omega + \Omega)$$

$$h = \tan\frac{i}{2}\cos\Omega$$

$$k = \tan\frac{i}{2}sin\Omega$$

$$L = \Omega + \omega + \nu$$

(3.7) Equinoctical Orbital Elements

Where *v* is the true anomaly.
Considering $\alpha_{i,}$ with i = 1 to 6, a set of orbit elements which, together with t, uniquely fix position and velocity of a satellite relative to a fixed Cartesian frame having the center of attraction as origin, a perturbative acceleration can be expressed as the gradient of a disturbing function R = R(x). Then

$$[\alpha_j, \alpha_i] \frac{d\alpha_j}{dt} = \frac{\partial R}{\partial x_i} \frac{\partial x_i}{\partial \alpha_j} = \frac{\partial \tilde{R}}{\partial \alpha_j} \tag{3.8}$$

Where $[\alpha_j, \alpha_i]$ is a Lagrangian bracket, and $\tilde{R}$ is the disturbing function expressed in terms of α and t. Inverting equation (3.8), it gives the equation of motion

$$\frac{d\alpha_i}{dt} = (\alpha_j, \alpha_i) \frac{\partial \tilde{R}}{\partial \alpha_j} \tag{3.9}$$

Where (α_j, α_i) is a Poisson bracket. So derived, these equations of motion are unique. Nevertheless, the right hand side can be expressed in many equivalent forms. R indeed is independent of velocity ẋ, and hence $\tilde{R}$ always satisfies three identities:

$$\frac{\partial \tilde{R}}{\partial \alpha_j} \frac{\partial \alpha_j}{\partial x_i} = 0 \tag{3.10}$$

Adding multiples of the left-hand sides of $\frac{\partial \tilde{R}}{\partial \alpha_j} \frac{\partial \alpha_j}{\partial x_i} = 0$ into the right-hand side of

$$\frac{d\alpha_i}{dt} = (\alpha_j, \alpha_i) \frac{\partial \tilde{R}}{\partial \alpha_j}, \tag{3.11}$$

many different forms of the equation may be generated [8].
This freedom does not exist in the Gaussian form, where the perturbative forces are uniquely defined. By differentiating equations (3.7) with respect to time, the derivatives of the modified equinoctial elements can be found in terms of classical ones (see equations (3.12)).
The results obtained from the simulation demonstrate that no significant changes occur for eccentricity, inclination and latitude of the perigee; a slight decrease of the semi-major axis is foreseen after 2 years and finally the RAAN variation is like expected.
The study has been simulated in the Simulink environment, for a whole lifetime of 2 years.

$$\frac{dp}{dt} = \frac{2pc}{w}\sqrt{\frac{p}{\mu}}$$

$$\frac{df}{dt} = \sqrt{\frac{p}{\mu}}\left\{S\sin L + \frac{[(w+1)\cos L + f]C}{w} - \frac{g(h\sin L - k\cos L)N}{w}\right\}$$

$$\frac{dg}{dt} = \sqrt{\frac{p}{\mu}}\left\{-S\sin L + \frac{[(w+1)\cos L + f]C}{w} - \frac{f(h\sin L - k\cos L)N}{w}\right\}$$

$$\frac{dh}{dt} = \frac{s^2 N}{2w}\sqrt{\frac{p}{\mu}}\cos L$$

$$\frac{dk}{dt} = \frac{s^2 N}{2w}\sqrt{\frac{p}{\mu}}\sin L$$

$$\frac{dL}{dt} = \sqrt{\mu p}\left(\frac{w}{p}\right)^2 + \sqrt{\frac{p}{\mu}}\frac{(h\sin L - k\cos L)N}{w}$$

(3.12) Derivatives of the EOE

Where $w = \frac{p}{r} = 1 + f\cos L + g\sin L$ and $s^2 = 1+h^2+k^2$

C, *S*, *N* are the components of the perturbing acceleration in the directions perpendicular to the radius vector in the direction of motion, along the radius vector outwards, and normal to the orbital plane in the direction of the angular momentum vector.

In the next figures from 3.7 to 3.10 there are shown the result in terms of keplerian parameters' changes both for an orbit period and for the whole lifetime.

Orbital perturbations generate no particular issues for this satellite. The altitude at the end of life will be slightly reduced; this would cause a negligible change in the number of bits exchanged, shown in Table 3.5

Table 3.5. Degradation in communication parameters due to the semi major axis' decrease

Altitude	MBits downloaded per week	N. of pictures
800 Km	4047	19
750 Km	3888	18

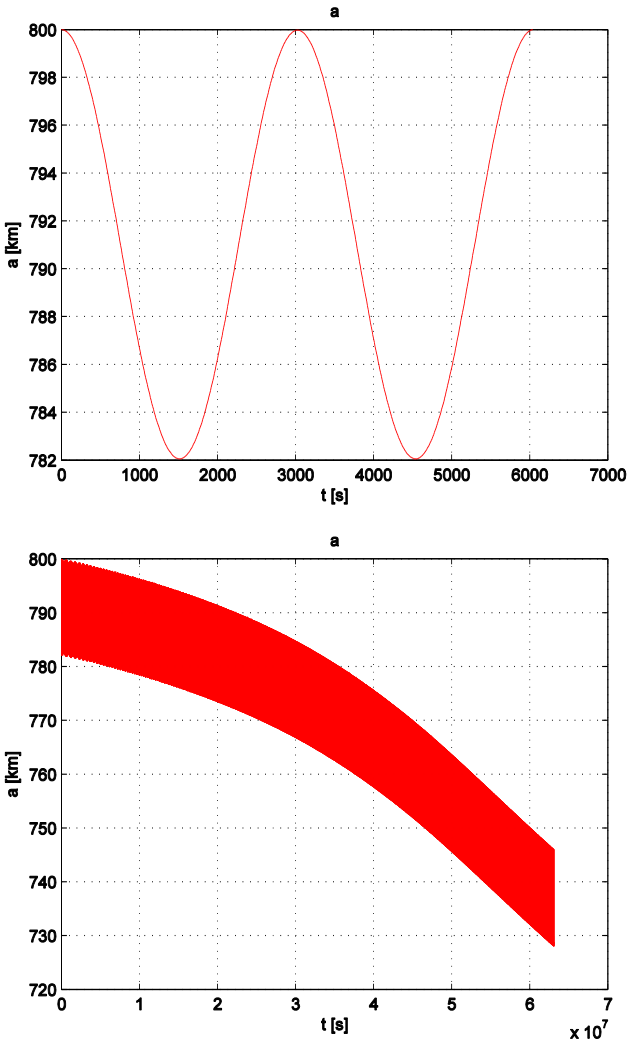

Figure 3.7 Orbital and secular variations of the semi major axis

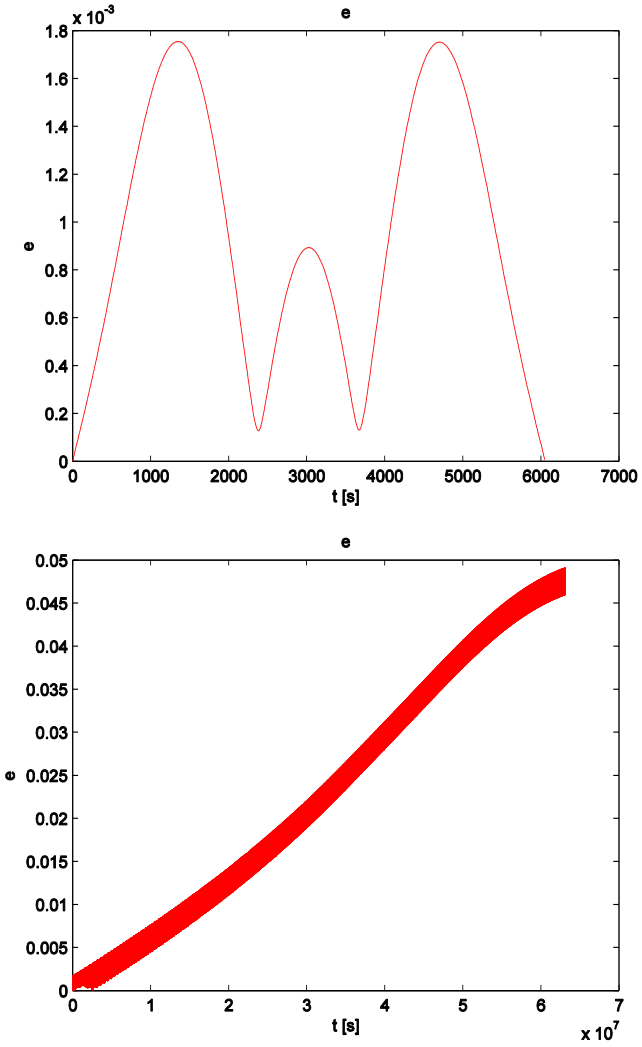

Figure 3.8 Orbital and secular variations of the eccentricity

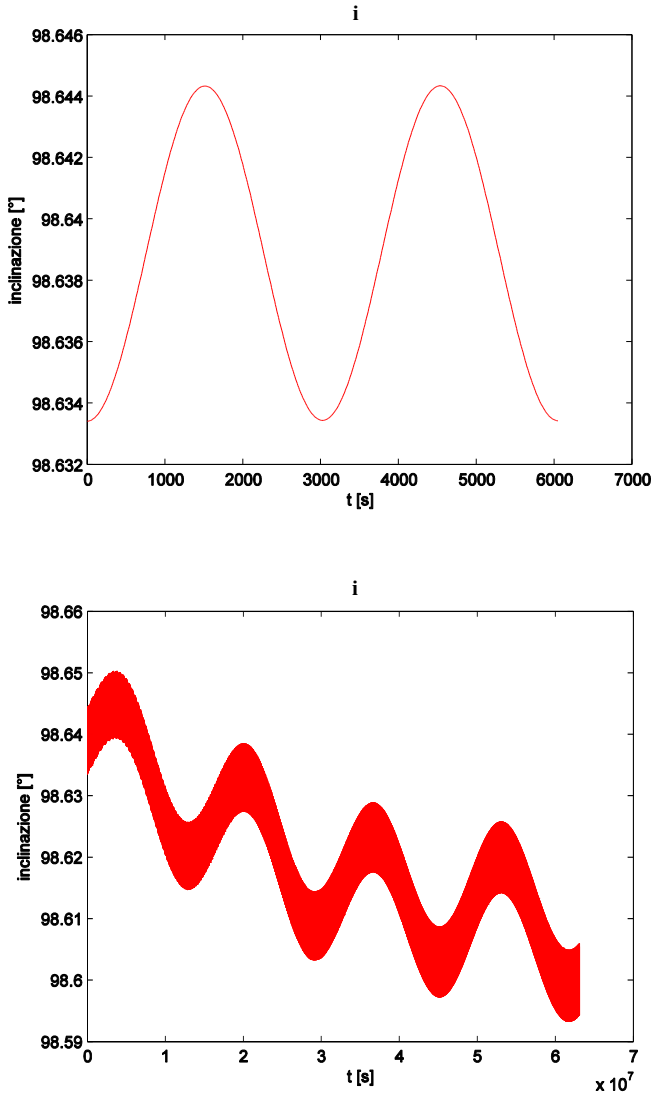

Figure 3.9 Orbital and secular variations of the inclination

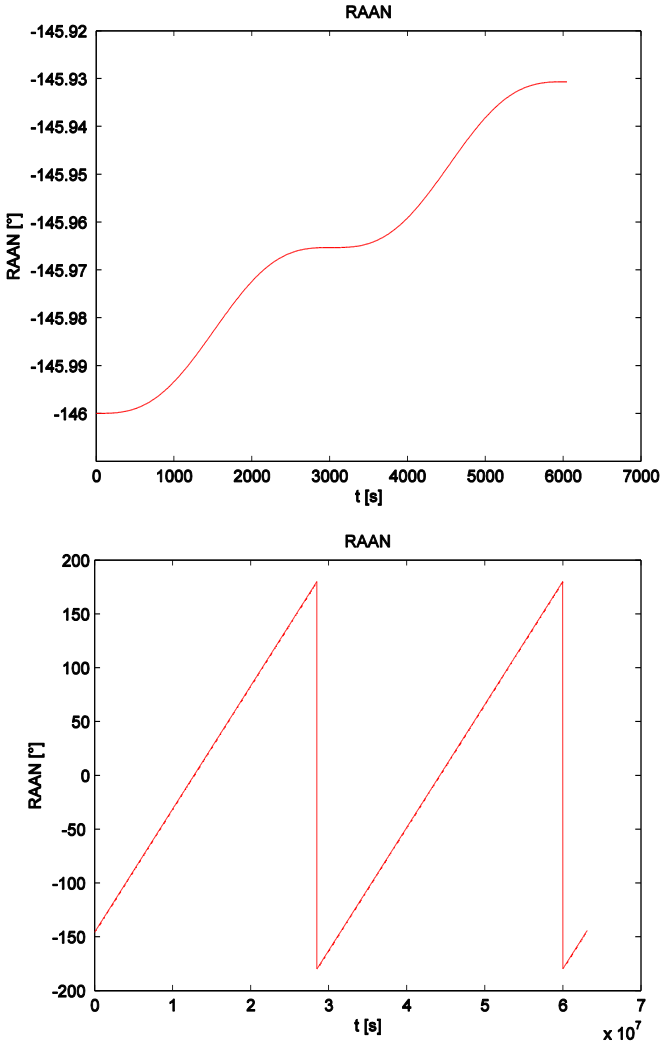

Figure 3.10 Orbital and secular variations of the RAAN

Eccentricity is nominally 0, implying the lack of definition for the argument of perigee. Inclination is maintained around its initial value while the RAAN has the desired trend. It performs a full turnaround per year.

4 Telemetry, Tracking and Communication Subsystem

The primary goal of the communication subsystem is to provide a link to relay data and send commands to and from the Cubesat. Telemetry and command subsystems will ensure communication between the ground stations and Obisat after separation from the launcher.

4.1 Subsystem requirements

The most important requirements of this subsystem are:

- To send at least about 20 images from Africa to Milan per week;
- COTS products have to be preferred in order to reduce costs and manufacturing times.
- Reliability in order to guarantee a minimum life time of 2 years.
- An Operational requirement is set on frequency choices: amateur frequency slots should be used if possible.
- A performance requirement is set on noise margins: a link margin of at least 5 dβ has to be achieved.
- Data stored can't overcome the memory size, namely 16 GB

4.2 Subsystem design

The sizing of the Communication subsystem has been defined based on the downloading segment, since the uploading from African stations requires only 1/3 of the downloading data rate and it is less impactful to the overall satellite subsystems.

4.2.1 Frequency and data rate selection

The main driver of frequency selection is the bandwidth available for each frequency slot. Nowadays the maximum typical frequency band available for Cubesats is the S band. Figure shows the different link phases.
An increase in frequency implies an increase in terms of power required for transmission, as they are directly proportional to each other.

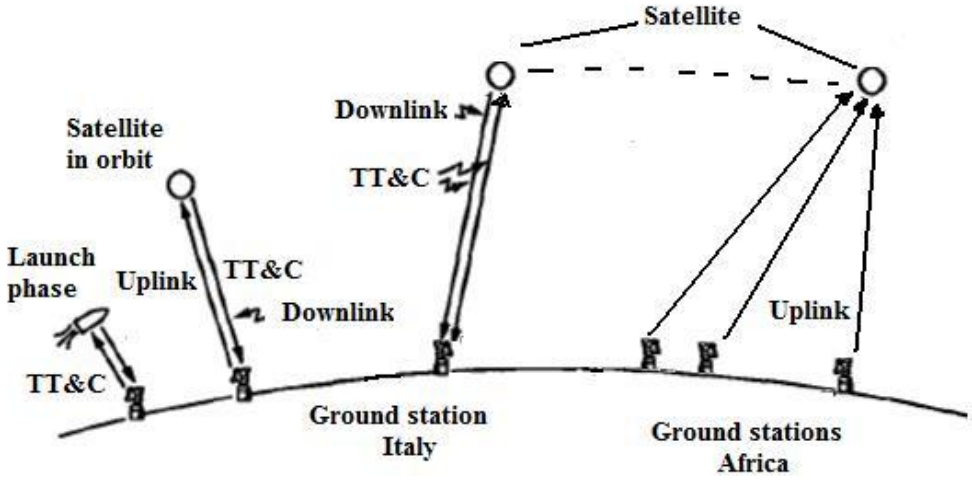

Figure 4.1. Communication architecture: Satellite and Ground stations interconnected with Communication links

Going through an integrated analysis between power and communication, and, at the same time, analyzing on-the-market transmitter-receiver systems, it results that no frequency exceeding the S band could be afforded even for Obisat. Indeed higher bands imply higher frequency components that are larger and heavier than the ones used for lower frequencies. The minimal frequency threshold for the choice is driven by the needed bandwidth. The narrower is the bandwidth, the lower is the frequency, and the lower is the power consumption. For this reason, since images are large and the orbit is not geosynchronous, a narrower bandwidth can be obtained improving the connection performance at the best affordable level so to guarantee an efficient transmission at the lower possible frequency. The analysis of the bandwidth is strictly connected to the data rate values

A sensitivity analysis has shown that even if a lower data rate gives higher access time, the best performance in terms of data exchanged is achieved letting the data rate be as high as possible. The analysis has been carried on with Simulink with constraints in terms of BER and Eb/No.
Ground antenna dimensions which, considering easy availability of ground components, is chosen large enough to let the space segment be as much compact and small as possible, has a diameter of 2.3m.

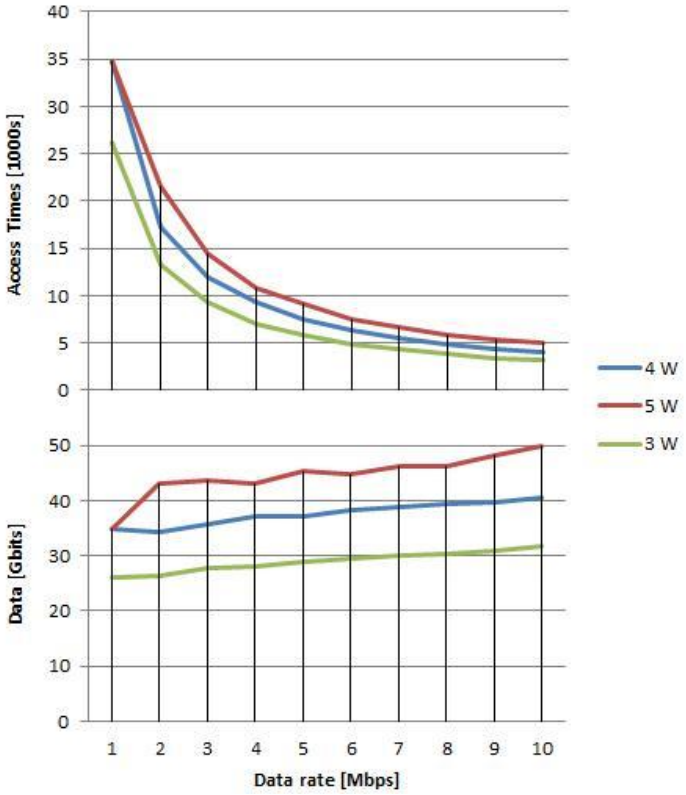

Figure 4.2. Data and access times VS Data Rate for different power values

Figure 4.2. Data and access times VS Data Rate for different power values shows the dependency of the exchanged data to the data rate for three different values of output power, namely 5, 4, and 3 W. The value of 5 Watt is the maximum RF output power that compact transmitters can afford. Unfortunately, due to power constraints of the EPS system, the peak manageable power level for Cubesat, is nowadays 30 W. The RF power of 5 W means an amplifier input power demand of more than 30 W, unfeasible for the system.

For the same technologies limitations reason, data rate threshold cannot exceed 10 Mbps, as standard items use data rates in the range of Kbitps [9].

Using a RF power of 4 W, the maximum number of images transmitted, (266 MB each one), is 19 per week. Due to the reduced system possibilities, this value is considered enough. From system From system possibilities arises a constrain on the available power, therefore a relaxation in the number of images requirement has been introduced.

These considerations led us to choose specific items not properly designed for Cubesats, but this project proves that if used, they can fit and comply with Cubesat requirements.
In addition to data rate and out power selection, the frequency needs to be selected in order to be compliant to AMSAT regulations.
The frequency alternatives listed in Table 3.1 are Exclusive Amateur Satellite Band in the official frequency scheme, internationally allocated. A subset of the entire table of the free amateur frequencies is here reported [10]:

Table 4.1. Amateur frequency slots

International amateur satellite frequency allocations				
Range	Band	Letter	Allocation	Notes
VHF	2 m	V	144.000 MHz - 146.000 MHz	
	70 cm	U	435.000 MHz - 438.000 MHz	
UHF	23 cm	L	1.260 GHz - 1.270 GHz	Only uplinks
	13 cm	S	2.400 GHz - 2.450 GHz	
SHF	9 cm	S2	3.400 GHz - 3.410 GHz	

The major drawback of these bands is that they have no protection and transmit considerable noise and interference which occurs especially in urban areas.

Table 4.2. VHF VS S bands: Pros and Cons

Band	**Pros**	**Cons**
VHF	Better use of available band Simpler ground system, Yagi antenna possible Lower power required in Tx Low cost antenna on board	Pathologies already have an antenna system for higher frequencies Since it would fit just the uploading, two antennas would be necessary
S	Antenna's dimensions are reduced Same antenna used both for up and downloading	More power required in Tx

Nevertheless, these frequencies may be used also if the ground station is located in sites where interference from these short-range applications would not be a problem.

The simulations made shows that using the VHF band it implies the use of Yagi antennas, for their higher gain compare to the Mono/Dipole ones. Still it would not be enough to guarantee communication. STK simulations show that no data could be transmitted, due to the low gain of both on board and ground antennas. Thus, the utilization of S band, 2400-2450 GHz, is the right choice. It allows a compact and smart patched antenna which will be later discussed coupled with a parabolic ground antenna which let us have much higher gain instead of the previous one. Table 4.2 lists all PROs and CONS of the different bandwidth analyzed, showing that S Band is the only solution to our requirements.

4.2.2 Modulation and coding

Modulation is the process by which an input signal varies the characteristics of a radio frequency carrier. Phase or frequency modulations are preferred because the transmitter can operate at saturation for maximum power efficiency. The chosen modulation technique and the respective encoding depend on the used transmitter. A basic choice in terms of power saving, BER performance and system simplicity is a BPSK modulation. Due to the complexity of coding techniques and relative hardware, it has been chosen to keep the signal uncoded. Coding would require in fact wider bandwidth and more complex systems, but it would increase the access time by a release on Eb/No constraints. However an analysis with modulation and coding sensitivity has been carried on to point out the differences in terms of access times, always considering a ground antenna of 2.3m and a RF power of 4 W [11]:

Table 4.3. Possible Modulation Types at a Data rate of 10Mbps

Modulation	Eb/No for BER = 10^{-5} (dβ)	Spectrum utilization	Pros	Cons	RF Power [W]	Access Time
BPSK	9.6	1	Good BER performance	Susceptible to phase disturbances	4	4047
BPSK Plus R-1/2 Viterbi Decoding	4.4	0.5	Excellent BER performance	Higher complexity. Reduced use of spectrum	4 3	11357 8843

These frequency locations are mostly suitable for special applications like alarm and security systems, horn automation, remote control, surveillance, toys and remote keyless entry.
Actually, an increase in access time if it is positive on one side, on the other side it would determine an increase in power demand which wouldn't be supported by the power system..
A lower value of RF power has also been simulated:
RF 3 W: if no encoding technique is used the downloading access time is 3165 s per week; using the Viterbi encoding it is 8843 s, which considering the occupation of the frequency spectrum, namely double, it is comparable to the 4 W case, without decoding. This would release the peak power on the EPS system, since Transmitter block would use about 20W, but it would be demanded for a longer time.
Unfortunately EPS cannot sustain such a long time of communication activity even if at lower average power. In fact results give:
Power required is 4.2 W while PSA (Power from Solar Arrays) is 4.05 W.
Based on these calculations and considering the good performance the system can achieve also without any coding, no coding is provided for the link. It makes the system simpler and less impacting on EPS subsystem.

4.3 Analysis of access times and Results

The value of access time computed for the Downloading mode is 4047 s of communication window per week. Namely it has a mean value of 255 s per access with a variance of 22 %.
Multiplying the access time times the data rate, dividing by 8 (number of bits per byte) and again by 15 (compression rate) the maximum number of images exchanged during a week is obtained, namely 19 pictures. Calculations are shown in Table 4.4.
The obtained results show that:

- To send at least 19 images per week, it is needed:
  A transmitter with at least 4 W of RF power, in a S frequency band at a data rate of about 10 Mbps;
  A receiver which can afford data rates up to 1 Mbps;
  No special requests in terms of coding;
  A dish ground antenna of at least 2.3 m diameter for downloading and 1.8 m diameter for uploading;
- To send more images, up to 30 per week, there is the possibility to consider a second configuration, which counts a 3m ground antenna with a Viterbi coding. The longer access time would require though a different sizing in

terms of power and thermal subsystems, which could be achieved with a configuration which takes in consideration deployable solar panels for an increase of the Psa.

Table 4.4. Results for Downlink: Data rate Vs. RF Power

RF Power [W]	**5**	**4**	**3**	**5**	**4**	**3**	**5**	**4**	**3**
R [Mbps]	**Access Times [s]**			**Data [Mbits]**			**N. of pictures**		
1	34732	34732	26159	34732	34732	26159	16	16	12
2	21522	17172	13225	43044	34344	26450	20	16	12
3	14510	11922	9279	43530	35766	27837	20	17	13
4	10796	9279	7009	43184	37116	28036	20	17	13
5	9068	7409	5796	45340	37045	28980	21	17	14
6	7457	6370	4922	44742	38220	29532	21	18	14
7	6618	5532	4296	46326	38724	30072	22	18	14
8	5783	4922	3804	46264	39376	30432	22	18	14
9	5367	4418	3432	48303	39762	30888	23	19	14
10	4987	**4047**	3159	49870	**40470**	31590	23	**19**	15

Table 4.5. Used downlink parameters

Parameter	**Value**
Analysis Period	1 week
Frequency	2,4 Ghz
Eb/N_0	9,6 DB
Link margin	5 DB
Ground Antenna diameter	2,3 m
Obisat Antenna gain	6 DB
RF power	4 W

4.1 Uplink

The uploading phase consists in the transmission of images from Africa to Obisat. The volume of data transmitted during upload must not exceed the one during download phase. An uncontrolled accumulate of data could bring the system to a memory congestion.
The variables to work on in order to design the correct communication system are: the RF power, data rate and diameter of the ground antenna.
The most critical one is the data rate. The maximum access window, for a 10-5 BER and a link margin of 5 dB on the 9.4 dB required, is 3843 s per day for each facility, but as soon as the data rate increases, the access window quickly decreases. In fact the following formula shows the influence of the data rate on the overall link:

$$\frac{E_b}{N_0} = \frac{P_{Tx} L G_{Tx} G_{Rx}}{k T_s R} \tag{4.1}$$

Where *P* is the emitted power, *L* the losses, *G* the gains, *K* the Boltzmann's constant, *R* the data rate, T_s the noise temperature and Eb/N_0 the ratio of received energy-per-bit to noise ratio.
As R increases the value of Eb/N_0 decreases, and as it is one of the constraints applied in the STK simulation, the access window shrinks.

The philosophy that has been followed is that of selecting an average amount of data to be transmitted and, keeping this constant, to point out the best combination of the previous variables to optimize the system. Obviously, the data sent by each facility will never be the same, as they depend indeed from many different local factors. Since this orbit cannot be a repeated ground track one, the times of visibility and access will be different for every passage. A proper design should be an algorithm which has as input the data to be sent from each venue, and through an orbital propagation, it gives as output the needed connection slots from each venue in the same connection window. Figure 4.3 shows a typical connection window. The center connection slot is shared by the all three African venues.
In this phase of the project, it is not possible to divide connections among the different places according their needs, thus, considering that it is possible to adjust times to reach the desired amount of data , an equal value is here considered for the all three places.
Being the downloading data per week 40470 Mbits that is 5780 Mbits per day, it is necessary that the amount of data to be uploaded is about the same (considering all telemetry data really minor than the payload ones). Thus, dividing the total upload volume by three (that is the total number of sites), the

maximum volume of data by each facility in Africa is 1930 Mbits maximum per day.

The run simulation takes into account:

- Data rate [from 0.6 to 1 Mbps]
- Ground Antenna Diameter [from 1 to 2.3 m]
- RF Power [10, 15, 20, W]
- Fixed amount of sent data: 1930 Mbits

Figure 4.3. Typical uploading connection window (3 orbits)

Results are represented in Figure 4.4:

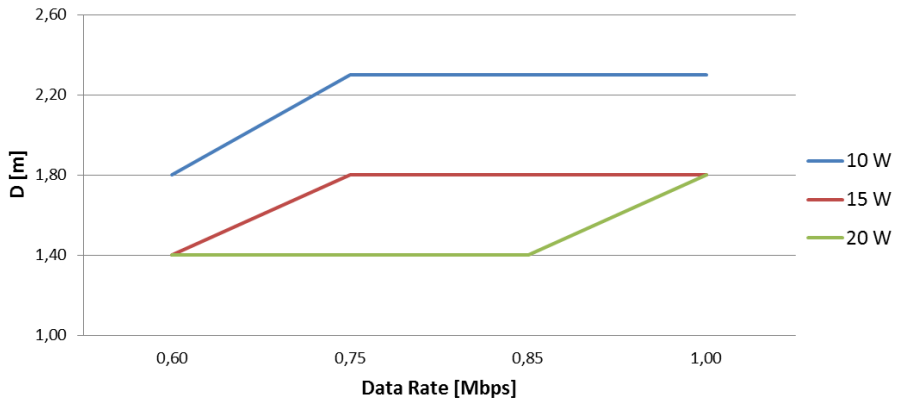

Figure 4.4. Diameter of ground antenna VS Data rate for a fixed amount of data

It is possible to see that the best result is obtained when the data rate is 1 Mbps using 15 W of RF power. Our priority is indeed to maximize the data exchanged in the achieved time window and this leads the system to the highest possible data rate.
Since the connection to the different locations in Africa happens simultaneously. It is needed a choice of a selection technique to decide how to divide the connection window. At a first analysis, the TDMA access method appeared to be the perfect choice, as it would require no changes in frequencies, therefore less hardware, obtaining a more simplified system. But this is partially true, because even if this is the simplest access of the multiple access series, it requires fast switches from a carrier to the other that still require a higher complexity in terms of hardware than the next choice. The simplest way to divide connection is to reserve each passage of the satellite for just a single venue even if it takes more time and is less efficient. In fact this choice implies a loss of possible data uploaded as the system could not fully utilize the slot of access time available for each orbit: when a connection with the dedicated venue ends, the system cannot connect to the next available one. This is necessary to keep the satellite as simple as possible, without the use of diplexers or complicated software controls which would need more sophisticated on board computers.

As the connection times per site, must be dedicated in every passage to a single facility, the best combination has been studied as a trial. Every day two big communication windows occur as already shown in the Figure 4.5. Brazzaville and Lusaka often share the communication windows. It is convenient, from the calculations executed, to let them alternate in gathering the highest frame day by day, while Antananarivo has always sufficient dedicated access.

Figure 4.5. Access times per day

This the selected time period it would make the system to reach an average value of 5449 Mbits total per day sent to Obisat. This way could seem not efficient, but considering the limited capabilities of Obisat hardware, the lack of multiplexers to implement a FDMA (Frequency Division Multiple Access) for evident reasons, it is considered it to be the best one.

4.2 Hardware

4.2.1 Transceiver

The transmitter is the one of the most critical point of this project.
It has to have particular requirements in terms of RF power, dimensions and data rate which is difficult to find in a Cubesat device. After a detailed analysis of many of them available on the market, the one which better fits these requirements was chosen.
It is the only device which can fit the Obisat dimensions and able to transmit up to 5 W or RF power at 10 Mb data rate. The unit includes latch-up detection and mitigation for applications with higher radiation exposure. It is composed by 3 blocks, namely the transmitter, the receiver and the High Power Amplifier. In order to achieve such functionality, it has to be coupled with the High Power Amplifier module. The receiver runs at bit rates from 1-8 Kbps instead of the required 1 Mbps and this makes it unfeasible for such a Cubesat. Many receivers have been analyzed but no one was found which could bear the requested datarate.

Table 4.6. S Band transponder from Aeroastro [12]

Feature	Value
Flight Heritage	MOST, NASA NM/ST5
Input Voltage	22 to 39 Vdc
Acquisition time	< 0.5 s
Output power	From 0.5 to 5 W RF
Interface	RS-422/EIA 485 software command interface
Operating temperature	-22 to 60 °C
Dimensions	Three modules, each (8.9 x 5.1 x 2.5 cm)
Mass	660 g (total)
Power input	42 W (peak)

Nevertheless it is possible to adjust a typical S band receiver with typical data rate up to some hundreds of Kbps, to achieve the desired higher characteristics. It is possible in fact to modify the acquisition filter in few months, without relevant technological matters. The filter's change implies no repercussions on the system in terms of masses but it brings a slightly increase of power demand which has already been taken into account.

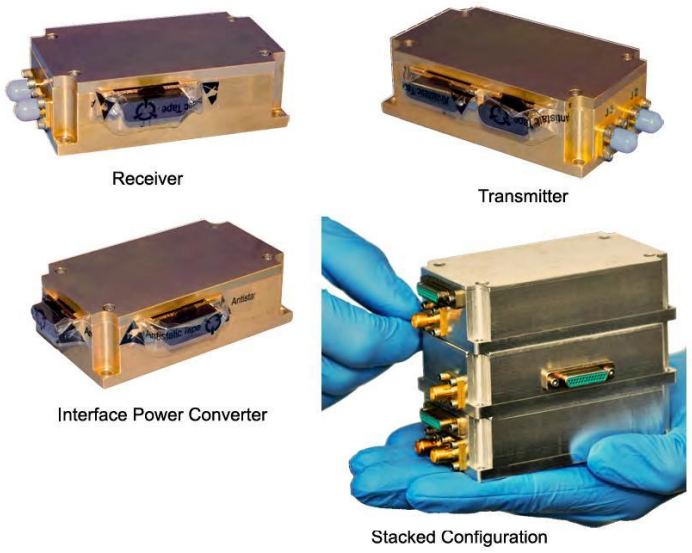

Figure 4.6. S band transponder (the receiver is shown for illustrative purposes)

A detailed description of the transmitter block is reported in Figure 4.7. Block diagram for TX

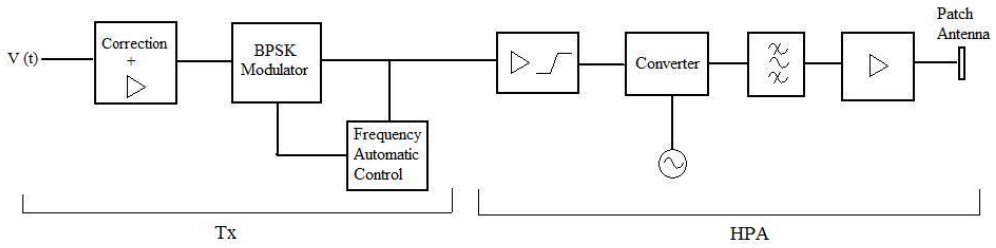

Figure 4.7. Block diagram for TX

The first part is namely the transmitter (Tx): it starts with a correction/amplifier block to give the signal the proper values in terms of gain-frequency in the selected modulating band. The FAC block is necessary to assure that the right frequency is achieved.
The second part is the High Power Amplifier (HPA): it is a system of power amplification; the first block is an amplifier followed by an amplitude clipper; it is needed to dump any introduced amplitude modulation which could add noise to the system. The converter brings the signal to the transmission frequency through an input coming from an oscillator. Finally the signal is amplified to reach the desired RF output power.

4.2.2 On-Board Antenna selection

The choice of an S-Band antenna is useful to contain antenna's dimensions. Considering costs and data sheets, a patch antenna compatible with other S-band systems, has been chosen.

Table 4.7. Patch RHCP Antenna from Cubesatshop [13]

Feature	Value
RF Bandwidth (3 DB)	50 MHz
Gain	6 dBi
Polarization	RHCP
Opening angle	Approx. 85 deg
Input power	Up to 10 W

A patch antenna (also known as a rectangular microstrip antenna) is a type of radio antenna with a low profile, which can be mounted on a flat surface. It consists of a flat rectangular sheet or "patch" of metal, mounted over a larger sheet of metal called a ground plane. The current flow is along the direction of the feed wire, so the magnetic vector potential and thus the electric field follow the current, as shown by the arrow labeled "E" in the figure below. A simple patch antenna of this type radiates a linearly polarized wave. The radiation can be regarded as being produced by the ‘’radiating slots’’ at top and bottom, or equivalently as a result of the current flowing on the patch and the ground plane.

The antenna pattern for this patched antenna is here shown: it is equal both in E and H planes.
The antenna selection took in consideration many other configurations. The VHF/UHF antennas which are very common for Cubesat purposes cannot fit the S band requirements, thus other configurations have been analyzed.
To have a consistent communication link, at least a gain of 13 dBi is required. Consequently a beamwidth of about 60 degrees apply for such a configuration, which is too narrow and does not t guarantee a sufficient access time. Moreover this model would have beams at least 7 cm long and they should point toward Earth. Therefore a deploying customized system should be considered.

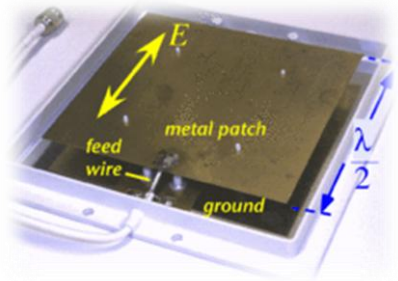

Figure 4.8. Patched Antenna characteristics

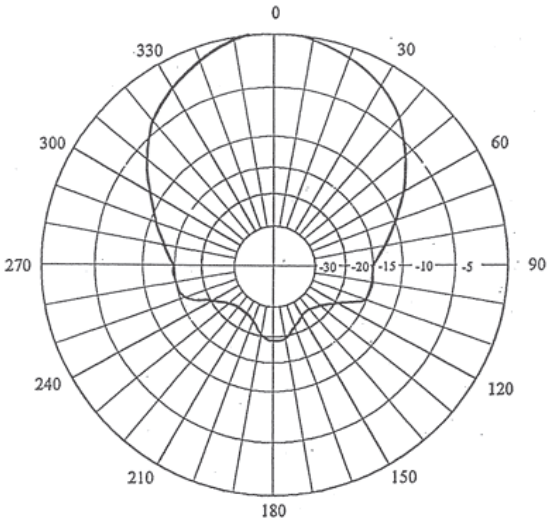

Figure 4.9 Antenna gain pattern 2350-2500 MHz - 6dBi Gain

A Yagi antenna has been taken in consideration. Gain and bandwidth for a typical Yagi follow the table [14]:

Some analysis been done also to Phased arrays antennas; unfortunately, even if they are very compact and with good gain they present several issues from results given from the electronical control of the beam's direction,. The number of antennas to be used would increase, usually four, implying the presence of 4 phase shifters.

Table 4.8. Yagi antenna's gains

Gain [dBi]	Beamwidth [deg]
0	360
3	180
6	90
9	45
12	22.5
15	11.25
18	5.125
21	2.5625

Not only costs would be very high, but also power consumption of the 4 phase shifters would be around 1 W. Such a system requires a highly robust control and software in terms of attitude precision and mounting items tolerances.
Parabolas have dimensions which do not fit with Cubesat size, or whereas a customization would be possible, maybe with a deployable one, that means more complicated systems, thus a non- Cubesat philosophy.

4.2.3 Ground segment design

The desirable ground antenna must accomplish the satellite lacks in terms of gain. It is designed to have the same frequency of the on board one. Yagi antennas do not have a gain as high that allows them to be chosen. Therefore dish antennas should be used. Several antenna diameters have been taken in account; considering communication is one of the critical requirements of this system, it is suggested to try to maximize its dimension. 2.3 m diameter and 3 meters diameter have been considered for the downlink: the first one is a 2.3 m parabolic antenna, with an efficiency of 50%, Gr=31.47 dβ while the second one is a 3 m one with a Gr of 34.95 dβ.

Table 4.9. Data acquired for different antennas' types

Diameter [m]	Gain [dB]	G/T [dB/K]	Data per week [Mbits]
2.3	31.47	10.59	4047
3	34.95	12.9	6485

Both are easy to be found. An interesting item is produced in Guangzhou, made of either 8 or 4 sections, with a reflective material Rolled Expanded Mesh. It has a 90° of pitch adjust range and 360° azimuthal one. The Net weighs 62 Kg (8 sections).
From the calculations previously done it results:

- Downlink: a parabolic antenna of 2.3 m is enough to achieve the desired performances.
- Uplink: the diameter needed for the parabolic antenna is 1.8m.

Figure 4.10. Possible ground antenna from Alibabà [15]

4.3 Link Budget

Link budgets for both downloading and uploading modes are reported in

Table 4.11. Values obtained are similar to those obtained through the use of the software STK and show that a sufficient margin level is achieved.
The noise spectral density N_0 is given by equation (4.2)

$$N_0 = 10\log(kT_S) \tag{4.2}$$

k is Boltzmann's constant = 1.38 x 10-^{23} J/K, while T_S is the system noise temperature. It is calculated taking into account the achieved temperatures of the antenna system on board and some statistical data for antennas [11]. In particular, data from Table 4.10 have been used.
No rain attenuation is here considered as it has a relevant influence from a starting frequency of 8 GHz. Clouds and other atmospheric factors at the frequency of 2.4 GHz produce an attenuation of about 0.7 DB which compared to the link margin reached is negligible.

Table 4.10. System Noise temperature for up and downlinks

Noise Temperature (K)	Downlink	Uplink
Antenna	150	290
Line loss	35	35
Receiver	36	289
System (Ts)	221	614

Table 4.11. Link Budget analysis

	Units	Source	Downlink	Uplink
Transmitter				
Frequency	GHz	Input	2,42	2,42
Transmitter Power	W	Input	4	10
Antenna Gain	dBW	Input	6	32,6
EIRP	dBW	Output	12,02	42,6
Antenna Noise Temperature	K	Input	150	290
Transmission Medium				
Distance	Km	Input	800	800
Losses	dB	Output	-158,19	-158,19
Receiver				
Receiver Noise Temperature	K	Input	36	310
Gain	dBW	Output	32,60	6
Rate-Modulation-Coding				
Data Rate	Mbps	Input	10	1
Modulation	-	Input	BPSK	BPSK
BER	-	Input	10^{-5}	10^{-5}
Received Iso Power	dBW	Output	-114,57	-110,59
R	dB-Hz	Input	-70	-60
No	dB/Hz	Output	-203,8	-200,8
Eb/No achieved	dB	Output	19,2	30,2
Eb/No required	dB	Input	9,6	9,6
Link Margin	dB	output	9,6	20,6

5 On Board Data Handling Subsystem

On Board Data Handling subsystem is that part of the satellite which is in charge to manage all telemetry data from instruments and to perform calculation of general station health status. Furthermore it has to be able to deal with and store the digitized images provided by the TT&C subsystem, so it needs to have an adequate mass memory and a processor fast enough to accomplish all these operations. A tradeoff has been carried out trying to optimize reliability factor with mass and costs: the aim is to guarantee a lifetime of at least two years, respecting the basic constraints on budgets, proper of a Cubesat philosophy. A basic redundancy will be provided where it doesn't impact significantly on mass and costs budgets.

5.1 Requirements:

- Components should be preferably COTS (Commercial Off-the-Shelf)
- Components have to be certified for at least 2 years to resist at the radiation dose correspondent at an orbit altitude of 800 Km
- The subsystem has to provide enough mass memory for images and telemetry to be stored, namely 8 GB
- Components have to respect power limits and volume constraints in accordance with the others subsystems and be able to communicate with them (interfaces, power, speed…)
- Onboard software should be based on high level language (modular) and be able to be updated and maintained remotely from ground
- The system has to identify and autonomously react to critical events (software malfunctions) and event detection (Sel events) for example timers for watchdog functions as well as running time delayed commands are required.
- The chosen system has to match the Rs-422 port from the Aeroastro communication block. Architecture Analysis and Design

5.1.1 Memories

To evaluate the amount of needed memory, it is necessary to study the time intervals during which data need to be stored after the uploading process from Africa and the completion of the downloading process in Italy. The longest time

interval between two downloading links depends on the orbit and it is 34920 sec; since memory hardware is not critical in terms of costs and mass, the memory has been chosen in order to store all the data collected during a period two times bigger than the maximum one.
To estimate the total amount of data flows for CPU clock in terms of MIPS, a data budget has been made, as shown in Table 5.2.
To satisfy the memory requirements a set of non-volatile memories for long time storage has been selected, in addition to a set of volatile memory for fast operations. Furthermore a non-volatile memory for system software load and reset was chosen (Eeprom). Total memories are summarized in Table 5.1:

Table 5.1. Evaluation of the necessary memories

Feature	Value
Total storage time	35000 s
Total uploading time	3500 s
Total memory needed	3,50E+10 bits
Total memory needed (100% margin)	8,76E+09 Bytes
DDR2 RAM	2 GB
Flash memory	8 GB (2x)
EEPROM	8 MB

5.1.1 CPU

A throughput analysis was made for each system module and operations to identify the most appropriate CPU typology and architecture. From statistical data from Wertz 1999 the amount of math operations, science elaborations and telemetry data processing, in term of MIPS were estimated. More accurate values would come from software data, unknown in this phase. The throughput data comes from the number and the type of sensors aboard, and from the type of operations to perform. An example of throughput calculation is summarized in Table 5.3:
From the throughput analysis done, the microprocessor to be chosen should be able to sustain 13 MIPS. For this reason, the best solution would be to design and develop a customized system. Unfortunately as a customized solution is usually very expensive, this is not the best solution in terms of cost efficiency, therefore a typical satellite on board system will be preferred.
Typical Cubesat OBC (On Board Computers) have the right requirements for being chosen but they mostly have Can/l^2p interfaces which can't afford high

data rates (the transmitter requires 10Mbit/s), customization is quite expensive therefore a typical satellite on board system will be preferred. The most of the on board microprocessors support mostly two types of interfaces: the RS-232 and RS-485 logic ports. Since the first one can only achieve 115 Kbps the second one has to be chosen (more than 10 Mbps). It is compatible with the RS-422 interface and doesn't require any converter thus.

Table 5.2. Data rate budget (statistical data from [11])

Measurement	Type	Ch.	SR [Hz]	Word size [bit]	DR [bps]
EPS					
solar cell sensor	V	3	0,03	8	0,72
bus sensor	V	1	0,03	8	0,24
battery sensor	V	2	0,03	8	0,48
management	digital data	1	1	8	8
TCS					
sensor	T	5	0,02	16	1,6
ADCS					
sun sensor	digital data	1	10	8	80
magnetometer	digital data	1	2	16	32
magnetotorquers	digital data	2	2	8	32
wheel	digital data	1			
controller	digital data	1	2	16	32
TT&C					
Antenna	T	1	0,03	8	0,24
	V	1	0,03	8	0,24
Cable-other com's	V	1	0,03	8	0,24
power	V	1	0,03	8	0,24
TM data processing	digital data	1	10	16	160
commands processing	digital data	1	10	16	160
picture processing	digital data	1	125000	8	1000000
Total telemetry					**508**
Science					**1000508**
Total data flow					**1001016**

The market offers different solutions for this kind of computers like the 32-Bit Atmel AVR Microcontroller. The AT32UC3A is a complete System-On-Chip microcontroller running at frequencies up to 66 MHz;

Table 5.3. Throughput analysis

Function	Typical throughput (KIPS)	Typical execution frequency (Hz)
Communication		
Command Processing	7	10
Telemetry Processing	3	10
Picture Processing	10000	
Attitude Sensor Processing		
Sun Sensor	1	1
Magnetometer	1	2
Attitude Determination & Control		
Kinematic Integration	15	10
Error Determination	12	10
Precession Control	30	10
Magnetic Control	1	2
Orbit Propagation	20	1
Autonomy		
Complex Autonomy	20	10
Fault Detection		
Monitors	15	5
Fault Correction	5	5
kalman Filter	80	0,01
Power ss	5	1
Thermal control	3	0,1
Total	**10224**	
Total with Margin (25%)	**12780**	

It is a high-performance 32-bit RISC (Reduced Instruction Set Computer) microprocessor core, designed for cost-sensitive embedded applications, with particular emphasis on low power consumption, high code density and high performance.

Table 5.4. Main characteristics of the AT32UC3A from Atmel [16]

Feature	**Good for Obisat**
MPU (Memory protection unit), fast interrupt controller for modern operating systems and real time operating systems	√
High computation capabilities thanks to Digital Signal Processing (DSP)	
On-chip Flash and SRAM memories for fast access	√
Peripheral Direct Memory Access controller (PDCA) enables data transfers between peripherals and memories without processor involvement	√
Class 2+ Nexus 2.0 On-Chip Debug (OCD), that is a non-intrusive real-time trace system	√

5.1.2 Data Bus

Referred to Cubesat standards, Can interface or l^2p data bus were chosen for OBDH. Most of Cubesat systems require these two types of bus interface and this make them the adopted choice. The communication block, since the Aeroastro transmitter data rate is at 10 Mbps, requires instead as data bus the RS-422 interface, , which matches all systems requirements in terms of bound per seconds, thanks to its high commands transmission speed (faster than Spacewire).

5.2 Design choices

The chosen final architecture is shown in Figure 5.1.
The number of memories and other components has been chosen considering also a reliability analysis; reliability (namely the no failure probability) goes as $e^{-\lambda t}$, where t is the time and λ is an index which increases with memory size, as shown in Figure 5.2.

Finally, the elements of the OBDH subsystems are:

- Microprocessor of 1.49 DMIPS / MHz
- 2 Flash memories of 8 GB each
- DDR2 of 2 GB
- EEPROM of 8 MB
- Standard bus l2c
- Bus RS-422 for transmitter

Instead of 1 memory of 8.76 GB, two memories have been chosen, each of which of 8 GB. A failure analysis has been done as well, but since a failure in download would imply no transmission in upload (higher data rate due to the shorter time interval couldn't be supported by the transmitter) it's not that relevant. As memory redundancy does not affect mass or power budgets, a higher value of memory has been chosen.

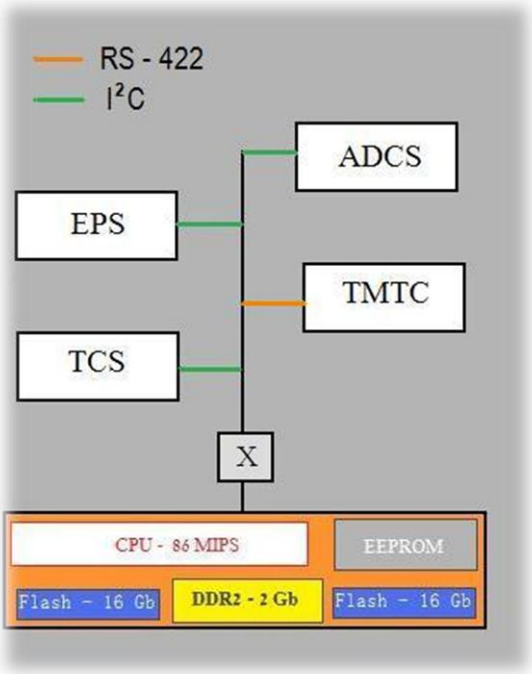

Figure 5.1. OBDH internal configuration

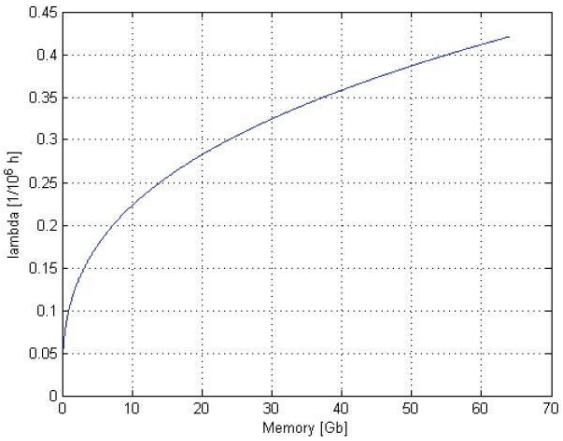

Figure 5.2 Reliability index VS Memory size

5.3 Budgets

In Table 5.5 mass and power data for OBDH's main components are summarized. A first estimation of cable length has been made for weight calculation, as RS-422 link has an average specific weight of 40 g/m and a maximum length of 0.7 m. Every cable length was multiplied by 1.3 to consider a folding margin. An EEPROM of 8 Mb has been chosen, namely a non-volatile memory used in space systems to store small amounts of data that must be saved when power is removed. This one, combined to the DDR2, gives more than enough level of reliability and redundancy for the Obisat system.

Table 5.5 Mass and Power budgets for OBDH

Item	Mass [g]	Power [W]
DDR2 RAM	1,5	0,001
Flash memory	6	0,006
EEPROM	7	0,001
Processor	10	0,5[1]
Data Bus	60	0,004
Total	84,5	0,512
Total with margin (25%)	105,625	0,64

[1] 0.5 W during stan by mode. 1.3 W during communication activities.

This system has been compared to a typical cubesat OBC, whose data are reported in Table 5.6.

Table 5.6. OBC from Clyde Space [17]

Feature	Value
Frequency	20 – 40 MHz
Interfaces	Low-Speed I2C Bus- 400 kbps High-Speed SPI Bus- 1 mbps
Memories	2 GB [Standard] 16 GB [Optional]
Ram	Up to 64 MB
Prom	Up to 1MB
Power consumption	1.2W to 2.5W
Mass	70 g

It is possible to see taht the values of a typical on board system are absolutely comparable to the designed ones.

6 Thermal Control Subsystem

The thermal control subsystem (TCS) is designed to serve two interconnected purposes for Obisat; to establish and maintain a thermal balance between the spacecraft and the environment and to keep the other spacecraft subsystems within their appropriate temperature ranges during flight operations.
In order to limit costs due to budget constraints, in a Cubesat system, mass and power are necessarily very strict and it would be preferable not to use any active control. A spacecraft thermal subsystem is classified as *passive* if the desired thermal balance is maintained using surface coatings or layers of specially selected insulating material. They are typically low cost due to a lack of complicated or complex control sub-components.
In space applications, radiation is the main method of heat transfer between the spacecraft and the environment. Radiant heat transfer can also occur within the spacecraft itself if there are components that dissipate heat during operation.
The TCS design process has been developed following specific steps summarized as follows:

- Identify heat sources: external, internal
- Identify cold and hot case
- Identify temperature ranges
- Select passive thermal control components: materials, coatings, paints, OSR
- Perform a single node thermal analysis for the hot case and for the cold one (if needed)
- Perform a multi node thermal analysis in Simulink
- Numerical analysis through the use of the Comsol software
- Compile the mass and the power budgets for the TCS.

6.1 Requirements

In a satellite system if temperatures threshold are crossed, the overall system efficiency and even the ability to obtain planned goals could be compromised. For this reason a TCS subsystem must:

- guarantee that temperature limits are not exceeded;
- keep the overall environmental limits into prefixed range;
- be a passive subsystem in order to simplify the whole system and limit costs;

6.2 Heat transfer dynamics

In space, only conduction and radiation heat transmission modes are present.
Conduction heat transfer is governed by Fourier's law that for an isotropic material is defined by equation (6.1):

$$\vec{q} = k\vec{T} \tag{6.1}$$

where k is the constant thermal conductivity and where q is the heat flux. This equation can be rewritten in the case of a steady unilateral flow through a surface of thickness L and constant area S as follows :

$$Q = qS = \frac{kS}{L}\Delta T = GL_{(i,j)}\left(T_i - T_j\right) \tag{6.2}$$

This defines the thermal conductance $GL_{(i,j)}$ between the isothermal surfaces i and j. Radiation heat transfer is governed by Stefan-Boltzmann's Law which is:

$$Q = \sigma\varepsilon AT^4 \tag{6.3}$$

Where ε and A are respectively the body's emissivity and emitting surface while σ is the Stephan Boltzmann's constant.
In space heat transfer analysis, thermal engineers made the following assumption: thermo-optical properties are assumed to be constant in two spectral regions:
- the infrared spectrum, from l = 4.25*m*m to 40*m*m, corresponding to temperatures between 70K and 700K.
- the visible spectrum, ranging from l = 0.3*m*m to 2.5*m*m associated to a temperature range going from 1150K to 10000K.

As a spacecraft temperature is always between the 70K-700K ranges, the emitted radiation is infrared. Nevertheless the main source of the incident radiation to a spacecraft is the sun which can be considered as a blackbody emitting at 5776K. Actually, ESA and NASA thermal engineers adopted the following convention: they call ε the (constant) emissivity (and absorptivity) in infrared wavelengths and α the (constant) absorptivity (and emissivity) in visible wavelengths. This convention will also be adopted in this work as well. An useful parameter is the Gebhart factor B_{ij}: It is defined through the following equation, valid for diffuse reflection[2] :

2 A theory has been developed to take partial specular reflection into account [32] but it will not be used in this work because the reflections encountered here are mainly diffuse

$$B_{ij} = F_{ij}\varepsilon_{ij} + \sum_k F_{ik}(1-\varepsilon_k)B_{kj} \tag{6.4}$$

this factor takes into account multiple reflections and represents the portion of the radiation emitted by a surface *Si* incoming to the surface S_j. The Gebhart factor does not only depend on geometry but also on thermo-optical properties of the surfaces *i* and *j*, namely the view factor F_{ij}, later discussed.
The radiative coupling between two surfaces, defined as Q_{ij}, flowing from S_i to S_j, is equal to the difference between the power emitted by S_i, and absorbed by S_j $\left(\varepsilon_j S_j B_{ji}\sigma T_i^4\right)$ and the one emitted by S_j and absorbed by S_i $\left(\epsilon_i S_j B_{ij}\sigma T_i^4\right)$.
At equilibrium, $Q_{ij} = 0$ and thus $\epsilon_i S_i B_{ij} = \epsilon_j S_j B_{ji}$. Out of equilibrium:

$$Q_{ij} = \epsilon_i S_i B_{ij}\sigma T_i^4 - \epsilon_j S_j B_{ji} T_j^4 = \epsilon_i S_i B_{ij}\sigma\left(T_i^4 - T_j^4\right) = GR_{(i,j)}\sigma\left(T_i^4 - T_j^4\right) \tag{6.5}$$

This defines the radiative exchange factor $GR_{(i,j)}$ between two surfaces i and j.

6.3 Heat sources:

External heat sources are: solar flux radiation, Earth albedo and IR radiation. The following picture shows the different external sources and how they interact with the Obisat system;

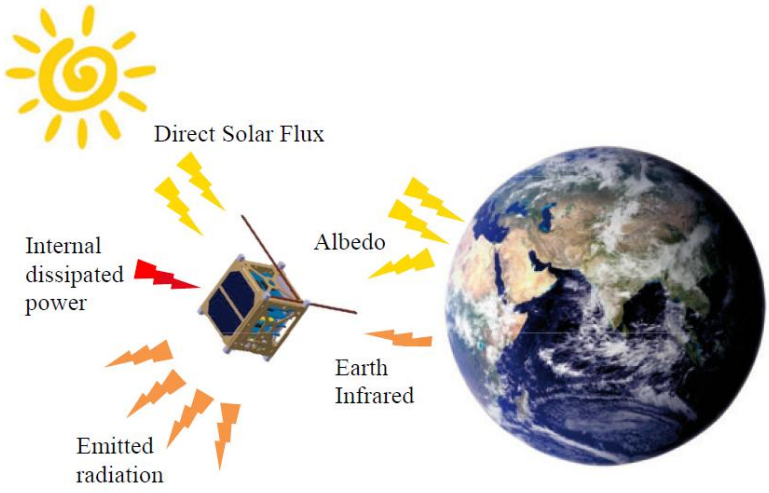

Figure 6.1. Power balance

6.3.1 Solar flux

As the sun distance is extremely large, the rays coming from the sun are assumed to be parallel. Furthermore, seeing the cubic shape of the satellite, there is no coupling between the faces, i.e. any ray that is reflected by one face will never hit another face. Therefore, the solar flux on each face is simply obtained as in equation (6.6), where in brackets it is the scalar product between the normal to the face and the sun direction.

$$q_{S,i} = C_s(\hat{n} \cdot \hat{r}_{sun}) \quad [\mathrm{W/m2}] \tag{6.6}$$

The Sun's intensity varies slightly over the orbit of the Earth due to Earth orbit's eccentricity; however, using the average value of the sunlight's intensity is a common praxis, since the introduced error is negligible. It is known as the *solar constant* and its value is C_S = 1367 W/m^{2,}.

6.3.2 Albedo flux

Albedo flux is more complex to compute. Indeed, it depends on many parameters such as the satellite's position from the sub solar point, Earth view factor and many others. In order to simulate the Albedo flux using the Simulink model, two references are combined. The first one is a simple formula (see equation (6.7)) derived from the notes of [18]

$$q_a = C_S a[cos(0.9\theta)]^{1.5} F_E \quad [\mathrm{W/m2}] \tag{6.7}$$

where a is the albedo reflectivity coefficient 0.37 [11] , θ the "sun-earth-satellite" angle, F_E the view factor between the face and the Earth, as shown in Figure 6.2. The 0.9 coefficient in the cosine means that even if the satellite has just come above the shadow part of the Earth, reflected rays are still hitting the satellite. When θ = 0, the satellite is at the sub solar point and the albedo is maximum.

Equation (6.7) and Figure 6.2 show that even if the scalar product $\hat{n} \cdot \hat{r}_{sat}$ is negative (i.e. ρ < 90° and the face does not point directly toward the Earth), the view factor is not null and the face still absorbs albedo or infrared flux. This can be explained by the fact that the incoming rays are no more parallel as it is the case for the sun rays since the satellite is close to the emitting body that can no more be considered as a point. In the Obisat case, the face always points to Nadir, so ρ is always 180°, and the formula gives us F_E = 0.78 and q_a as reported in the figure, with a mean value of 27 W/m^2:

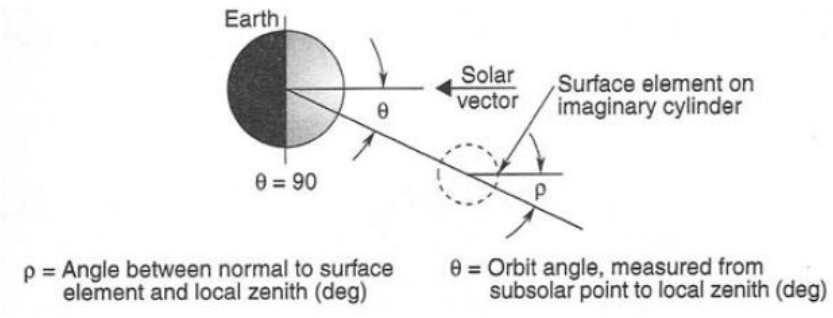

Figure 6.2. Incident albedo irradiation on a surface element in Earth orbit

where $r = \frac{R}{R+h}$ with R the Earth radius and h the orbit altitude.

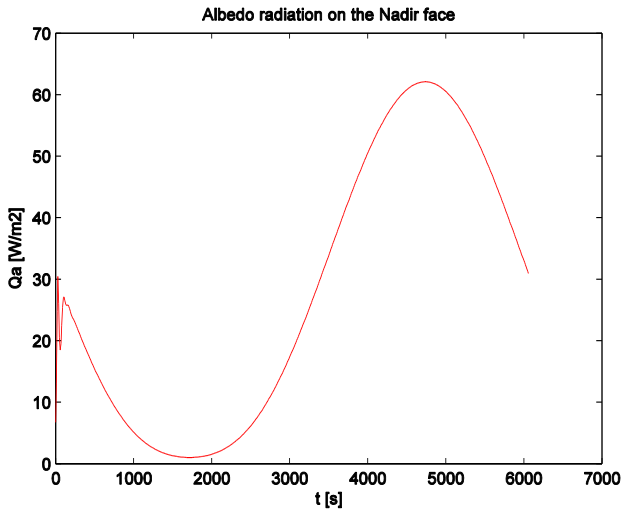

Figure 6.3. Albedo flux on the Nadir face

The second equation for Albedo computing, used as a comparison for the first one, is quite similar to the previous one, but this time the orbit geometry is taken into account inside the view, is defined by equation (6.8):

$$q_a = C_S a F_{albedo} \tag{6.8}$$

From Table 6.1, using θ = 90°, namely the angle between Nadir and Sun direction one gets $F_{albedo} = 0.03$, thus $q_a = 16$ W/m^2

For the FEM model it has been chosen to use the mean value of 27 W/m^2; it was taken from the carried out simulation combined with the first formula.

Table 6.1 Geometric factor for Earth albedo on a flat plate [11]

Albedo	θ	F_{albedo}
500 (0.0784 R_E)	0	0.8587
	30	0.7437
	60	0.4293
	90	0.0232
1000 (0.158 R_E)	0	0.7381
	30	0.6392
	60	0.3688
	90	0.0344

6.3.3 Earth infrared flux

Earth's infrared flux, also depending on the same view factor is now easier to compute since F_E is already known. By neglecting diurnal and seasonal variation in the temperatures of the earth and considering it as an equivalent 255K black body (thus emitting diffusely in all directions), the earth infrared flux is obtained from the equation (6.9) [11]:

$$q_{IR} = 244\, F_E \quad \frac{W}{m^2} \tag{6.9}$$

Where 244 W/m^2 is the Earth emitted IR radiation [11].
In conclusion, the following table summarizes the power by surface incoming to Obisat by the different external sources at the conditions and constrains explained before:

Table 6.2 Summarizing table of the different external heat fluxes sums up all the external fluxes radiating to the satellite

6.3.1 Internal heat sources

Internal heat sources come from thermally dissipated power by every subsystem and depend on the operational modes. Table 6.3 reports the internal heat sources to be dissipated. They are evaluated taking into account the different power consumptions and the relative efficiencies.

Table 6.2 Summarizing table of the different external heat fluxes

Heart sources	W/m^2
Solar flux	1367
Earth Albedo	27
Earth IR	197
Total radiation	2014

Table 6.3 Internal heat sources for the different subsystems

Heat Sources	Hot case [W]	Cold case [W]
OBDH	1.3	0,5
TT&C	23.5	-
EPS	0,16	0,16
ADCS	1	1
TOTAL DISSIPATED POWER	29.96	1.66

6.4 Thermal design

In order to estimate the thermal environment in which the satellite will operate, a simulation has been implemented.
As solar irradiation is constant, hot case happens when Obisat is downloading to Italy; since the transmitter has the highest power demand, and thus the highest power dissipation. Cold case happens when no communication activities are performed during the winter solstice. Indeed during this period of the year the satellite is subjected to a short eclipse time frame.

6.4.1 Temperature ranges

Table 6.4 shows a list of the main components of every subsystem and their acceptable temperature ranges. The most critical components are the batteries, the memories and the wheel with a more limited temperature range than the other ones while the less while the widest range belongs to the solar arrays, spanning between -40 and +125 °C.

Table 6.4 Temperature ranges for Obisat components (operative)

Component	Tmin [°C]	Tmax [°C]
EPS		
Ac/Dc Converter	-55	125
PCU	-35	70
Batteries	-10	50
Solar Array	-40	125
TT&C		
A/D Converter	-40	85
Transmitter/HPA/Receiver	-20	60
Antenna	-25	85
OBDH		
Memory	0	70
Processor	-40	85
ADCS		
Magnetotorquers	-35	75
Reaction wheel	-20	50
Sun sensor	--25	50
Magnetometer	-50	85
ADCS board	-40	80

6.4.1 Single node Steady State Analysis

As first, a one-node steady state analysis has been performed, both for the hot and the cold cases. The analysis made is based on this simple steady-state equilibrium referred to a sphere with the same volume of the considered spacecraft:

$$Q_{int} + Q_{ext} = Q_{emit} \tag{6.10}$$

Where Q_{int} and Q_{ext} are the same parameters referred in previous paragraph and Q_{emit} is the power emitted by the equivalent sphere, calculated with Stefan-Boltzmann law. In particular it is:

$$Q_{int} + q_S \alpha A_C + q_A \alpha A_N + q_{IR} \varepsilon A_N = \sigma \varepsilon A (T_S^4 - T_a^4) \tag{6.11}$$

In Table 6.5 are shown the different parameters used for equation (6.13). Except for the internal heat to be dissipated which depends on the operative mode, the other parameters do not change.

Table 6.5. Parameters and results for the single node thermal analysis

Parameter	Description	Value	
		Communication	**Stand by**
Q_{int}	Internal heat	22 W	3 W
q_S	Sun heat flux	1367 W/m^2	
q_A	Albedo heat flux	27 W/m^2	
q_{IR}	Earth IR heat flux.	244 W/m^2	
A_N	Area pointing to Nadir	0.01 m^2	
A_C	Section Area of the sphere	0.02 m^2	
ε	Sphere emissivity	0.85	
α	Sphere absorptivity	0.9	
T_a	Space temperature	3 K	
σ	Boltzmann's constant	5.67 x 10^{-8} W/m^{2}K^4	
T_S	Sphere temperature	20 °C	68 °C

While the temperature for the stand by case is acceptable, on the contrary the one referring to the communication mode is out of boundaries.
The use of this simplified formula is clearly not enough to simulate the thermal behavior of this system; the high power dissipation, occurring for short time frames during communication, forces us to a transient analysis as time scale is indeed absolutely comparable to the components' capacitances.

6.4.2 Multi node Transient Model

A multi node transient analysis is required, as it would give more detailed values for the temperatures reached, for the chosen nodes representing different parts of the system.
The basic equation used here, is the lumped parameter equation, written for the general multiple nodes model, which comes from the heat balance on the node i:

$$Q_{int\,i} + Q_{ext\,i} - \sum_{i,j=1}^{n} GL_{i,j}(T_i - T_j) - \sigma \sum_{i,j=1}^{n} GR_{i,j}F_{i,j}(T_i^4 - T_j^4) = C_i \frac{dT_i}{dt} \tag{6.12}$$

Being $Q_{int\,i}$ the total internal dissipated power for the node i, $Q_{ext\,i}$ the total external power incoming on the node i,; $GL_{i,j}$, $GR_{i,j}$ and $F_{i,j}$ are respectively the conductive, the radiative links and the view factor between nodes i and j. Ti is the temperature on the node i and it C_i is heat capacity. Finally n is the number of nodes.

For Obisat it has been made an 8 nodes analysis, one node for each external panel and two internal ones. The internal configuration could be ideally divided into 2 parts: the communication block will form a standalone block since it reaches higher temperatures than the rest of the satellite, and the other subsystems' boards. The following picture explains better this choice:

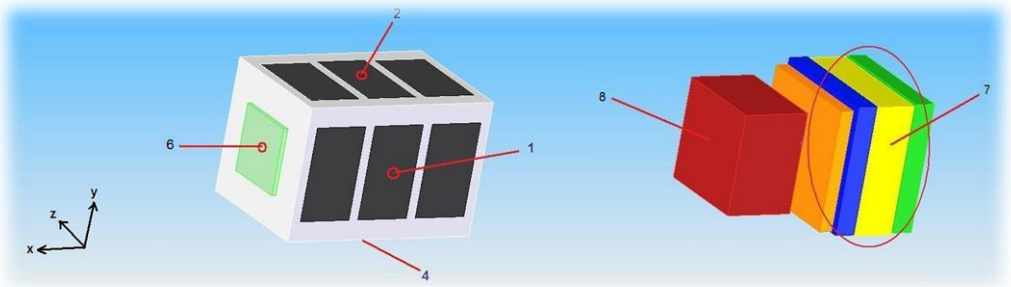

Figure 6.4. Nodes distribution

To simulate the thermal dynamics, a Simulink program has been developed as it is shown in the following picture:

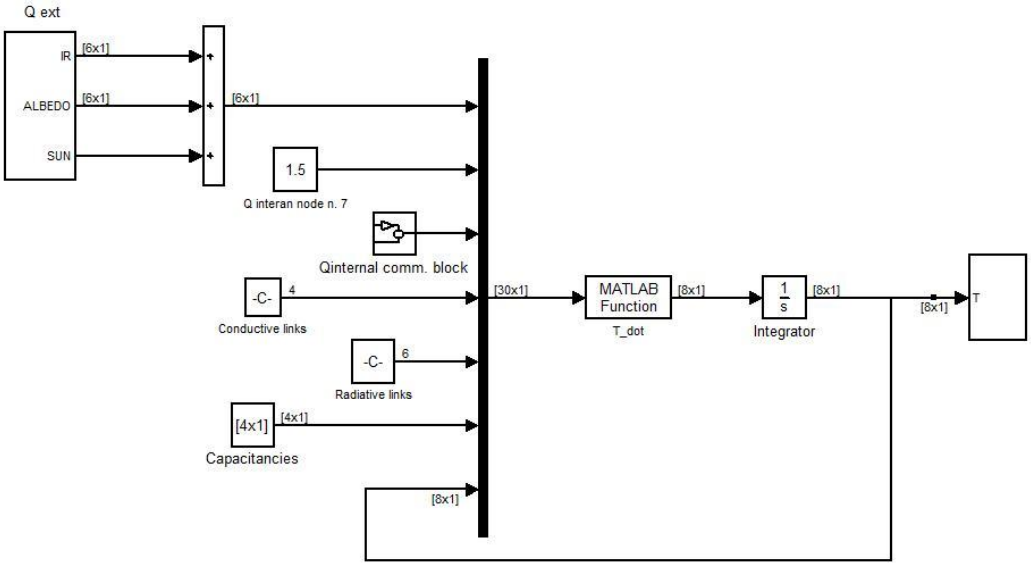

Figure 6.5. Simulink model

The different blocks will be now analyzed.

External Heat Sources: Total External heat is given from the multiplication of the flux incident on face *i* by its corresponding equivalent absorptivity/emissivity (α for solar and albedo and ε for IR) and then summed up for all faces:

$$Q_{ext} = Q_S + Q_A + Q_{IR} = \sum_i^{n\ faces} A_i\left(\alpha_i q_{S_i} + \alpha_i q_{A_i} + \varepsilon_i q_{E_i}\right) \quad (6.13)$$

Internal Sources: They are lumped in the nodes 7 and 8. The alternation of Rx, Tx, and stand by modes is simulated.

Heat Links: The following two inputs are those computing the heat links GL and GR respectively the conductive and the radiative ones.

Conductive Heat Links

As regards the GL conductive heat links, the simulation considers all typology of conductivities present within the system:

- GL side_top = Heat link between two adjacent faces
- GL between HPA and side panel
- GL board to board
- GL spacer to structure

GL Side_Top:

The values assumed for the conductive links are the following:
$GL_{side\text{-}top} = GL_{ij}$ with i = 1,2,3,4 and j = 5,6
This formula has been taken from [19] where the author conducted a FEM analysis assuming a temperature gradient of 10 °C across the two half faces of the 2 frames. The software was then able to compute the resulting flux proportional to the temperature gradient. Thus the thermal link was calculated:

$$GL = \frac{Q}{\Delta T} \quad (6.14)$$

giving as result GL_{st} = 0.055 W/K between two side faces of Obisat. This conductivity could seem very low considering that panels are based on aluminum but it turns reasonable due to the very small contact area.

It has been decided to calculate the heat link between two side faces by multiplying the previous one times 1.5. Since heat link is directly proportional to dimensions, it appears to be a good first estimate.
$GL_{(side)}$ = 0.055 x 1.5 = 0.0825 W/K

GL HPA / Panel:

The heat exchange between the HPA and the panel face has to guarantee a sufficient high thermal conductance. A hypothetic contact area has been estimated in 1912 mm^2. This assumption is based considering a perfect link between the device and the aluminum frame. Moreover the area of the HPA was divided by 2 to take into account the fact that the contact may happen between the face of the HPA and the skeleton frames instead with a whole flat panel; as a consequence the frame area has been estimated to be half of the entire surface as well.
The Thermal link has been evaluated according to its definition:

$$GL = \frac{A}{R_{tot}} = \frac{A}{\left(\frac{s_1}{k_1}+\frac{s_2}{k_2}\right)} \tag{6.15}$$

where k is the thermal conductance [W/mK], A is the contact area [m^2] and s is the distance between the nodes. Using the values reported in the picture, GL = 6.4 [W/K] is obtained.

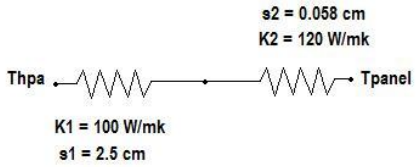

Figure 6.6. Heat link between the HPA and the Panel

GL board and structures

The evaluation of the conductive link between the stack (node number 7, namely all the boards except from the communication subsystem) and the side panels has been taken from [19], where the author imposed a temperature gradient, and by evaluating the reached temperatures, the transfer link was calculated.
Thus they are:
GL board to board = 0.58 [W/K]
GL spacer to structure = 1.42 [W/K]

Radiative Heat Links

As far as concern the GR radiative heat links, it is given by the product of the emitting area times the emissivity factor. A list of the absorptivities and emissivities for the main components participating in the thermal exchanges is reported in Table 6.6

Table 6.6. Radiative properties of the main Obisat's parts

Part	Material	Surface type	α	ε	Reference
Aluminum panels, inside	7075 aluminum alloy	Alodine 1200		0.1	[20]
Aluminum panels, outside	7075 aluminum alloy	2mil Kapton foil on Alodine 1200	0.87	0.81	EADS Astrium measurements
Solar cells	Triple junction GaAs cells	Anti reflecting coating	0.91	0.81	[21]
PCBs	FR4 + copper			0.8	[22]

Thus the following values have been used:

Table 6.7. Radiative links

GR	X 10^{-3} [m^2]
GR_{17}	7.6
GR_{57}	8.5
GR_{18}	3.25
GR_{68}	4.8
$GR_{side,environment}$	12.1
$GR_{side,environment}$	8.1

Where GRij is the radiative factor between the surface i and the surface j.
GR will be thus multiplied for the respective view factor in order to get the right values as in equation.
View factor computation could be very difficult when numerical analyses are carried on; the chosen method for the evaluation is the Monte Carlo one. With this approach, F_{12} means that random points are selected on the surface 1, from these points many shots with random directions are thrown and if they hit the

surface 2, the counter will be incremented. In a spherical coordinate system, these vectors have been created through the use of the angles ranges:
φ $[0,2\pi]$ and ϑ $[0,\frac{\pi}{2}]$

ϑ distribution has to respect the shape given from the definition of view factor:

$$F_{ij} = \frac{1}{JiAi} \int_{Ss_j} \int_{S_i} \frac{I_i \cos\theta_i \cos\theta_j}{r^2} dA_1 dA_2 \tag{6.16}$$

Where J_i considering diffused surfaces, I_i loses its dependency from the position and $J_i = \pi I_i$, thus having

$$F_{ij} = \frac{1}{\pi Ai} \int_{Ss_j} \int_{S_i} \frac{\cos\theta_i \cos\theta_j}{r^2} dA_1 dA_2 \tag{6.17}$$

Then, after identifying the number of rays which hit the second surface, the view factor will be given by the formula:

$$F = \frac{n\ centers}{n\ shoots} \tag{6.18}$$

In the following table, view factors are analyzed:

F_{17}	0.5	F_{71}	1
F_{57}	1	F_{75}	1
F_{68}	0.57	F_{86}	1
$F_{2,}$ F_{48}	0.2	F_{82}, F_{84}	0.82
F_{18}	0.1768	F_{81}	0.6855

Table 6.8 View factors

Heat Capacity computation

For heat capacities values in Table 6.9 have been used:
The capacity of the 7th node, namely the PCBs stack with boards, is calculated considering the influence of two materials, aluminum and FR4. Their respective values are 790 and 6000 J/KgK. A weighted average on the thickness of the different boards has been made, thus multiplying the heat capacity of FR4 [23] times 0.2 while the aluminum one was multiplied for a factor of 0.8.

Table 6.9. Heat capacities

Element	Value
Panels	700 J/KgK
Node 7	1287 J/KgK
Node 8	790 J/KgK

For ADCS PDM and OBDH the value of 1832 J/KgK has been therefore adopted. For batteries the following value has been used: C = 1012 J/KgK [24]. For the only PCB the value has been taken as the heat capacity of copper 385 J/KgK estimating it in 30 % and the value of the FR4 composite. The result is 4400 J/KgK

The simulated system has returned the following values for the temperatures:

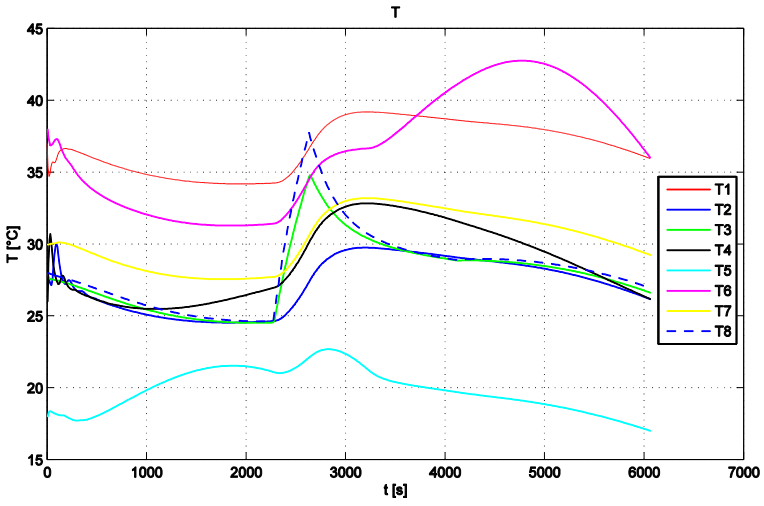

Figure 6.7. Temperatures' ranges

It is clear from the results that, based on reliable assumptions and formulas calculation approximation, the temperatures distribution over an orbit for every subsystem are within their respective temperature ranges. It is also possible to notice a steep variation of the temperatures of the nodes 3rd and 8th. This is due to the activation of the HPA module, which is characterized by high power dissipation; the strong thermal link to panel #3 causes its temperature to rise with almost the same slope.

FEM Analysis

The previous temperature distribution is computed considering specific approximations and assumptions. As a results it gives a value of temperature Ti as a constant equal distributed on each element "i" at time "t", while in reality the temperature is not only a function of the time "t" but also a function of each point in the sub-systems' components.
That's said, in order to have a more realistic and punctual temperature distribution, a Finite Elements Model needs to be evaluated.

To conduct the FEM analysis the Comsol software has been used.
The first step was to model the external structure in order to be as much as possible equal to the real one. For internal components different blocks have been created each one having the same physic properties of the real one. For the most critical components, namely the hottest ones (amplifier, panels) a "Surface to surface radiation model" has been defined.
In order to completely characterize the heat transfer matrixes, each node must be fully characterized. In particular the information needed are:
1. Internal power
2. External fluxes: solar, albedo, IR
3. Linear and radiative conductances from one node to each other.

To model the external flux, the mean value for each surface has been considered. This engineering choice is based on the fact that the largest amount of power comes on surfaces 1 and 2 and it is quite constant, the others vary with a cosines distribution, but as a simplified model, their power is not much influent and the mean value instead of the real one has been adopted.
The analysis has been computed following three phases: Uploading (Rx), Downloading (Tx), and stand-bye. They are summed in Table 6.10 with the relative adopted margins.

Table 6.10. Simulation steps

Steps	Type	Time expected	Time simulated	Margin [%]
1	Rx	1094	1367	25
2	Tx	323	355	10
3	-	-	4331	-

The first is the uploading period which can vary widely depending on many factors such as the number of pictures to be sent, the availability of the African center, and the other variables already discussed in chapter 1. Thus this margin

has been considered higher than the one in downloading, for which a detailed analysis can be afforded. The margin for this last parameter is set in 10 %.

Model:

This paragraph presents the numerical choices made to build up the finite element model as much as possible equivalent to the real one.
As concerns the conductive links between the PCBs, there are two main heat flow paths: through the spacers and through the connector. According to the PC/104 specification [41], the connector is made up of 104 phosphor bronze pins and only pins contribute to the link since connector's housing height is such as there is no contact with the above PCB. Conduction through the M3 endless screws is neglected seeing the clearance with the PCB holes and spacers. The spacers are made of 6061- T6 aluminum and the contact between spacers and PCBs is considered to be perfect. A spacer is a small hollow aluminum cylinder with diameters of 3.3mm (interior) and 4.5mm (exterior). Spacers are shown in Figure 6.8:

Figure 6.8 PCB board

The PCBs stack has 8 contact points with the external structure: four at the top with the COM PCB and 4 at the bottom with OBC PCB. The top links are ensured by the "midplane standoffs" as presented in Figure 6.9. Two midplanes ensure the fixation with the face "four" and "two".
Again, perfect contact is assumed between the PBC and the frame. The FEM model tries to approximate the real model, by selecting the heat conductancies as much as close to the real ones. PCB is both a heat conductor and structure support, it is a composite material made of cupper (layers and pins) and FR4

composite. Its conductance has been calculated by the sum of the contributions of the two materials in an approximated way since no detailed data were found on it, depending on the fact that its structure can vary significantly. Since the FR4 conductance is about 4 W/mk while the cupper one is near 400 W/mK, and considering that a good thermal link to panels is required, it has been decided to assume 200 W/mk for the PCBs. This value is not that far from the ones found in literature [25].
Figure 6.9 shows highlighted in blue the main contributors to thermal exchanges.

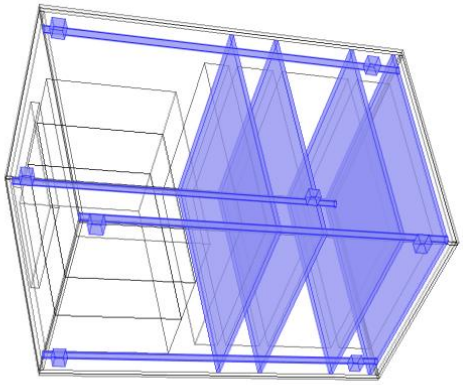

Figure 6.9. Main heat transfer contributors

The link to the structure is guaranteed by fastening screws, namely the NC 4-40 series. The model takes as equivalent link an aluminum block which sizes are equal to the real one, neglecting the discontinuity given by the screws.
The results obtained are described in the following picture:

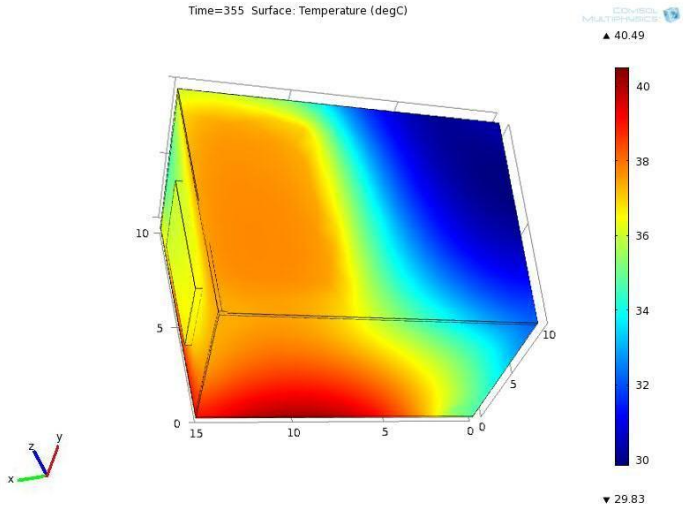

Figure 6.10. External temperatures

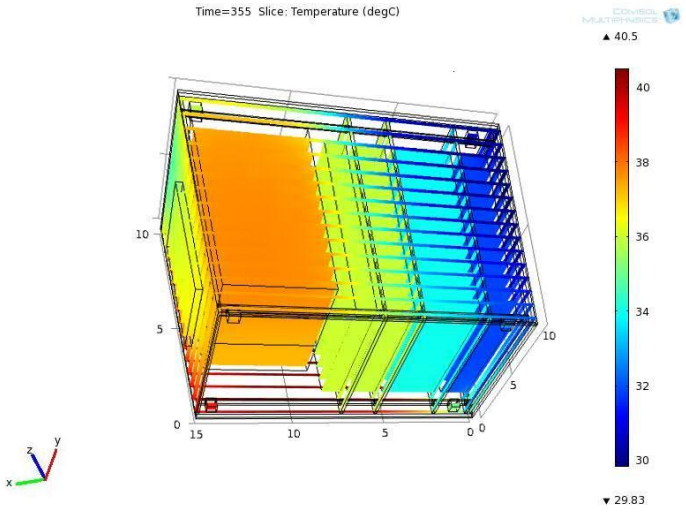

Figure 6.11. Internal Temperature distribution

The same study has been done considering no transmission occurring and choosing a time interval long enough to let the temperatures reach static values. The simulation has produced the following results:

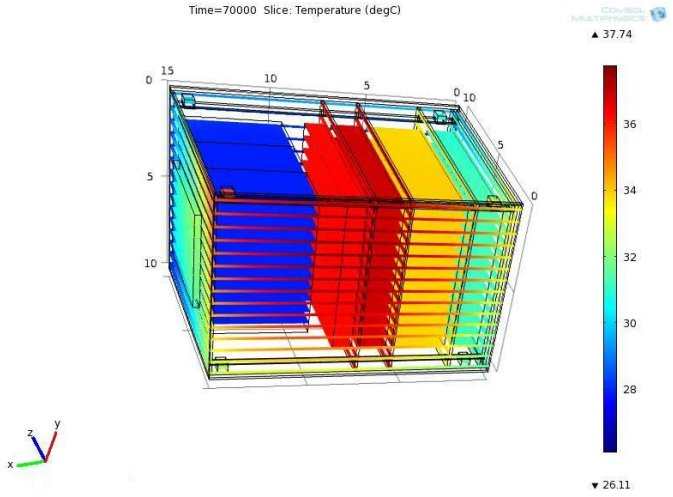

Figure 6.12. Steady state results

6.5 Cold case analysis

The low altitude of the orbit coupled with the inclination of the ecliptic plane give the birth to some short eclipse periods. It starts on the 12th of May and ends on the 13th of September. The maximum time Obisat spends in eclipse is 1086 s. During this period, no albedo and no sun power hit the satellite, thus it represents the cold case for our study. The FEM simulation conducted revealed that temperatures stay in the boundary limits, thus no active thermal control is required.

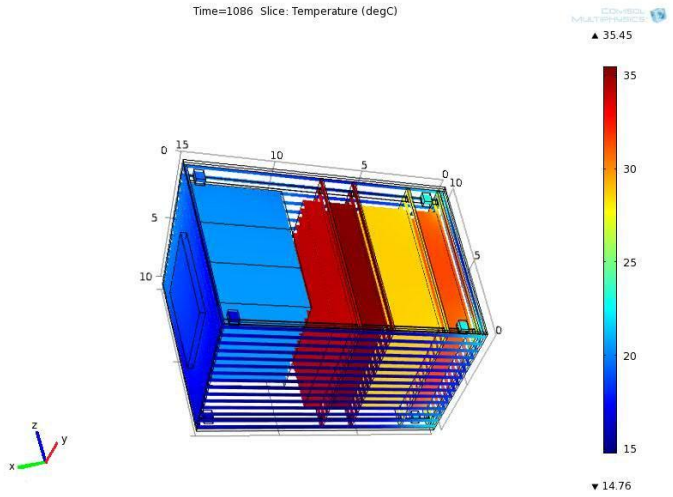

Figure 6.13. Temperature distribution after eclipse time

6.6 Results and considerations

ESA ECSS-E-10-03A prescribes ±15 °K of margin for uncertainty during phase A on temperatures.
Results show that the COTS selected products perfectly fit the temperature limits, allowing the system to be the simpler possible.

From the analysis it is evident that the critical case is the hot one since the satellite never goes in shadow. This condition, in addition to the small dimensions of the system, makes the heat from solar panels moving towards the entire structure rising the temperature above the internal one. The communication block made of Tx, Rx and HPA needs to dissipate the high amount of heat generated while transmitting; thus requiring high values of conductance towards the panel, so it has considered attached to the aluminum internal frame structure. The transmitter will be sustained by a PCB or some joints which should be appropriately studied since this component is not namely a cubesat standard.
The analysis shows that all the temperatures keep staying in the safety ranges.

Table 6.11. Reached temperatures

Component	T min	T cold	T hot	T max
EPS - PCU/PDM	-35	34	35	70
Batteries	-10	31	33	50
Solar Array	-40	20	41	125
Tx / HPA / Rx	-20	23	42	60
OBDH	0	34	37	70
ADCS board	-40	30	32	80

Figure 6.14 and Figure 6.15 show two graphs of the reached temperatures for both the hot and cold cases.

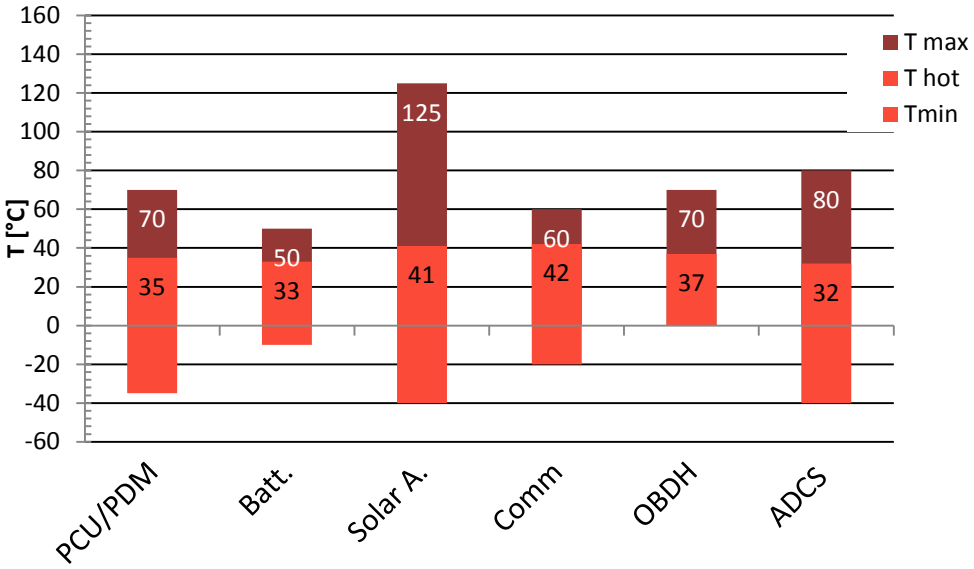

Figure 6.14 Temperature distribution. Hot Case

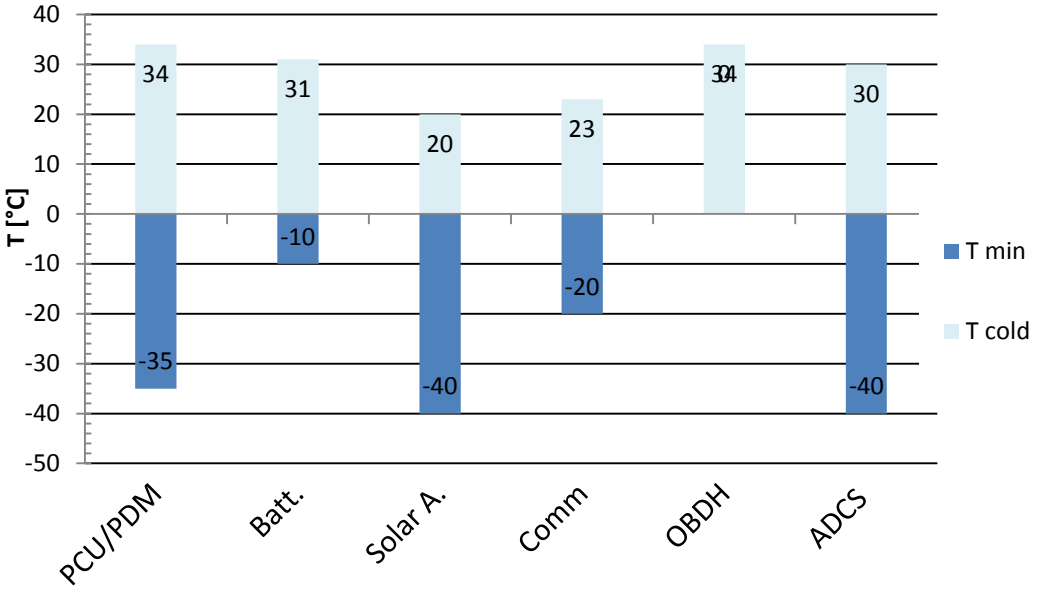

Figure 6.15. Temperature distribution. Cold Case

From the next chart it is possible to see that since no active systems are used to control temperature, only a short time of transmitter use can guarantee the system's survivability.

An interesting study is the evaluation of the temperatures in the case of a longer activity of the transmitter device. Trying the system at different time intervals, temperatures remain between the thresholds. This means that more communication activity could be foreseen according to thermal issues, since this would not compromise the system environment. The double time of a single connection is thought to be a proper simulation since access times are always about 355 s, from every possible venue using 10 Mbps data rate, having thus same heat dissipation needs.

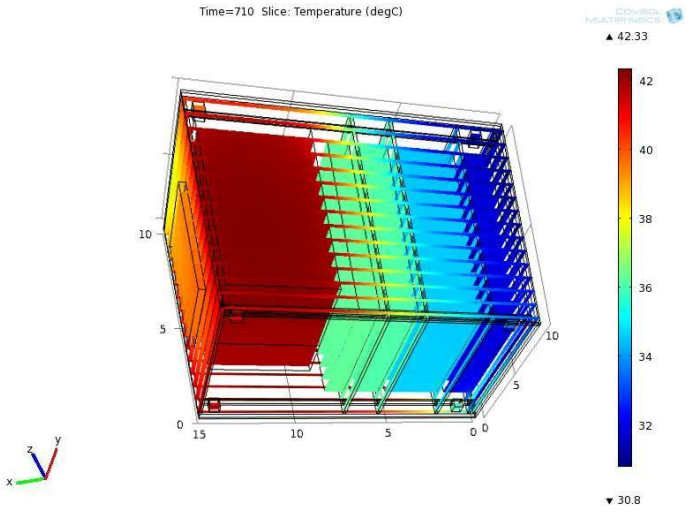

Figure 6.16. Temperatures reached after a longer period of transmission

7 Electrical Power Subsystem

The Electrical Power Subsystem (EPS) provides, stores, distributes and controls spacecraft electrical power.

7.1 Subsystem requirements

EPS must be able to:

- Provide power to the loads during the whole mission lifetime, in every operative mode. In particular it must provide power for at least 2 years after release in orbit and face high power demands during transmission.
- Generate, store, condition, control, and distribute power within the specified voltage band to the whole bus and payload equipment.
- Guarantee a basic protection of the power system components in case of faults.
- Minimize costs and complexity.

7.2 Power sources

For a Cubesat system the most used power source is the solar power. It usually satisfies Cubesat demands and it is the most efficient in terms of mass, volumes and constraints among all possible ones. All other means of power generation are too heavy or too expensive to be used in such a cheap and small system. When Solar arrays (SA) are not able to sustain the peak spacecraft power request or during eclipse times, packs of batteries are used. No other technologies to store power are here analyzed because they do not fit Cubesat requirements

7.2.1 Solar Panels

Solar cells convert the available power from the Sun (1367 W/m2 on average in LEO) thus providing a stable, lightweight, reliable and low cost energy source.
A solar cell is composed by:

- Different layers of semiconductor material
- A metallic grid
- Transparent cover

The most important parts of a solar cell are the semiconductor layers. There are many different materials suitable to constitute these semiconducting layers, and each has benefits and drawbacks. Unfortunately, there is no ideal material for all types of cells and applications. In addition to the semiconducting materials, solar cells consist of a top metallic grid or other electrical contact to collect electrons from the semiconductor and transfer them to the external load, and a lack contact-layer to complete the electrical circuit. Then, on top of the complete cell there is typically a glass cover or other type of transparent encapsulant to seal the cell and keep weather out, and an anti reflective coating to prevent the cell from reflecting the light back away from the cell itself.

For Cubesat missions requiring more power, many producers have developed self-contained deployable solar panels that require no spacecraft structure modification. Their manufacturing techniques have been developed based on traditional solar array assembly techniques, but adapted to reduce assembly costs in order to meet the tighter budget of the Cubesat satellite community.

Key features of these solar panels include:

- GaAs Triple-junction solar cells from AZUR Space
- Assembly processes tried and tested on Carbon Fibre composite,
- ISIS Aluminum and PCB substrates.
- Low-cost assembly method based on traditional techniques using heritage, space-qualified materials.

They are typically multilayer Printed Circuit Board (PCB) substrates with a space rated Kapton facesheet. To ensure good thermal design, copper fill on the top and bottom layers is used and the underside of the cells is flood with vias for thermal conductivity purposes. There is no wiring on them and they are designed to produce a minimal magnetic field.
All solar panels are assembled to a high quality and inspected to ESA standard. PCB substrates can incorporate magnetotorquers (MTQ) coils and other sensors (temperature sensors are standard fit). Coarse and fine sun sensor on panel options are available. These solar panels have been supplied for about 50 Cubesats to date.

As far as concern the number of solar panels, they are 6, one for each face, in order to assure that the right amount of power is collected. Some faces are supposed to be never in sunlight, but since COTS panels are produced with solar arrays inbuilt; this would let the satellite have enough power in case an unexpected launch problem, or unforeseen disturb that would cause the satellite rotation. Principal parameters for the selected solar panels are reported in Table 7.1:

Table 7.1. Clydespace solar cells' characteristics for a 1.5 U Cubesat; panels' thickness depends on the desired MTQ performances.

Feature	Dimension	Value
Cell Width	(mm)	39.70
Cell Length	(mm)	69.11
Corner crop length	(mm)	5.00
Cell Area	(mm^2)	2719
Parameters at temp.	°C	28
BOL Efficiency	%	28.3%
Cell Vmpp	(mV)	2350
Cell Impp	(mA)	443.17
dVmpp/dT	(mV/°C)	-6.50
dImpp/dT	(mA/°C)	0.03
Cell Voc	(mV)	2665
Cell Isc	(mA)	464
dVoc/dT	(mV/°C)	-5.90
dIsc/dt		0.14
STRING LENGTH		3
No. STRINGS/PANEL		1.00
BOL Voc at -40°C	(V)	9.20
BOL Vmpp at -40°C	(V)	8.38
BOL Vmpp at 80°C	(V)	6.04
BOL Vmpp at 28°C	(V)	7.05
BOL Power at -40°C	(W)	3.7
BOL Power at 80°C	(W)	2.68
BOL Power at 28°C	(W)	3.12
Mass 1.6mm PCB no MTQ	(g)	48
Mass 1.6mm PCB w/ MTQ	(g)	59
Mass 2.4mm PCB w/ MTQ	(g)	79

A magnetorquer is integrated into the PCB in ten internal layers thus taking up no extra space inside the spacecraft, and with an effective area of 1.6 m2 it is by far enough to detumble and control the attitude of a Cubesat. This point will be later discussed in the next chapter. A temperature sensor is mounted close to the diode to enable compensation for its temperature drift. The attitude determination electronics on the panel interfaces connect to the on-board computer via a single connector including power supply and the dedicated bus

for temperature sensor and output from sun sensor. The magnetorquer uses its own connector allowing high switching currents, and the solar cells also use a separate connector to connect to the power supply system.

Degradation factor

All the products built from Cubesat factories have a minimum lifetime of 2-3 years. These solar panels are guaranteed for a minimum lifetime of 2 years. The degradation factor for these solar panels is reported in the following table:

Table 7.2. Degradation factor for different life times.

2 years	3 years	5 years
0,94	0,92	0,87

7.3 Power generated VS Power demand

7.3.1 Power demand

The power demand for Obisat is quite high and it strongly depends on the choice of the Downlink parameters. Figure 7.1 shows the power required by each subsystem in the different operative modes. The Eps' value comes from the efficiency of the Power Distribution Module (PDM) which is supposed to be different in each different phase, but since no additional data were provided and due to its negligible value it was taken 0.16 W for all the operative modes.

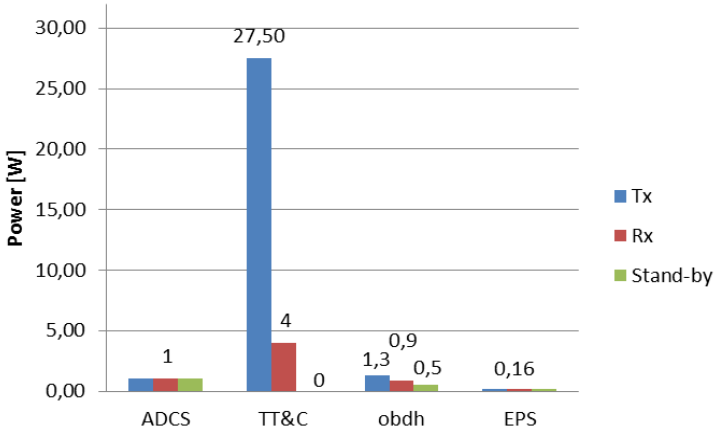

Figure 7.1. Power demand for every subsystem during Tx, Rx and stand-by

It's evident that the highest power is required by the transmitter which, with the HPA module, can consume up to 30 W. Table 7.3 shows all the power demands for the various subsystems in the different operative modes:

Table 7.3 Power demands from each subsystem

SS	Tx	Rx	Stand-by	Reference
ADCS	1,00	1,00	1,00	[26]
TT&C	27,50	4,00	0,00	[12]
OBDH	1,30	0,90	0,50	[16]
EPS	0,16	0,16	0,16	[27]
TOTAL (25% margin)	24,96	6,97	1,88	

The Psa, namely the power in W provided by solar arrays, is given by the equation (7.1):

$$P_{sa} = 1.25 \frac{\frac{P_d T_d}{X_o} + \frac{P_u T_u}{X_o} + \frac{P_{sb} T_{sb}}{X_{sb}}}{T_{cycle}} \quad (7.1)$$

Where *Pd*, *Pu*, *Psb* and *Td*,*Tu* and *Tsb* are respectively the powers required, during the downloading, the uploading and stand-by phases, and their correspondent time durations. *Xo* and *Xsb* are respectively the efficiency performed by batteries during operations and stand-by phases in which solar arrays directly provide power to loads, and their values are respectively 0.65 and 0.85 [11]. *T cycle* is the time elapsed from the last downloading phase to the beginning of the next uploading phase. To explain how this value has been estimated it is needed to introduce the hypotheses made. The cycle chosen is the worst case for our system as it takes into account two transmissions in two consecutive orbits, letting the batteries having less time to be recharged. Figure 7.2 shows the three phases in which this cycle is divided

Table 7.4 gives the duration is seconds of each phase. *T cycle* is thus the time window in which one download and 3 or 4 uploading phases occur and it is the time on which is based our sizing. From Figure 7.2 it is the time frame one minus the total time of uploading (3550 s). Results are presented together with the generated power in Figure 7.6

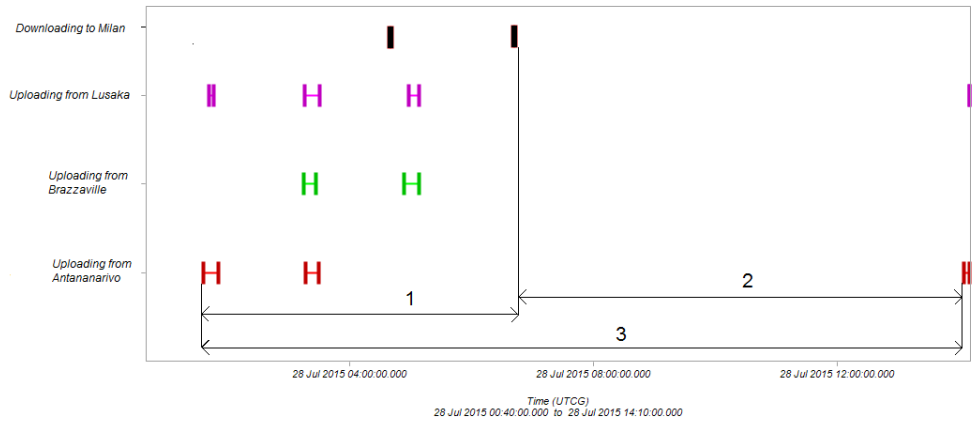

Figure 7.2. A full cycle example

Table 7.4 Description of the three phases encountered in the previous cycle

Phase	Description	Duration [s]
1	Discharging	17548
2	Recharging	27324
3	Full cycle	44872

7.3.2 Power generated

To choose the right solar panels configuration a power analysis has been conducted. Simulating the income of energy for different types of orbits it has been seen that no eclipse must be present in order to collect the highest amount of energy. This choice fits also thermal requirements. The simulation combining the satellite's altitude, faces' orientation and satellite-sun vector, gives as output the amount of power generated by each panel as shown in Figure 7.3. On average the power that can be provided by a side solar panel of a 1.5 Cubesat header with perpendicular sun, @ 1 AU and at a temperature of 28 °C is about 3.12 W. Considering the hypothesis of an uniform temperature on the panel of 40°C as it is stated in the thermal analysis, the amount of power gathered at BOL (Begin of Life) from all the panels with their correspondent orientation in an orbit period is 4.3 W.

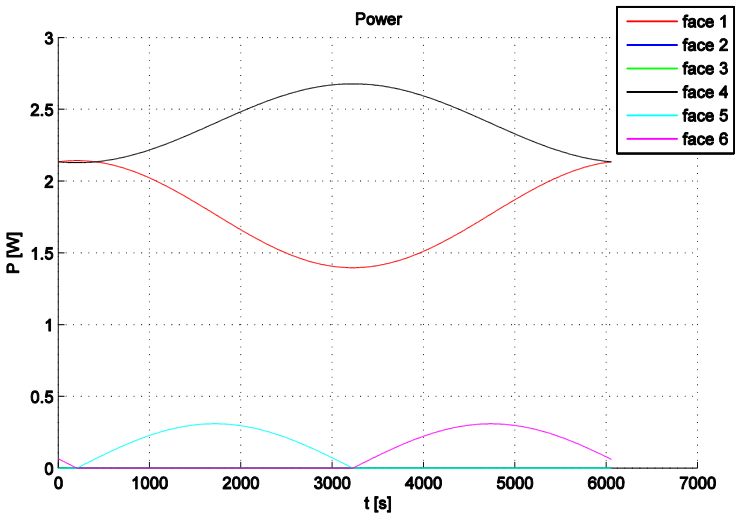

Figure 7.3. Power generated from each face

By summing the mean values of all the panels, the total PSA generated on board is obtained, as shown in Figure 7.4:

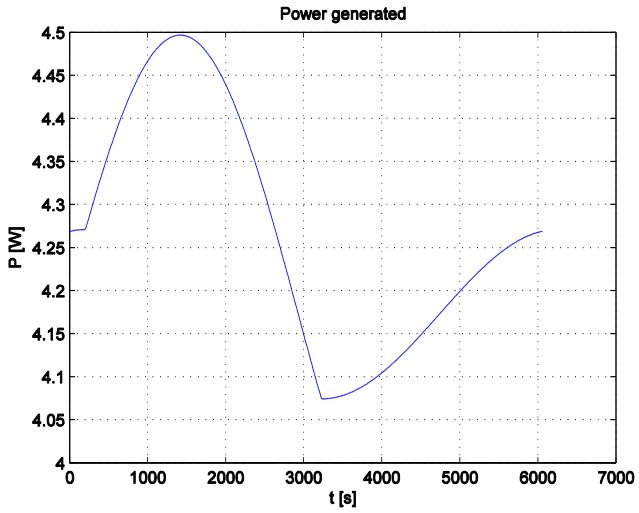

Figure 7.4. Total power generated on board

Figure 7.5 shows the variation of the panel produced power versus temperature..

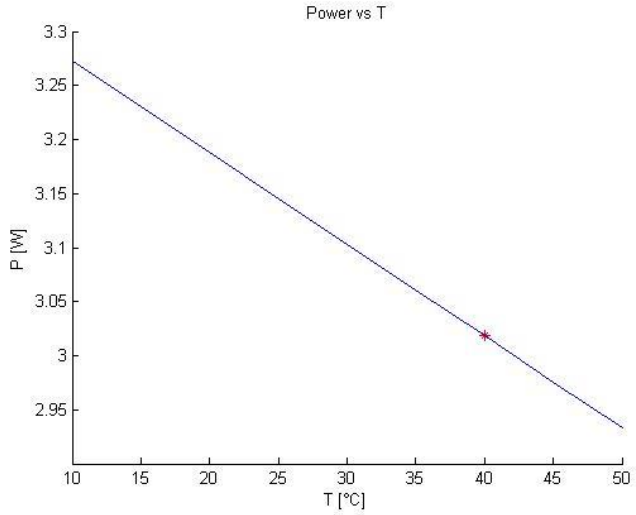

Figure 7.5 Power production VS temperature

Figure 7.6 reports both the power demand and the obtained one for a lifetime up to 5 years.

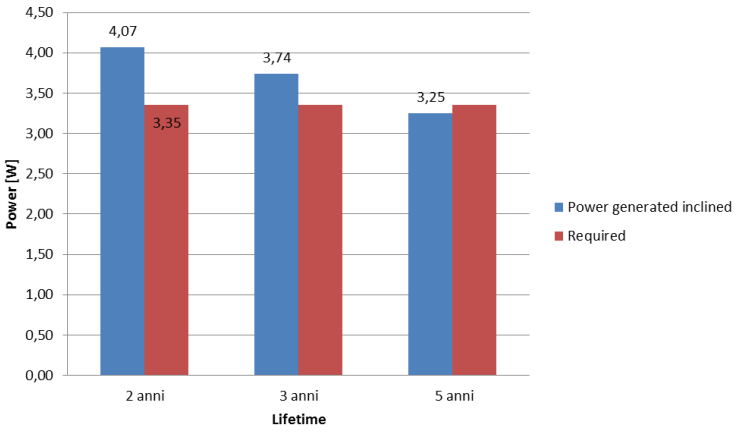

7

Figure 7.6. Power demand VS power generated for different lifetimes

The power demand has been increased by a margin with 25 % in respect to the real one, thus the system sizing is well satisfied.

Power analysis need to consider also the charging system for the batteries.

At present, EPS board and Power Distribution Module for Cubesats cannot afford to feed loads with different voltages from the entire I2C feed system and can reach a total peak power of 30 W tops.
The HPA has particular needs in terms of voltage, current and power. It cannot be powered by the solar arrays as they cannot afford such high demand, so an additional dedicated system of batteries is needed to satisfy the power high demand.
Since currently there are no technologies on any Cubesat system that can enable the split the power input between solar panels and batteries, the powering system of the communication subsystem is entirely provided by batteries. Moreover, as Cubesat batteries cannot be recharged during discharge, this implies some inefficiency as an amount of power, equivalent to the one collected during the sum of downloading and the uploading times, is wasted. Considering a time frame between the last uploading phase and the next downloading one that is about 45000 s, the time wasted is thus about 4000 s.

7.4 Eclipse analysis

The cold case analyzed for thermal purposes is here integrated with consideration upon the power system. The charging period must take into account the shadow generated by the Earth due to the low altitude of the satellite. Thus, having a shadow period of 1086 s, the following power balance has been obtained (see Figure 7.7.).

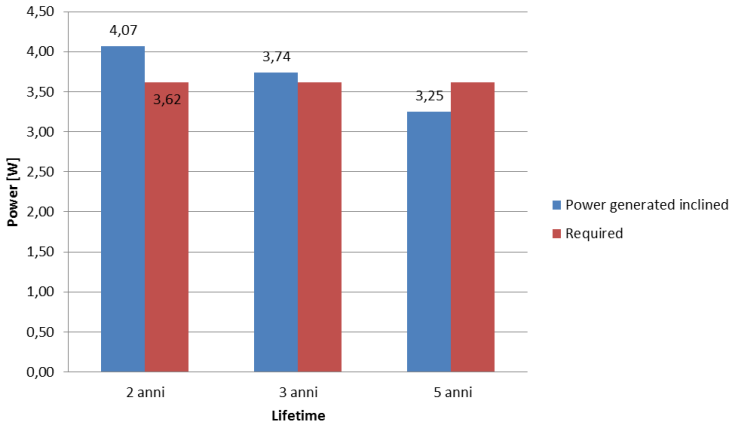

Figure 7.7. Power balance during eclipse occurrences

At 3 years the required power overcomes the generated one. Since 2 years is the basically wanted lifetime and the high margins applied it is reckoned to be fine.

7.5 Batteries

The battery pack will provide power to the communication block since its power demand is too high to be supported by solar arrays. At the moment the battery technologies with the highest specific energy are based on Lithium polymers.
The batteries produced by Cubesat industries meet our requirements except for the highest output power offered which will force us to oversize their capacity. According to Obisat constraints in terms of masses, volumes and power demand, typical Cubesat batteries match the design needs.
For example SAFT cells offer an output voltage of 3.6 V with a weight of 150 g each; To reach the required 22 V needed by the communication subsystem, a total number of 6 cells, with a total weight of 1,2 Kg, would be needed to produce such a voltage, and this is absolutely unfeasible in terms of masses.
No primary batteries are needed on board; therefore only secondary ones will be here analyzed. Clyde Space batteries utilize Lithium Ion Polymer technology to offer power to mass ratios in a form factor ideally suited to the volume constraints of Cubesats. In addition to this, testing has been carried out by both ESA and NASA, and the batteries have also been cleared for launch on NASA manned flights. The major reasons to choose them are:

- Availability in 8.2V and 32.8V versions as standard; custom voltages also available
- Lithium Polymer for increased performance:
- Low magnetic signature due to aluminum foil casing
- Verified cycle life of 5000 cycles (accelerated life test); 35000 cycle life though expected (usage conditions dependent).
- Cycling Tests at reduced pressure (15-20mbars) give as a result 30% DoD, at C/2 (half the highest possible current) Charge/Discharge

The batteries required on Obisat should be able to afford in the worst case 7000 cycles, including a 20% margin on the real one. This is computed estimating 6 uploading connections per day plus 2 downloading ones, for a two years period, with a margin of 20%. This has been computed considering a discharge/charge happening for each activity performed by the communication system and it is namely the product of the 8 cycles per day times 2 year of lifetime.
Namely, a single pack of batteries has a capacity of 10 Wh and is made of 2 cells connected in series. To match our need 3 packs of batteries are required, whose characteristics are reported in Table 7.6. To reach the desired 22 V output capacity, 6 cells have to be used, thus having a 30 Whr battery stack instead of the needed 20 Whr one. A further study could be carried on to analyze the possibilities to produce the desired battery with lower capacity to reach the same

desired voltage output. In this preliminary phase it's impossible to evaluate whether buying them in the 30 block is more convenient in terms of costs and times than making a plan to customize them. The first estimation of the battery capacity in W-hr has been done using the equation (7.2)

$$C_r = \frac{P_d T_d + P_u T_u}{DOD\ n} \tag{7.2}$$

Cr is the battery capacity in *W-hr*, *Pd* and *Td, Pu* ant *Tu* are the power and duration of the downloading and uploading phases, *DOD* is the battery depth of discharge at the end of life and *n* is the transmission efficiency between the battery and the loads.

Table 7.5. Parameters used for battery sizing

Parameter	Value	Reference
n	0.9	[11]
DOD	0.5	[28]
Pd	30 W	
Tc	355 s	
Pu	7 W	
Tu	3555 s	

Considering the values reported in Table 7.4, the battery capacity results to be 22 W-hr. This value is based on the hypothesis that no recharging happens from first upload to last download highlighted as time-frame #1 (see Figure 7.2). Recommended DOD at the end of every discharge phase is 20 %, and this value, since Obisat's batteries' capacity is oversized, will be widely respected.

Table 7.6. Charge/Discharge properties for the LiPo stream

Discharge					**Charge**		
V	Ah	A	Whr	Depth of Discharge	Kg	EoC V	Charge Current (max)
24.66	1.25	1.25 (C)	30	75%	0.260	24.66	1.25 (C)

It is possible to build a graph in which it is shown the battery capacity profile through all the different phases as shown in Figure 7.9. It starts with the downloading phase, followed the uploading one, to end with a recharging period which guarantees the fully recharge of its capacity. All the uploading phases, have been lumped in one equivalent phase. Since this study was made to point

out the lowest discharge level of the batteries (it has to be higher than the 20% of its capacity), it is a conservative hypothesis which help us to simplify calculation in this first estimation process; In such a way 2 cycles per day will be performed, having thus 1470 cycle in 2 years with an applied margin of 20 % instead of the previous 7000, with a consequent saving in batteries' performance. In this case the power budget with a margin of 20 % on the required power value, due to a restriction in time charging becomes (see Figure 7.8):

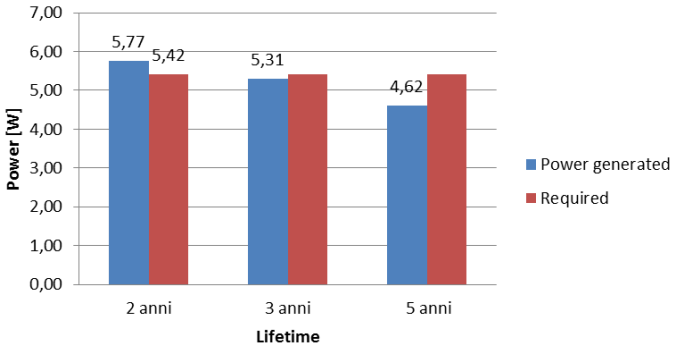

Figure 7.8. Power demand VS Power offer for shorted charging period

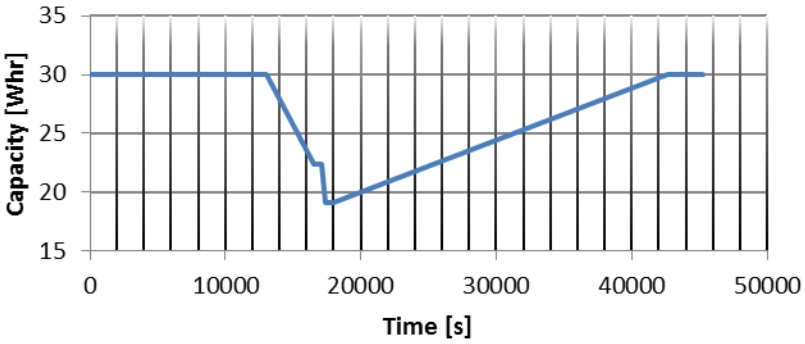

Figure 7.9. Battery capacity VS time

7.6 Charge Methods

The BCR (Battery charge regulator) system has two modes of operation: Maximum Power Point Tracking (MPPT) mode and End of Charge (EoC) mode.

MPPT Mode

If the battery voltage is below the preset EoC voltage the system is in MPPT mode. This is based on constant current charge method, operating at the maximum power point of the solar panel for maximum power transfer.

EoC Mode

Once the EoC voltage has been reached, the BCR changes to EoC mode, which is a constant voltage charging regime. The EoC voltage is held constant and a tapering current from the panels is supplied to top up the battery until at full capacity. In EoC mode the MPPT circuitry moves the solar array operation point away from the maximum power point of the array, drawing only the required power from the panels. The excess power is left on the arrays as heat, which is transferred to the structure via the array's thermal dissipation methods incorporated in the panels.

8 Attitude Determination & Control Subsystem

In this chapter Attitude Determination and Control System (ADCS) sizing is described. Firstly requirements and constraints will be identified. Then perturbance torques will be inspected to finally find the proper solution to contrast their effect and to give to Obisat the right attitude performance.

8.1 Requirements analysis

The ADCS subsystem must provide vehicle stability and maintenance of the correct attitude through all Obisat's life.
In each phase ADCS must be able to provide correct solar panel orientation in order to obtain enough electrical power and correct antenna pointing with a sufficient accuracy whilst communication.
The general phases that are critical for the subsystem are:

- Separation: after launcher last stage separation the spacecraft has to perform attitude determination and contrast residual rotation
- Operative life: Solar panels must be oriented towards the Sun while the antenna should point towards the Earth

To provide attitude control the ADCS uses a set of sensors and actuators. Low cost devices, as small as possible should be used, with the lowest power consumption as well. Furthermore they have to be compatible with the chosen bus. According to these requirements and considering the whole mission profile it has been decided to perform a 3-axis stabilized attitude control. 5 degrees of pointing accuracy seems to be a good compromise for a small economic system with strict constraints on power and communication. The attitude accuracies required in every mission phase are listed in Table 8.1. Pointing accuracies

Table 8.1. Pointing accuracies

Antenna pointing	SA pointing
±5°	±5°

8.2 Disturbances analysis

First of all an analysis of the main disturbances needs to be performed in order to understand the environment in which the satellite will operate. The main sources of disturbance are hereby listed:

- Sun radiation
- Earth albedo and IR radiation
- Magnetic Earth field
- Gravity gradient

To inspect intensity and profile of these disturbs a simulation in Simulink has been carried on. In the following paragraphs the main parameters used to build the model are discussed. The time of the simulation is computed during 10 orbits to show better what the behavior of the system is in a longer time than just one orbit. Nevertheless, disturbances are shown in an orbit period for a better visualization.

Sun Radiation

To compute the torque caused by the Sun's radiation on Obisat attitude, equation (8.1) needs to be used:

$$T_{sun} = \sum_{i}^{n} r_i \wedge F_i \tag{8.1}$$

r_i is the distance between the face *i* and the mass center of the cubesat, F_i is the force given from the Sun radiation acting on the face *i* coming from equation (3.3), *n* is the number of the Obisat's faces. T_{sun} is thus the torque disturbance inducted on the satellite. The simulation is conducted during an orbit to better visualize disturbance's behavior.
The disturb on the x axis is negligible respect to the other two, in fact the symmetry along *y* and *z* axes doesn't let the growth of any torque along *x*. The other components show a periodic behavior.

Magnetic Earth field

The residual magnetic induction present on the satellite generates a torque which is given by the following equation:

$$T_{magn} = m \wedge B \tag{8.2}$$

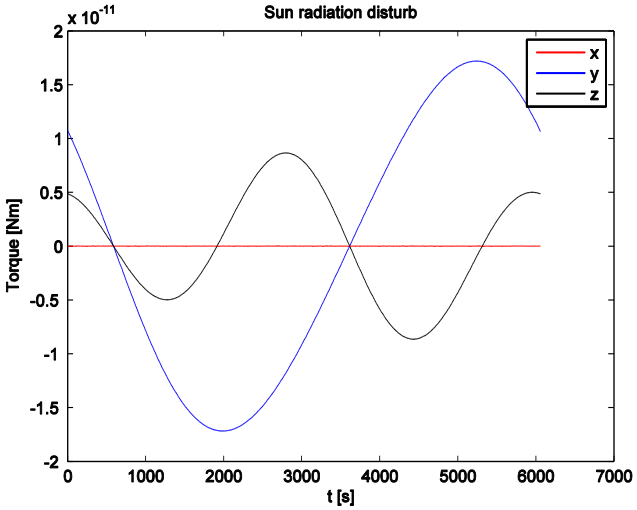

Figure 8.1. Sun's radiation disturb

m is the residual magnetic induction, and *B* the Earth magnetic field. The residual magnetic induction is difficult to be evaluated, it has thus been estimated from statistical data taken from other Cubesat systems [29] and its value is

$$m = \begin{Bmatrix} 0.6 \\ 0.6 \\ 0.6 \end{Bmatrix} 10^{-5} \quad \text{Am}^2$$

B is evaluated time by time by the simulation process.

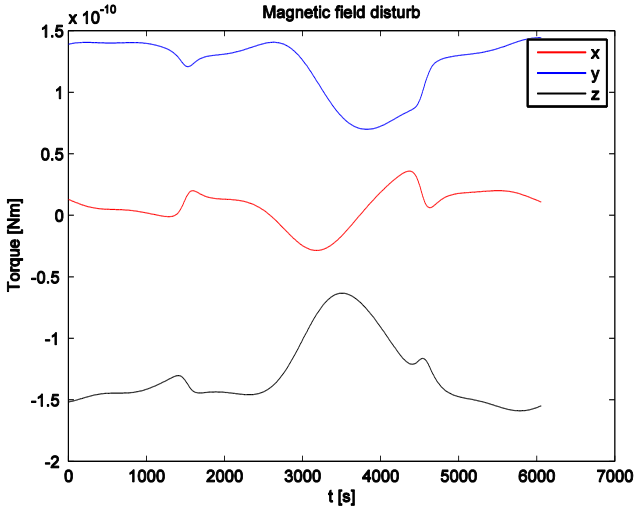

Figure 8.2. Magnetic earth field disturb

Earth IR and Albedo

Earth albedo and IR radiation cause a disturbance on the satellite as well. It is given by the same formula used for the Sun disturb, since it deals with radiation particles. The formula used is the same from the section 4.4 The disturbance caused is represented in Figure 8.3:

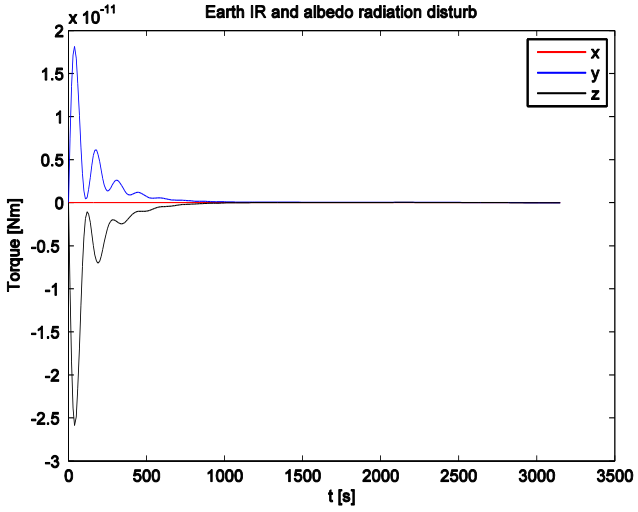

Figure 8.3. Earth albedo and IR radiation disturb

On contrary from the solar disturb, after the first oscillations, disturb inducted by Earth goes to 0 rapidly. It is due to the fact that the exposed area to Earth radiation is just face n. six which is square shaped so the torque generated on it is absolutely negligible.

Gravity gradient

This kind of disturb is generated from the non-equilibrium of the gravitational forces on the body. It is relevant especially for big bodies but also on a cubesat can have relevant effects. It is given by the equation:

$$T = 3n^2 \begin{Bmatrix} (I_z - I_y)c_3c_2 \\ (I_x - I_z)c_1c_3 \\ (I_y - I_x)c_1c_2 \end{Bmatrix} \tag{8.3}$$

Where *n* is the orbit angular velocity, *I* the moment of inertia of the satellite and *c* are the director cosines of the radial direction in the principal axes of inertia. If the *x* axis points to Nadir, then only c_1 will be different from 0, namely one and this would imply the lack of this disturb.
If the minor inertia axis points to Nadir, the Obisat dynamic eigenvalues will be in the stability zone, implying a return to the equilibrium state in case of little perturbations, which helps the attitude control actuators. In fact, as it can be seen, the gravity gradient is about 0 through all the simulation:

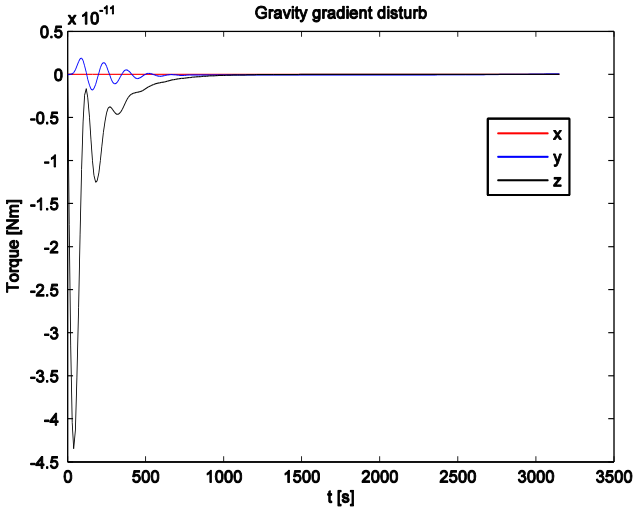

Figure 8.4. Gravity Gradient disturb for half period simulation

Total disturbance

Finally the total disturbance acting on the satellite is calculated in Figure 8.5 for an orbit time frame.

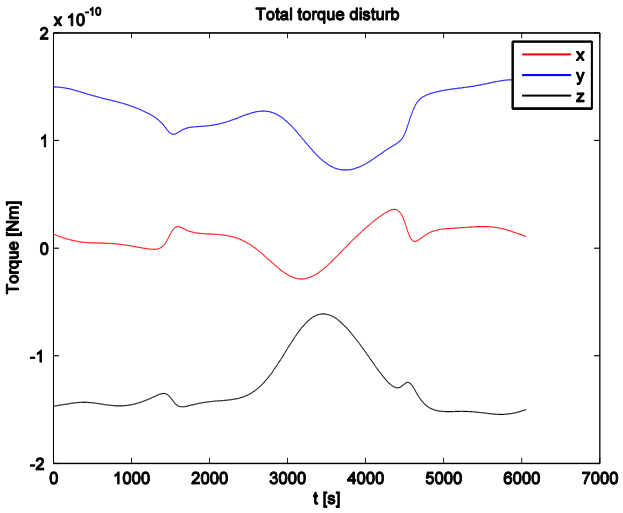

Figure 8.5. Total disturbance

The total disturbance is of the order of 10^{-10}, and while the pitch disturb is about 0, the roll and yaw ones are about 1.5 x 10^{-10} Nm.
This disturbance must be contrasted by a torque generated by the actuators driven from a control system.

8.1 Subsystem design

8.1.1 Sensors

Sensors are necessary to detect Obisat attitude. Trying to dump costs and masses, it was necessary to perform a trade-off between the main sensors systems. Star sensors are too expensive for a Cubesat, in fact the most used ones are Earth sensors, sun sensors and magnetometers. The first two sets cannot be used as stand alone but they should be coupled since each one requires an addiction measure to uniquely define the reference frame. Moreover, they are also heavier and bigger than the last group, thus magnetometers are chosen.

Magnetometers

The sensors are implemented as ceramic packages and co-located with drive electronics in a potted sensor head - ideally at the end of a rigid boom. The Magneto Resistance driver ensures the sensor maintains low noise operation by holding the sensor at its optimum position on the sensor transfer function. The sensor delivers the three components of the magnetics field plus a temperature measurement.

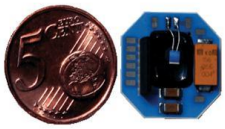

Figure 8.6. Magnetometers

In microsat applications, the additional electronics is integrated with the sensor head resulting in a very compact unit that is simple to accommodate. Its main characteristics are:

- Orthogonality: better than +/- 1°
- Measurement range: +50,000nT to -50,000nT
- Sensitivity: 10nT
- Power consumption: 400 mW
- Power supply: +5V and +15V DC or 28V unregulated option
- Serial (RS422 or I2C) options
- Sensor: 10x10x5mm

8.1.2 Actuators

To control the Obisat system it has been decided to use magnetotorquers, which are the simplest and low cost way to perform this aim. For Cubesat systems they come included directly into the solar panels; this results in a gain of space and efficiency. The most important characteristics for these Magnetotorquers are listed in Table 8.2:
Their size and weight is not provided because they are integrated inside the solar panels. Magnetotorquers alone cannot control Obisat. Indeed they work generating a magnetic dipole, which interacting with the magnetic Earth field, generates the control desired torque. The constraints coming from the fixed orientation of the Earth field, bar the system to get unconditioned values of magnetic dipole. This implies the use of just two components of the Earth

magnetic field to control 2 axes and to perform the 3rd axis attitude control through the use of a supplement actuator, namely a reaction wheel.

Table 8.2. Magnetotorquers characteristics

Parameter	Value
Operating Voltage	5 V
Power	0.2 W
Magnetic Dipole	0.114 Am^2
Total turns	318 (53 per layer on a 6 layer board)
Current	0.041A
Averaged area (due to loop decreasing size)	0.0086 m^2

The selected wheel could be the one built in the technical university of Berlin [30]. Its main characteristics are here reported:

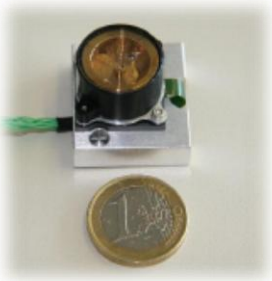

Figure 8.7. Micro wheel

Table 8.3. Main characteristics of the reaction wheel

Parameter	Value
Torque	4 x 10^{-5} Nm
Angular momentum	3.4 x 10^{-5} Nms
Moment of Inertia	117 gmm^2
Size	20 x 20 x 15 mm^3
Mass	9.2 g

8.2 Analysis and results

The principal inertia frame needs to be defined as first. It is given by the following values, calculated through the use of the software SolidEdge, the same used for the all 3D drawings:

- I_x = 0.0011 Kg m^2
- I_y = 0.0017 Kg m^2
- Iz = 0.0017 Kg m^2

The first thing to be done, is to create a target matrix that represents the desired attitude that the satellite should follow through its life.
The goals with the control system are:

- To keep the x axis aligned with the Nadir axis
- To let face 1 and 2 collect the highest amount of energy by letting them be lit with an angle between each face's normal and sun direction of 45°.

The chosen inertial frame is a geo-centric one with the first axis oriented in the direction of the vernal point, the second axis laying on the celestial equator is perpendicular to the first and the third is perpendicular to the both pointing towards the north pole.
This led to the definition of the desired Eulerian target angles between the inertial frame and the principal one:

$$\begin{Bmatrix} \varphi = 0 \\ \vartheta = 10 \\ \psi = 90 \end{Bmatrix} \text{deg}$$

These values have been used to define a target direction cosines matrix A_T (φ,θ,ψ) which, used as in the equation (8.4) , gives the error matrix.

$$A_S A_T^T = A_E \tag{8.4}$$

A_S is the attitude matrix based on sensors' acquisitions.
Errors are used to run the controller, which returns the control torques M_x, M_y, M_z. They are used as an input for the actuators system, which according to actuators' parameters returns the effective control action. The actuators' system behavior follows the system (8.5):

$$\begin{Bmatrix} -\dot{h}_x \\ D_y \\ D_z \end{Bmatrix} = \frac{1}{B_x} \begin{bmatrix} B_x & B_y & B_z \\ 0 & 0 & -1 \\ 0 & 1 & 0 \end{bmatrix} \begin{Bmatrix} M_x \\ M_y \\ M_z \end{Bmatrix} \quad (8.5)$$

Dy and *Dz* are the torques magnetic dipoles generated by the magnetotorquers, while $\dot{h}_x$ is the derivative of the angular momentum of the reaction wheel. Since the wheel cannot bear a higher level of angular momentum of ± 3.4 x 10^{-5} it is necessary to make an analysis of the highest level reached by this and of the possible desaturation cycles.

Figure 8.8 shows the behavior of the wheel's angular momentum which is just the integral of the x curve represented in Figure 8.10. It is possible to see that the first desaturation is required after 14.5 days. The angular momentum's trend seems to respect the fact that the torque has an almost constant trend, thus its integral has the obtained "linear" shape.

In Figure 8.11it is possible to notice a pick at the beginning of the simulation. It is due to the fact that errors start from 0, thus the angular acceleration becomes quite high, causing the torques' pick.

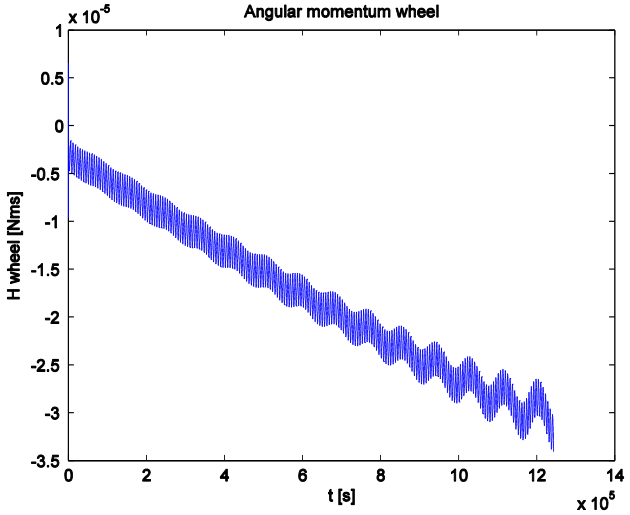

Figure 8.8. Angular momentum of the wheel until desaturation point

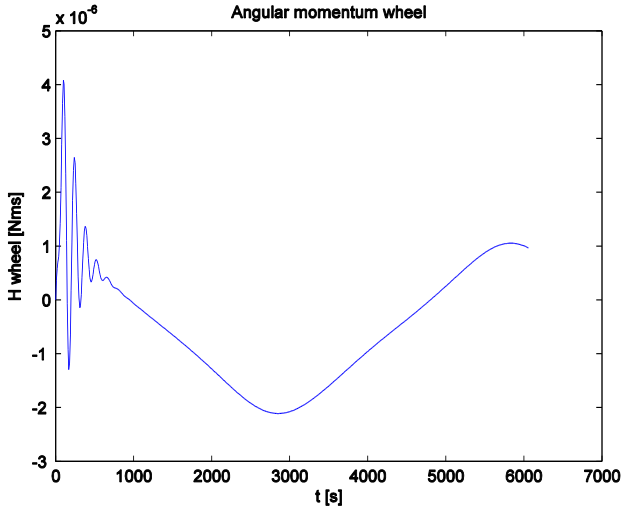

Figure 8.9. Angular momentum of the wheel during one orbit period

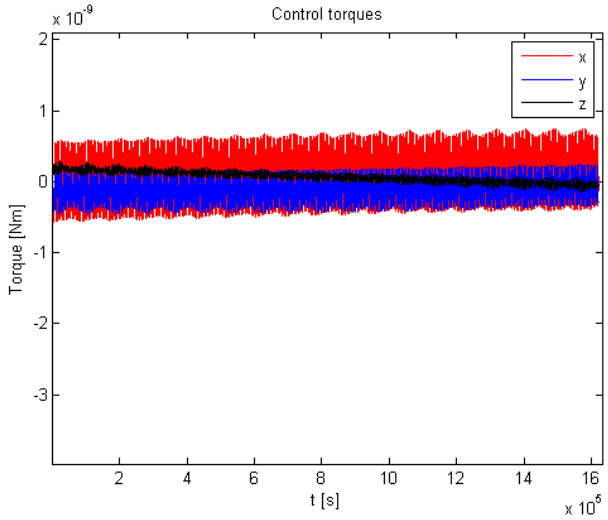

Figure 8.10. Control torques until desaturation point

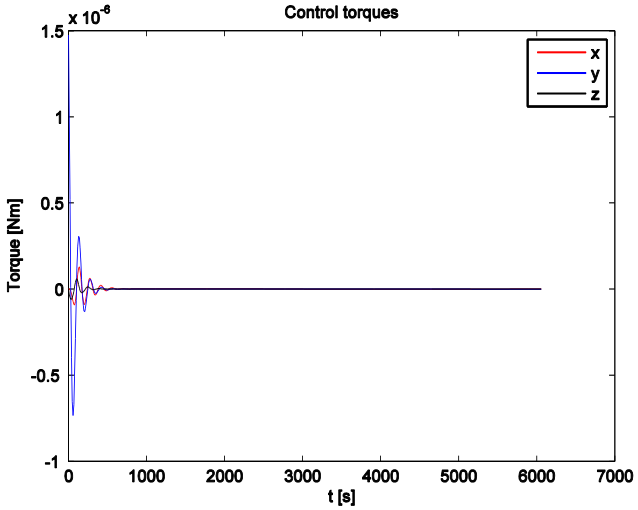

Figure 8.11. Control torque during an orbit period

It is possible to evaluate the pointing errors (α_x α_y α_z), namely the needed Eulerian angles to make the "target inertia principle frame" rotate to be coincident with the real one. They are calculated through the use of director cosines matrixes which give the principal inertia frame orientation in the fixed Geocentric one. α_i is therefore the rotation around the x axis. The order of the rotations is given by the director cosines matrix used which in this case is the A_{231}: first rotation around the second axis, then the third and eventually the first.
The simulation takes in account the maximum values for control torques which have been automatically considered in the saturation parameters.
Results in terms of pointing errors are shown in the next figures.

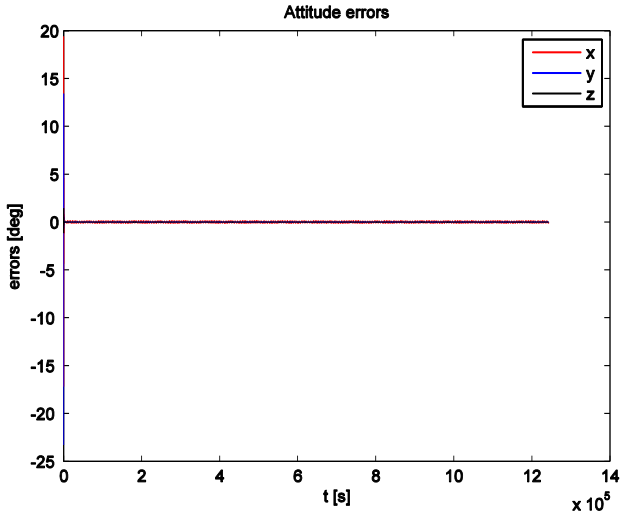

Figure 8.12. Pointing errors

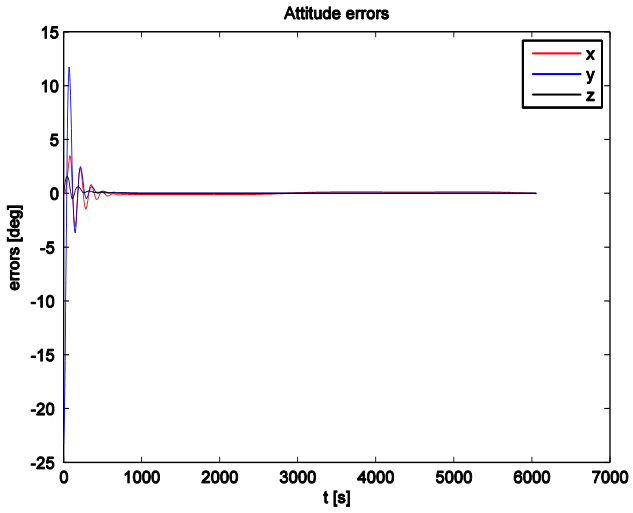

Figure 8.13. Errors (α_x α_y $\alpha_{z)}$ trend during one orbit period

It is possible to see how errors stay into the required ranges

In the next two figures the behavior of the control torques and errors responding to a variation of the initial conditions are shown. Changing the initial Eulerian angles from the target set with an applied error of ±40 deg, the following results are obtained:

With a set of angles with an error of 40 deg it is:

$$\begin{Bmatrix} \varphi = 40 \\ \vartheta = 50 \\ \psi = 50 \end{Bmatrix} \text{deg}$$

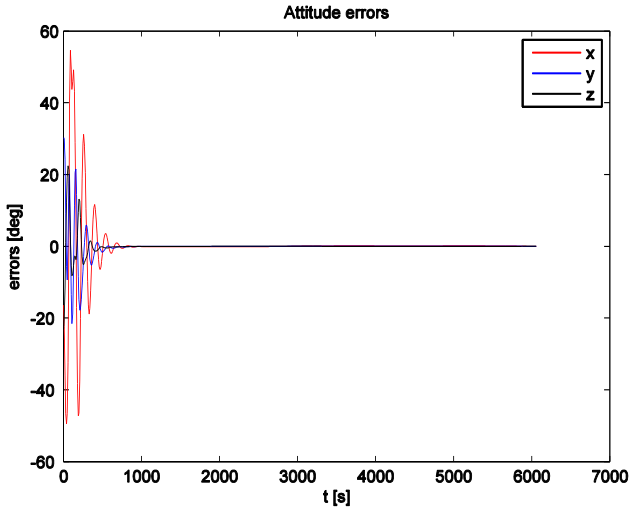

Figure 8.14. Attitude deviations with 40 deg initial error

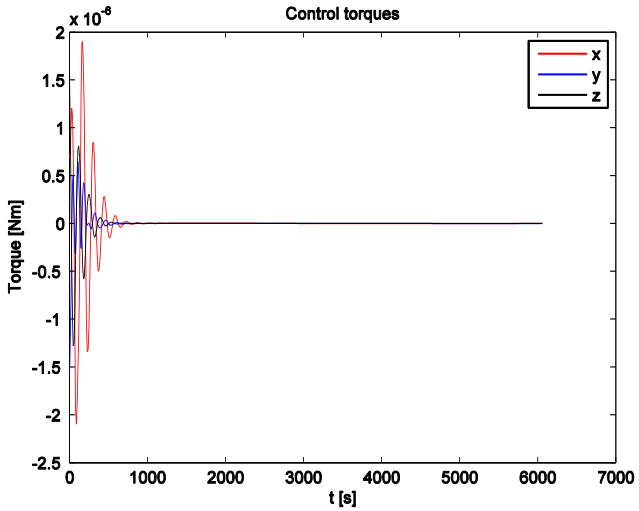

Figure 8.15. Control torques with 40 deg initial errors

The system is able to reach the target attitude in a reasonable time.

Now the response of the system at an initial disturbance both on the angular speeds of 1 deg/s and on the initial Eulerian angles of 35 deg is simulated:
These represent the stability threshold, since bigger deviations cause singularities.

$$\begin{Bmatrix} \omega_x = 1 \\ \omega_y = 1 \\ \omega_z = 1 \end{Bmatrix} \text{deg/s} \qquad \begin{Bmatrix} \varphi = 35 \\ \vartheta = 45 \\ \psi = 55 \end{Bmatrix} \text{deg}$$

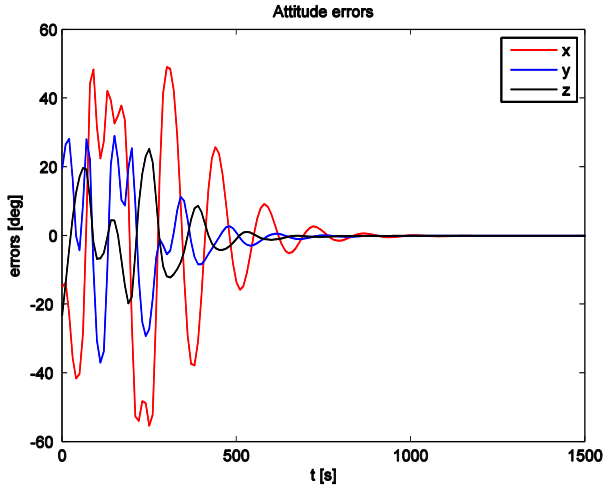

Figure 8.16. Attitude errors with initial deviations on angles and velocities

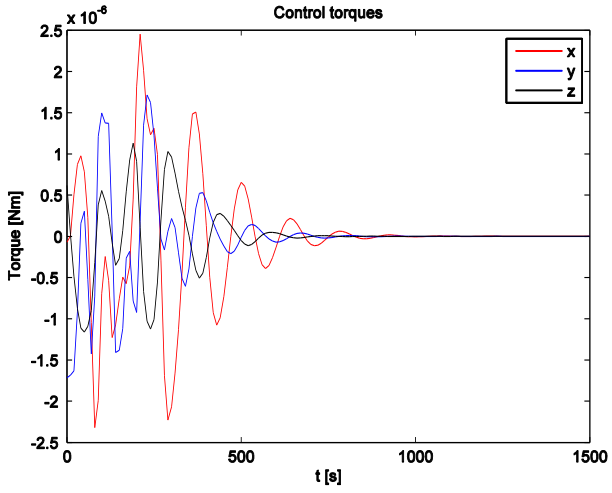

Figure 8.17. Control torques with initial deviations on both angles and velocities.

9 Mass, and Cost budgets

The following table shows a list of the contributes in terms of mass and costs for each Obi's element.

Table 9.1. Mass and cost [26] [13]

Feature	**Mass [g]**	**€**	**$**
Conversion rate ($/€)		**1,2485**	
PDM	60	6167	7700
Batteries	204	2883	3600
Solar panels	302	14738	18400
Cables	56		
EPS Total	*622*		
Obdh board	84,5	5000	
OBDH Total	*84,5*		
Magnetometers	15	9000	0
Sun sensor	5	2500	0
Reaction wheel	9,2		
Adcs board	170	7209	9000
ADCS Total	*199,2*		0
Tx/Rx/HPA	660	7000	0
Antenna	50	4600	0
Cables	50		
TT&C Total	*710*		
Structure	*150*	*3100*	*0*
Total	**1766**	**62197**	**77653**
Total with margin of 25%	**2207**	**77746**	**97067**

A 1.5 Cubesat can afford to sustain up to 3 Kg of mass. Nevertheless, the more it weighs, the more you pay for the launch.
An average cost for Cubesat launches is estimated in 50,000€ per unit. For a 1.5 Cubesat it can be evaluated in 75,000 €.

Including the average launch cost, the total cost for Obisat can be estimated on about 150,000€.

Table 9.2. Total costs

Feature	€
ObiSat System	77746
Launch by unit	50000
Total	*152746*

At a first analysis, this is an extremely high cost system, compared to all other systems on the market. In reality, we need to consider that this cost can be limited by the following factors:

- Launch costs can be limited or avoided considering the "piggyback" approach. As explained initially we could sign-off agreements with ESA in order to have the system launched whenever other missions are.
- We could extend the scope of the system both in terms of mission goals and venues and going beyond the POF scope. This would bring some additional costs not more than 10%, as evaluated but it would enable to sell the service to different customers for a certain period of time, having a ROI (return on investments) in the lifetime of the satellite itself.

In the following table, we have estimated the ROI considering an hypothetical rented connection service with speed rate conditions of 536 Kbps, 5 hours connection a day, 25 days a month for 2 years.

Table 9.3. ROI estimation

Price Month/ Kbps	Price/ period	# Custo-mers	Total Price [1000$]	Total Price [1000€]	Total Cost [1000€]	ROI Period	ROI Months
$4,7	$60.4	1	60.5	48.5	152	3.13	75.12
$4,7	$60.4	2	121	97	152	1.57	37.68
$4,7	$60.4	4	242	194	152	0.8	19.2

From the last row it is possible to see that a service rent to 4 customers could bring a return of the investment before the end of life. The scope of this work is indeed to point out whether this system could cost less than the on the market alternatives, and this can be obtained only with a shared service.
Such a study has to be accompanied by those regarding power and thermal considerations. This analysis wants to be just a brief anticipation of what could be the next step in the size of this system, with no pretention of accuracy.

To rent the service to 4 customers, considering the same downloading and uploading time windows as in chapter 7 but multiplied times 4, in the same period frame of 44872s a most powerful system has to be used. Using an attitude configuration which exposes just one side to perpendicular solar radiation using though double deployed panels (9.4 W – 3 faces exposed) we obtain a power income of 9.4 as shown in Figure 9.2.

Figure 9.1. Double deployed panels for a 3U structure [26]

It is possible to see that a sufficient margin is guaranteed and the system can still achieve the desired goals.

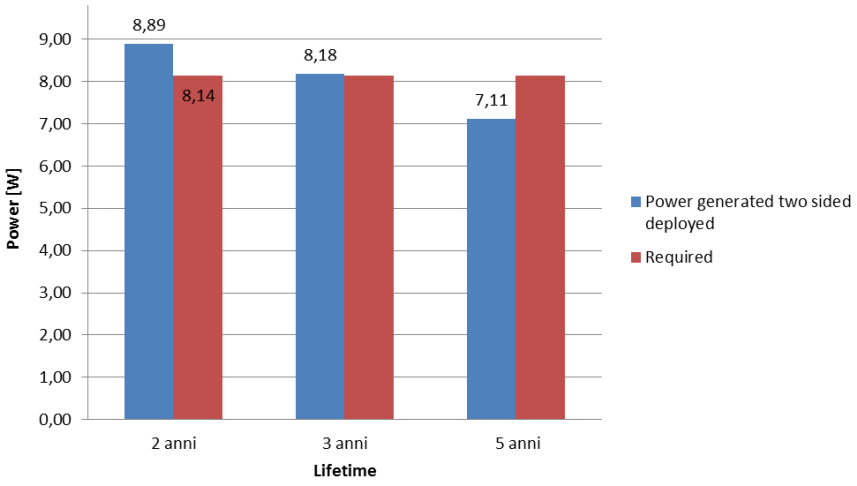

Figure 9.2. Power balance for extended transmission time

It is also necessary to study the temperature trend after such a long period of downlink connection. The simulation is conducted for all the 44872 seconds period.

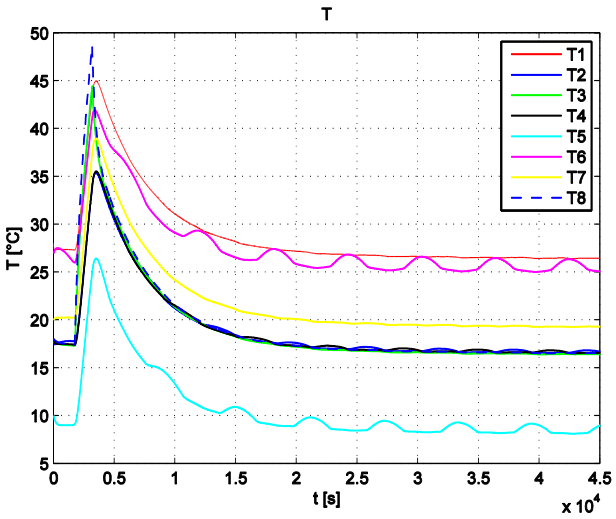

Figure 9.3. Temperature trend for extended transmission time

Temperatures are at the acceptance's border level but they still guarantee the proper system environment.
Thus a rental condition and a consequent increment of the transmission times could be afforded by the system.

10 CONCLUSIONS

The aim of this work was trying to help an organization of people, the "Patologi oltre frontier", who constantly spend their time and passion trying to treat people in difficult situations around the African continent. From the beginning it was clear that a dedicated satellite system was an expensive solution in terms of times, costs and responsibilities.

From a scientific point of view this work represents a way to investigate the possible use of broad band links at high data rates through the use of Cubesats. That's a challenge as this is the first time such a solution is tried with a cubesat. Up to now such high speed links have not been used on board of these small spacecraft, although some missions like the Canadian Most or the Nasa St-5 have used the same technologies.

The constraints met in terms of thermal loads and power demand have been faced in a analytical and technical way, presenting solutions based on configuration choices or through an accurate devise selection which let the system overcome these problems.

Through an economic analysis it has been pointed out, that on the market providers offer the service with quite unaffordable costs for a non-governmental association and partial covertures. The development of a dedicated system, through a possible rent of service to third customers could help saving some costs which could relief the big economic burden this work brings whit itself.

By adopting the new deploying structure available on the market, the system besides to have more gathered power, would be almost all, under shadow conditions, allowing a wider use of window connections, letting more payload to be transferred.

From the analysis carried out it is possible to see that this system, could be manufactured, although some critical issues should be firstly discussed and solved. They are:

- The achievement of the operative orbit
- Disposal
- Receiver customization
- Transmitter structural links with the panels' frames.

It would be desirable to include a propulsion system which could also serve for disposal needs. A possible future solution for the development of a similar low cost complex system, could be that of launching an interfaculty project which involves different areas such as, It technologies, telecommunications, electrical field, management engineering. By the internal customization and realization of some devices and through the specialized skills coming from all the components it would be possible to have the best results in terms of quality and costs with a consistent saving of money, emulating the ESA concept philosophy.

“At the moment Obi remains a compact fast efficient… kid”

List of acronyms

ACM: Adaptive and Coding Modulation
ADCS: Attitude Determination and Control System
AMSAT: American Satellite
AU: Astronomic Unit
BCR: Battery Charge Regulator
BER: Bit error rate
BOL: Begin Of Life
BPSK: Binary Phase Shift Keying
CIR: Committed Information Rate
COM: Communication
COTS: Commercial off-the-shelf
CPU: Central Power Unit
DDR2: Double Data Rate 2
DOD: Depth Of Discharge
DSP: Digital Signal Processing
DSR: Digital Slide Server
EEPROM: Electrically Erasable Programmable Read-Only Memory
EoC: End Of Charge
EPS: Electrical Power System
ESA: European Space Agency
FAC: Frequency Automatic Control
FDMA: Frequency Division Multiple Access
FEM: Finite Element method
FR4: Fire-Retardant glass laminate substrate material for electronic circuits.
GaAs. Gallium Arsenide
GL: Conductive Heat Link
GR: Radiative Heat Link
HPA: High Power Amplifier
I2C: Inter-Integrated Circuit Communications
IR: Infra Red
MIPS: Mega Information per Second
MPPT: Maximum Power Point Tracking
MPU: Memory Protection Unit
MTQ: Magnetotorquers
NASA. National Aeronautics and Space Administration
NGO: Non-Governmental Association
NPO: Non Profit Organization
OBC: On Board Computer
OBDH: On Board Data Handling

OCD: On-Chip Debug
ONLUS: Organizzazione Non Lucrativa di Utilità Sociale
OSR: Optical Solar Reflectors
PCB. Printed Circuit Board
PDCA: Peripheral Direct Memory Access
PDM: Power Distribution Module
POF: Patologi Oltre Frontiera
PSA: Power from Solar Array
RF: Radio Frequency
RHCP: Right Hand Circular Polarization
RISC: Reduced Instruction Set Computer
ROI: Return on Investment
Rx: Receiver
SA: Solar Array
SRAM: Static Random Access Memory
TCS: Thermal Control System
TDMA: Time Division Multiple Access
TT&C: Telecommunication Tracking and Control
TX: Transmitter

Bibliography

[1] Aperio, "Aperio Application Note," 27 12 2007. [Online]. Available: http://www.aperio.com/.

[2] "List of Cubesat Satellite Missions," [Online]. Available: http://mtech.dk/thomsen/space/cubesat.php.

[3] NASA, "History of on orbit satelite fragmentation," *Orbital Debree program office,* no. JSC62530, 2004.

[4] U. Nations, "Technical report on space debris," New York, 1999.

[5] A. Q. Giovanni Mengali, Fondamenti di Meccanica del Volo Spaziale, Pisa: Edizioni PLUS, 2006.

[6] P. F. Bernelli, *"Attitude Determination and Control" Courses Notes,* Milan, 2010.

[7] C. Clark, "Cubesat Components from Clyde Space," Clyde Space LTD, Glasgow, 2011.

[8] B. I. H. O. M.J.H. Walker, "A set of modified equinoctical orbit elements," *Nasa Astrophysics Data,* p. 11, 1985.

[9] "Cubesat S-band Transmitter," 03 2012. [Online]. Available: http://www.clyde-space.com/cubesat_shop/transceivers_rx_tx/transmitters/301_cubesat-s-band-transmitter.

[10] F. C. Commission, ""FCC Online Table of Frequency Allocations" (PDF)," 4 August 2011. [Online]. Available: http://transition.fcc.gov/oet/spectrum/table/fcctable.pdf.

[11] J. R. Wertz, Space Mission Analysis and Design, USA: Microcosm Press, 1999.

[12] Aeroastro, "Aeroastro S Band Transceiver," 2012. [Online]. Available: http://www.aeroastro.com/index.php/components/s-band-radio.

[13] Cubesatshop, "S-Band Patch Antenna RHCP for HISPICO," Cubesat shop, 2012. [Online]. Available: http://www.cubesatshop.com/index.php?page=shop.product_details&flypage=flypage.tpl&product_id=85&category_id=6&option=com_virtuemart&Itemid=70&vmcchk=1&Itemid=70.

[14] RadioRampage, "Yagis, Gain Beamwidth and Stacking," 2012. [Online]. Available: http://www.radiorampage.com/techpages/yagis.php.

[15] Alibaba, "aluminum mesh dish antennas," Jan 2012. [Online]. Available: http://www.alibaba.com/product-

gs/287587502/2_3m_3_0m_3_69m/showimage.html?newId=287587502&pn=1&pt=10&t=12&cids=.

[16] Atmel, "Atmel - Customer care and IT solutions," 2012. [Online]. Available: http://support.atmel.no/bin/customer.exe.

[17] Clydespace, "Mission Interface Computer," Clyde Space, 2012. [Online]. Available: http://www.clyde-space.com/cubesat_shop/obdh/mission_interface_computer/300_mission-interface-computer-sa-mic.

[18] I. Alet, Contrôle thermique des engins spatiaux, École nationale Supérieure de l'Aéronautique de l'Espace, 1998.

[19] L. Jacques, *Thermal Design of the Oufti-1,* Liege, 2009.

[20] P. Prat, "GLAST Large Area Telescope Calorimeter Subsystem Thermal," Laboratoire Leprince-Ringuet, Ecole polytechnique, Mar 2003..

[21] AzurSpace, "'Azur space solar power gmbh"," [Online]. Available: http://www.azurspace.com.

[22] A. Wiberg, "Thermal study with comparison between physical measurements and simulations"," ABB automation Technologies AB, May 2005.

[23] B. Guenin, "Electronics cooling," August 2002. [Online]. Available: http://www.electronics-cooling.com/2002/08/simplified-transient-model-for-ic-packages/. [Accessed 06 Jun 2012].

[24] M. K. Ahmad A. Pesaran, "Thermal Characteristics of Selected EV and HEV Batteries," in *Annual Battery Conference: Advances and Applications*, Long beach, California, 2001.

[25] D. B. Graham, "Thermal portal," 2011. [Online]. Available: http://www.tak2000.com/. [Accessed 06 June 2012].

[26] Clydespace, "Clyde Space," 2012. [Online]. Available: www.clydespace.com.

[27] K. Worrall, "CubeSat Power Distribution Module User Manual," Clyde Space Ltd., Glassgow, 2011.

[28] V. McLaren, "User Manual, Standalone 30 Wh Battery," Clyde Space Ltd, Glasgow, 2010.

[29] Wikipedia, "Wikipedia - Cubesat," 2012. [Online]. Available: http://en.wikipedia.org/wiki/CubeSat.

[30] F. B. K. B. M. H. H. Kayal, "Verification of Miniaturized Reaction Wheels for Pico and Nano satellites," TU Berlin, Berlin, 2008.

[31] D.Gilmore, Spacecraft Thermal Control Handbook: Fundamental Technologies, Aerospace Press, December 2002.

[32] P. Rochus, "Conception d'expériences spatiales," 2008.